JAERI-Tech
97-022

DESIGN OF ITER SHIELDING BLANKET

May 1997

Kazuyuki FURUYA, Satoshi SATO
Toshihisa HATANO, Ikuhide TOKAMI*
Kazunori KITAMURA, Hidenori MIURA
Yutaka ITO, Toshimasa KURODA
and Hideyuki TAKATSU

日本原子力研究所
Japan Atomic Energy Research Institute

本レポートは，日本原子力研究所が不定期に公刊している研究報告書です。
入手の問合わせは，日本原子力研究所研究情報部研究情報課（〒319-11 茨城県那珂郡東海村）あて，お申し越しください。なお，このほかに財団法人原子力弘済会資料センター（〒319-11 茨城県那珂郡東海村日本原子力研究所内）で複写による実費頒布をおこなっております。

This report is issued irregularly.
Inquiries about availability of the reports should be addressed to Research Information Division, Department of Intellectual Resources, Japan Atomic Energy Research Institute, Tokai-mura, Naka-gun, Ibaraki-ken 319-11, Japan.

編集兼発行　日本原子力研究所
印　　刷　日立高速印刷株式会社

Design of ITER Shielding Blanket

Kazuyuki FURUYA, Satoshi SATO, Toshihisa HATANO
Ikuhide TOKAMI *, Kazunori KITAMURA+, Hidenori MIURA+
Yutaka ITO+, Toshimasa KURODA and Hideyuki TAKATSU

Department of Fusion Engineering Research
Naka Fusion Research Establishment
Japan Atomic Energy Research Institute
Naka-machi, Naka-gun, Ibaraki-ken

(Received April 1, 1997)

A mechanical configuration of ITER integrated primary first wall/shield blanket module were developed focusing on the welded attachment of its support leg to the back plate. A 100 mm x 150 mm space between the legs of adjacent modules was incorporated for the working space of welding/cutting tools. A concept of coolant branch pipe connection to accommodate deformation due to the leg welding and differential displacement of the module and the manifold/back plate during operation was introduced.

Two-dimensional FEM analyses showed that thermal stresses in Cu-alloy (first wall) and stainless steel (first wall coolant tube and shield block) satisfied the stress criteria following ASME code for ITER BPP operation. On the other hand, three-dimensional FEM analyses for overall in-vessel structures exhibited excessive primary stresses in the back plate and its support structure to the vacuum vessel under VDE disruption load and marginal stresses in the support leg of module No.4.

Fabrication procedure of the integrated primary first wall/shield blanket module was developed based on single step solid HIP for the joining of Cu-alloy/Cu-alloy, Cu-alloy/stainless steel, and stainless steel/stainless steel.

Keywords:ITER, Shielding Blanket, Welded Attachment, Electromagnetic Analysis, Thermal Analysis, Stress Analysis, Fabrication Procedure, Separable First Wall

---

This work was conducted as an ITER Technology R&D and Design, and this report corresponds to the 1995 ITER Task Agreement for Design Task (Task No. G16TD18, ID No. D202).

+ Department of ITER Project

* On leave from Kumagaigumi, Co.

Mechanically attached separable first wall was also examined resulting in practicable difficulty based on a huge number of bolts to withstand electromagnetic force, questionable electrical insulation under high neutron loads, extremely accurate mechanical locking by in-situ remote handling, and so forth.

ITER遮蔽ブランケット設計

日本原子力研究所那珂研究所核融合工学部
古谷　一幸・佐藤　聡・秦野　歳久・戸上　郁英*・喜多村和憲+
三浦　秀徳+・伊藤　裕+・黒田　敏公・高津　英幸

(1997年4月1日受理)

支持脚のバックプレートへの接続を溶接接合構造としたITER遮蔽ブランケットに対し，モジュール構造概念，電磁力及び熱，強度解析等による特性評価，製作手順に関する検討等を行った。支持脚の溶接／切断用機器挿入スペースとして隣接モジュールの支持脚間に100mm x 150mmの空間を設けた。また，冷却水母管とモジュール内の冷却水ヘッダを接続する枝管として，EPPにおける増殖ブランケットで必要となるトリチウムパージ用ヘリウムガスの給／排気をも考慮した二重ベローズ構造を提案し，モジュール構造概念に反映した。

2次元熱及び熱応力解析により，第一壁部の銅合金ヒートシンク及び第一壁／遮蔽体部のステンレス鋼構造材はITERのBPPにおけるプラズマ立上げ及び立ち下げ，定常状態の運転に対して十分な強度を有することを確認した。一方，バックプレート及び真空容器を含めた3次元電磁力及び応力解析により，VDE時にはバックプレート下部及びバックプレートを真空容器に接続する支持構造に過大な応力が発生すること及びプラズマの定位置消滅時に発生するブランケット支持脚部の応力には裕度が少ないことから，設計改善が必要であることを明かにした。

遮蔽ブランケットの製作に関しては，特に重要となる第一壁部の銅合金／銅合金及び銅合金／ステンレス鋼，ステンレス鋼／ステンレス鋼の接合に対し，高温静水圧（HIP）法を用いてこれらを同時に接合する方法を提案し，これに基づく製作手順を検討した。

電磁力低減及び廃棄物量軽減等の観点から有利となる機械接続方式分離型第一壁についても設計検討を行ったが，電磁力支持に必要なボルト数が多大となること及び中性子重照射下での電気絶縁材料の性能不確定性，遠隔操作に対する機械的はめ合い構造の設置精度要求が過大となること等，種々の課題が残された。

本作業は，国際熱核融合実験炉（International Thermonuclear Experimental Reactor）の工学設計活動として，1995年設計作業計画（Task No. G16TD18, ID NO. D202）に基づいて実施した。

那珂研究所：〒311-01　茨城県那珂郡那珂町向山801－1
＋　ITER開発室
※　外来研究員（株）熊谷組

Contents

目　　次

1. Executive Summary

Mechanical design and analyses have been performed on the integrated primary first wall/shield (IPFW/SH) blanket and the separable first wall (SFW). Fabrication issues for the IPFW/SH and the back plate have been also investigated including the initial assembly of the back plate.

A concept of the IPFW/SH blanket module has been developed focusing on the welded attachment to the back plate. Two attachment legs of 70 mm thickness each are extruded from the back of the module to be welded to the back plate. For the working space of leg welding/cutting tools, the space of 100 mm x 150 mm is provided in-between the legs of adjacent modules. A concept of coolant branch pipe from the manifold to the module is also shown. This branch pipe includes bellows structure to accommodate to deformation due to the leg welding and differential displacement between the module and the manifold/back plate during operation.

Three-dimensional FEM structural analyses were performed with the model of overall structures including blanket modules, attachment legs, the back plate, back plate support structure connected to the vacuum vessel, and vacuum vessel for various loading conditions, i.e. component weights, electromagnetic loads during centered disruption and VDE, and differential thermal loads. Main conclusions derived from the analysis results are: 1) excessive primary stresses in the back plate and its support structure over the allowable limits with weight and VDE disruption loads, 2) therefore the reinforcement of the back plate at the bottom required, e.g. by either increasing the thickness or mounting poloidal ribs connected by a toroidal support ring, and also the stiffening and/or further optimization of the support structure required, 3) marginal stress in the attachment leg of #4 module with weight and centered disruption loads, thus further investigation required including the effect of stress concentration at the edge of the leg.

Detail thermal stress FEM analyses have been conducted with two-dimensional horizontal cross-sectional model of #4 module with attachment legs and the back plate. Transient behaviors of thermal stresses during plasma start-up and shut down as well as at steady state have been analyzed. Maximum stress in the DSCu in FW is observed during the start-up while maximum stresses in SS FW coolant tube and SS shield block at steady state. All these stresses satisfy the stress criteria based on ASME Section III for ITER BPP operation of 1×10^4 shots.

Fabrication procedure of the IPFW/SH module has been developed based on single step solid HIP for the joining of DSCu/DSCu, DSCu/SS and SS/SS. The joining method of Be armor to the DSCu needs further investigation.

Based on the assessment of welding and cutting methods to be applied to the module attachment leg, narrow-gap TIG welding and plasma cutting are proposed as reference welding and cutting methods, respectively. In addition, iodine laser is proposed as alternative for both of welding and cutting. Welding and cutting heads of these methods aiming at working in the 100 mm x 150 mm space have been designed. The heads access route and temporary module support have been also investigated including interfaces with remote maintenance equipment.

Mechanically supported SFW has been examined aiming at reducing the burden onto remote maintenance equipment, reducing radwastes associated with the reactor operation, and even reducing the EM force acting on the blanket module. Mechanical design, EM and thermo-mechanical analyses, and feasibility studies on two types of SFW have been extensively carried out. However, the requirement of a huge number of bolts to withstand EM force, the questionable electrical insulation under high neutron loads, the difficulty of accurate mechanical locking by in-situ remote handling, the unpredictable seizing/sticking of mechanical locking and bolts during reactor operation, and/or the less reduction of EM force than expected resulting in high eddy currents and stresses have never made us reach a viable solution of SFW. Thus another approach, i.e. the integrated first wall/blanket module with welded attachment leg, is proposed.

Fabrication procedure of the back plate has been developed beginning with manufacturing of one sector and up to assembling into the vacuum vessel during initial construction. Welding jigs and fixtures, and a back plate transporter during the assembly are also indicated.

2. Objectives

This task consists of mechanical design and analyses of the shielding blanket system for the integrated primary first wall/shield blanket and the separable first wall, neutronics analyses concerning to radiation streaming, and the back plate design. The report of the neutronics analyses is separately given as a specific neutronics task report. Thus this report includes other design works on the integrated primary first wall/shield blanket, the separable first wall and the back plate.

The objective of the mechanical design of the shield blanket system is to perform conceptual level design of the primary first wall and in-vessel shielding system to establish its ability to meet the ITER technical requirements. The first wall and shield shall be provided in 720 modules, of which 500 contain a primary first wall. The poloidal length of these modules will vary from approximately 1.4 to 2 m with a toroidal width varying from ~0.8 m (inboard) to ~1 m (outboard). The conceptual design of the module approach by addressing the following issues is to be developed.

1) Development of concepts for integrated first wall and shield modules.
2) Development of methods for attaching the first wall/shield modules to the back plate by welding.
3) Investigation of the methods for manufacturing the proposed first wall/shield modules.

In support of conceptual level mechanical design of the first wall and in-vessel shield modules and welded attachment scheme, stress analysis is to be performed. The first wall and shield modules will be subjected to large electromagnetic forces and heat loads during normal and off normal conditions. The work shall analyze: (1) the ability of the first wall to transmit the heat loads to the embedded cooling system while maintaining acceptable temperature and stress levels, (2) the capability of the first wall and shield structural arrangement to withstand the imposed mechanical loads, and (3) the integrity of the module's structural attachment to the back plate. The work shall maximize use of available Finite Element Analysis (FEA) codes and techniques. Specific areas to be analyzed include:

1) Determining thermal stresses and temperatures in the primary first wall.
2) Determining the stresses and deflections in integrated first wall/shield modules.
3) Determining the required weld thickness necessary to structurally attach the modules to the back plate. The analysis will also include a calculation of stresses in the back plate in the region of the connection and include recommendations on the required back plate thickness.

The investigation on the separable first wall aiming at a reduction of rad-wastes and an easy maintenance by reducing the handling weight and size shall be performed. Specific areas to be performed include:

1) Concept development.
2) Determining the stresses and deflections in separable first wall modules.
3) Assessment of the feasibility.

The objective of the back plate design is to identify methods of manufacture, assembly, and repair/replacement of the back plate, including the attached manifolds. The back plate is a toroidally continuous stainless steel thick wall similar in shape to a horse shoe when viewed in poloidal cross-section. The inboard section and outboard section must have an effective minimum structural thickness of approximately 8 and 10 cm, respectively. However actual thickness may be considerably larger in certain locations, such as those containing module attachment bosses. Manifolds that supply cooling to the modules are attached to the back plate. This work will address the following issues with the above concept.

1) Method of manufacturing the 20 compound curved, 44 tone and 26.5 meter long with variable width, sections required in each of the 20 machine sectors.
2) Method of obtaining the required local variations in cross sections of the back plates.
3) Method of manufacturing the manifolds and attaching them to the back plates.
4) Methods of installing the back plate and manifold sub assemblies including joining of adjacent sectors.
5) Methods of maintenance

3 Mechanical Design of Integrated Primary First Wall/Shield Module and Analyses

3.1 Module Concept with Welded Attachment to Back Plate

An overall concept of the integrated primary first wall/shield module with welded attachment to the back plate is shown in Fig. 3.1.1. The module No. 4 has been representatively taken for this concept development. Figures 3.1.2 and 3.1.3 show a horizontal cross-section at the upper coolant corrector and a vertical cross-section, respectively. The first wall consists of 10 mm-thick beryllium armor and 20 mm-thick Cu alloy (alumina dispersion strengthened copper: DSCu) embedding SS coolant tubes of 10 mm in outer diameter and 1 mm in thickness. The first wall is joined, e.g. by hot isostatic pressing (HIP), to the stainless steel (SS) shielding block in which coolant channels are drilled in an arrangement to accommodate the attenuating nuclear heating.

The module is welded to the back plate at the attachment legs extruded both from the back of the module and the front of the back plate. The thickness of the attachment legs is 70 mm to withstand the disruption electromagnetic forces. The space of 150 mm x 100 mm is provided in-between the legs of adjacent modules for the insertion of welding/cutting tools. Cover plates to protect the surrounding structures such as manifold pipes during welding/cutting and also to collect cutting dross are indicated in Fig. 3.1.2. However, there is not enough space to provide the cover plates with this manifold pipe arrangements, i.e. four 100 mm-diameter pipes. Thus, it needs to be examined, e.g. to reduce the number of manifold pipes or to change the manifold pipe location. Figure 3.1.4 shows an example the latter investigation, in which the manifold pipes are located at the back of the back plate keeping the total thickness from the first wall to the back of the back plate or the back of the manifold pipes. This concept has an advantage of easier piping to the top port of the vacuum vessel without penetration through the back plate. On the other hand, disadvantages of this concept are possible degradation of shielding performance, especially for rewelding of the legs and branch pipe connections, and possible interference with the back plate support structure attached to the vacuum vessel. Further investigation is required.

Branch pipes from the coolant manifold to the module are also described in the figures with a bellows structure for the pipe ends from the manifold and from the module to meet for welding and accommodate to deformation due to the leg welding and differential displacement between the module and the manifold/back plate during operation.

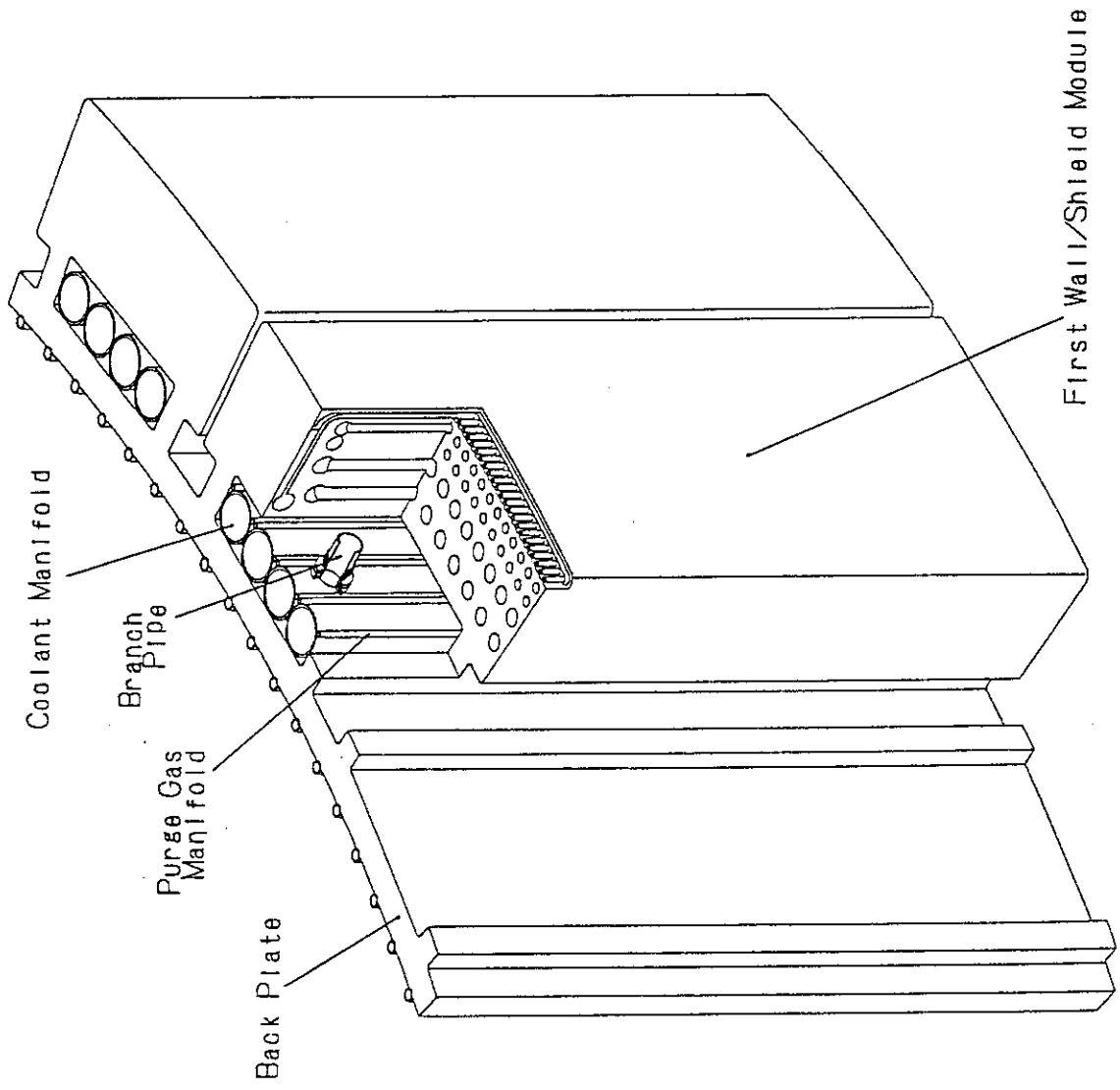

Fig. 3.1.1 Shielding Blanket Module (welded attachment)

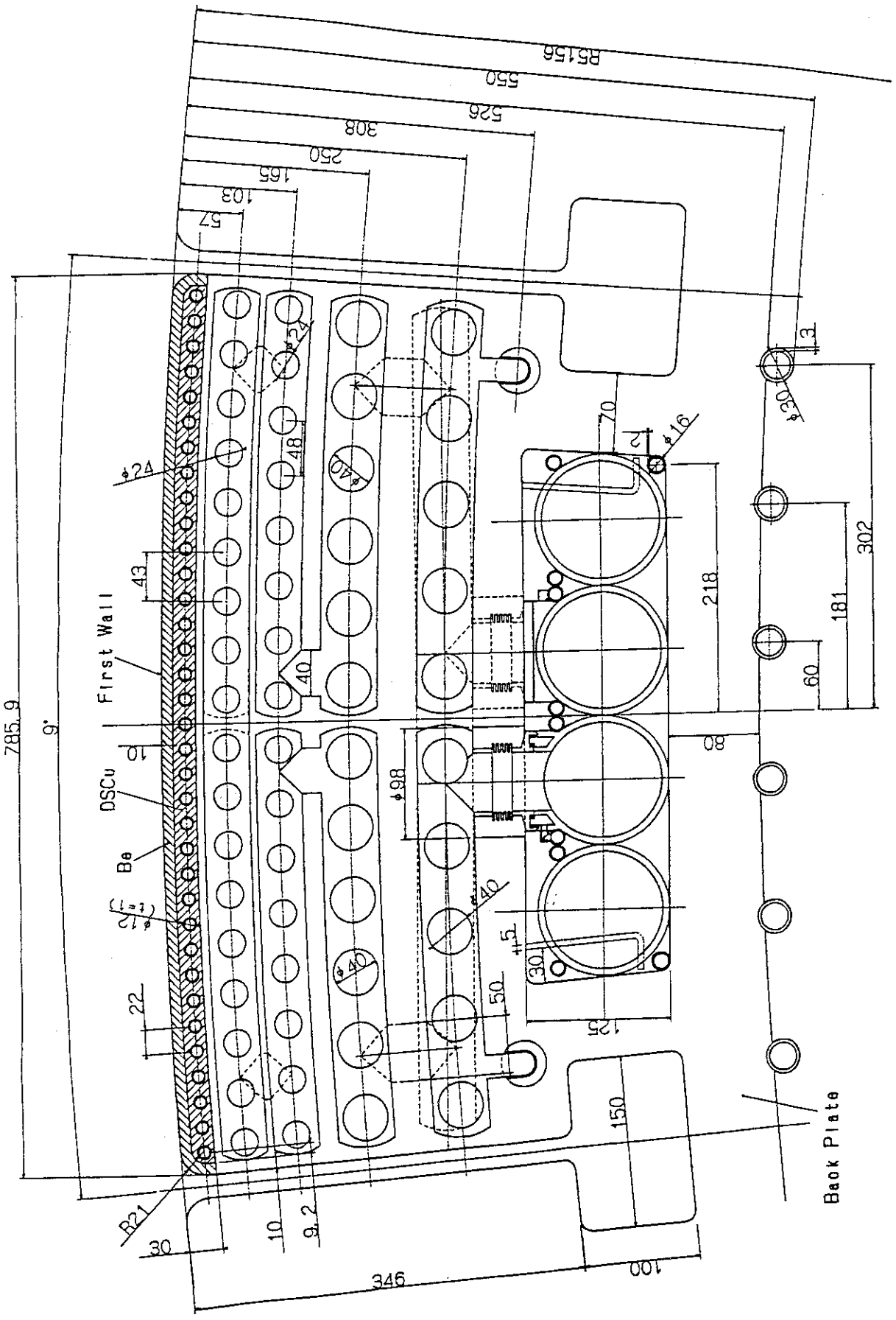

Shield Blanket Module (NO.4) with Welded Attachment to Back Plate (Section A－A)

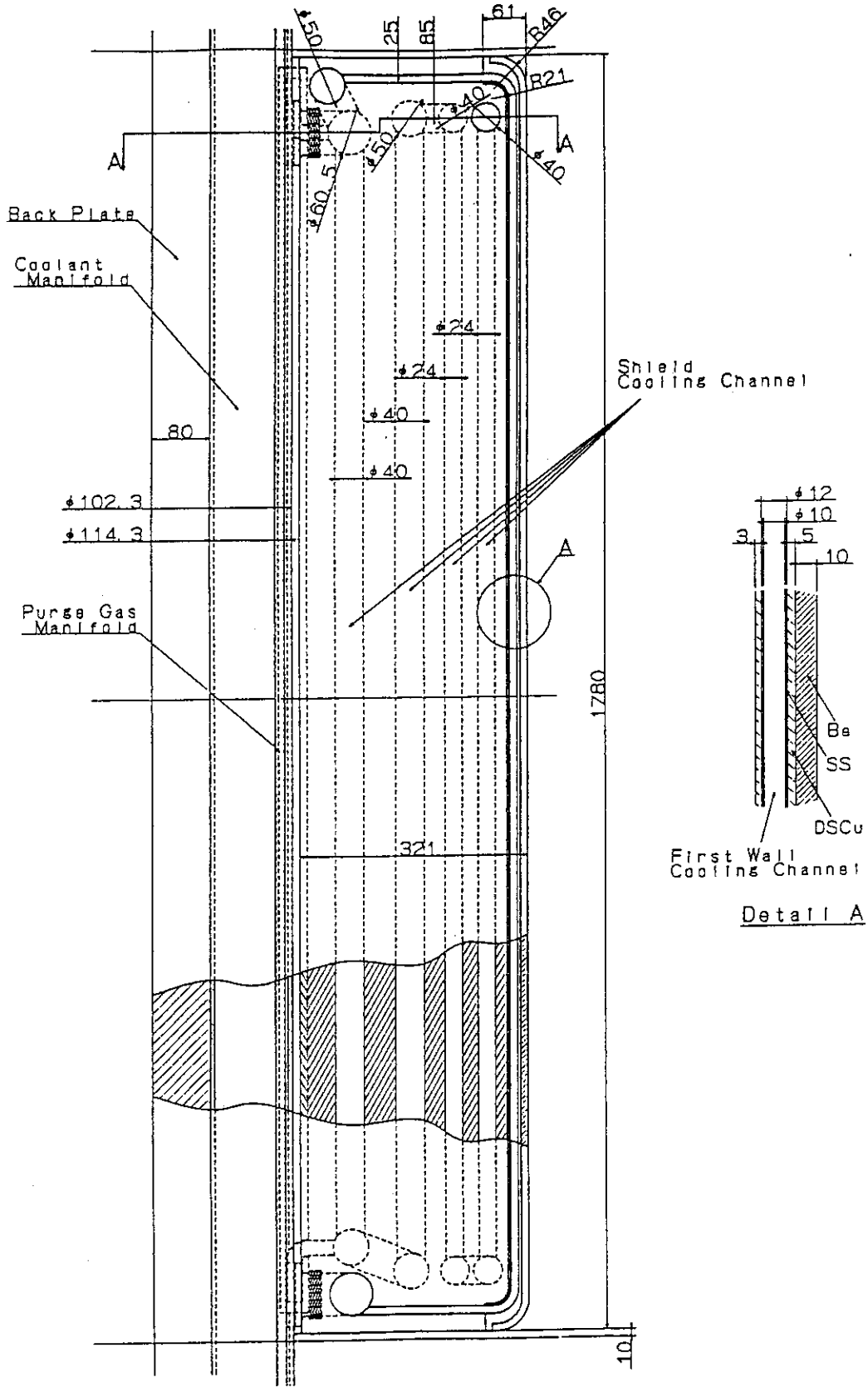

Fig. 3.1.3 Vertical Cross-Section of Shield Blanket Module (NO.4) with Welded Attachment to Back Plate

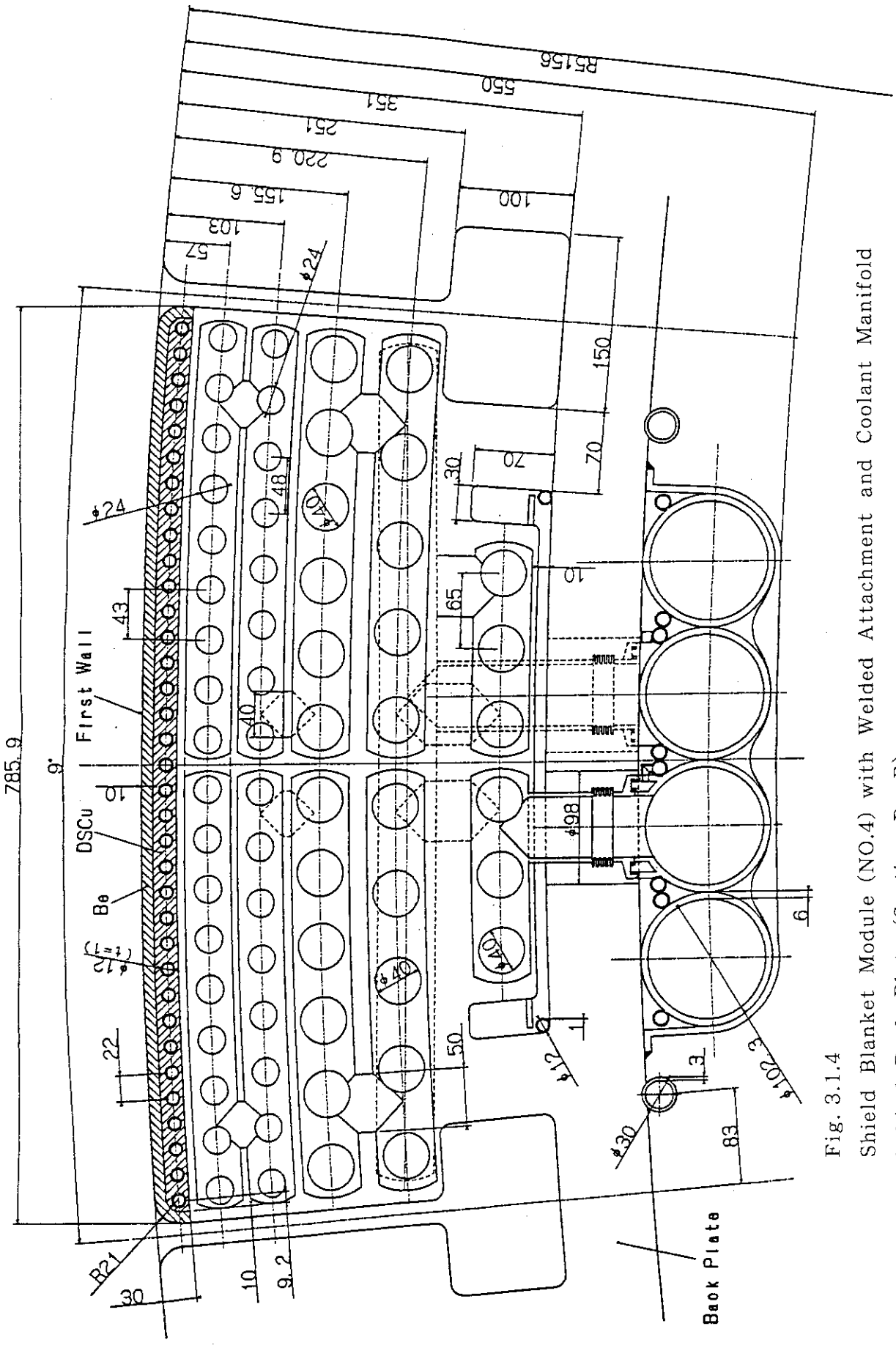

Fig. 3.1.4
Shield Blanket Module (NO.4) with Welded Attachment and Coolant Manifold behind Back Plate (Section B - B)

3.2 Thermal and Structural Analyses

3.2.1 Overall structural analysis of blanket support system

The blanket support system consists of blanket modules, module attachment support legs, back plate and blanket support structures. The blanket modules are welded to the back plate through the module attachment support legs, and the back plate with thick toroidal shell structure is supported with the inboard/outboard blanket support structures from double-walled vacuum vessel.

To investigate the structural integrity of the blanket support system, an overall structural analysis has been conducted with 3-D FEM model including blanket modules, module attachment support legs, back plate, inboard/outboard blanket support structures and double-walled vacuum vessel.

(1) Analytical conditions

(i) FEM modeling

All of structural components such as blanket modules, module attachment support legs, back plate, inboard/outboard blanket support structures and double-walled vacuum vessel are represented with shell elements. Table 3.2.1-1 shows materials and thickness of the components in the model. Figure 3.2.1-1 indicates the FEM model with 18° sector in the toroidal direction. Both toroidal side edges of the vacuum vessel and back plate are under the cyclic symmetry conditions. Details of the blanket modules and back plate, and details of inboard and outboard blanket support structures in the FEM model are shown in Fig.3.2.1-2 and Fig.3.2.1-3, respectively.

The shield block of the modules was represented with box structure of 100 mm thickness. The back plate has locally 200 mm thickness around the blanket support structures. The configuration of the blanket support structures are applied to the model, with multi-layered flexible plates proposed by the VV group in Garching JCT[3.2.1-1]. They have the configurations of 2-20 mm thickness/300 mm width/1160 mm length/7 layers for inboard blanket support structure, and of 4-12 mm thickness/600 mm width/1340 mm length/20 layers for outboard support structure. Though the lengths of both the inboard and outboard blanket support structures in the FEM model are different from actual dimension, equivalent bending stiffness are used in the analysis.

The modified reinforcements on the vacuum vessl components are shown

in Fig.3.2.1-4, which was determined in the VV Technical Meeting at Naka Co-Center on Oct.30-Nov.2, 1995[3.2.1-2]. The details of the VV gravity support leg are shown in Fig.3.2.1-5, with multi-layered flexible plates of 3 m length and box-type rigid support leg of 3 m length.

Two types of gravity support leg configurations on multi-layered flexible plates were considered, including separate type support leg as the reference design and integrated type one as alternative design. The lower edge of the box-type gravity support leg was absolutely fixed in the model.

(ii) Load conditions

Following loads were applied to the analysis, including weight loads, electromagnetic loads and thermal loads. The weight loads on the structural components were set to be 3.1 MN uniformly for 18° sector of the vacuum vessel, to be 0.6 MN and 1.9MN for 18° sector of the inboard and outboard blanket support system, respectively, and to be 0.38 MN and 0.38 MN concentratedly for 18° sector of the inboard and outboard divertor system at R=6.4 m and R=9.5 m (R: radius from machine center), respectively.

The centered disruption and VDE(Vertical Displacement Event) disruption loads were considered as the electromagnetic loads. The electromagnetic pressures on the first wall and shearing forces on both side walls of the blanket modules are shown in Fig. 3.2.1-6 as the centered disruption loads. The VDE disruption loads were applied to the lower parts of blanket modules and lower portions of the vacuum vessel corresponding to the divertor support rail locations. The VDE load has a load distribution with the averaged electromagnetic pressures on the first walls of #1, 2, 13, 14, and #15 blanket modules, as shown in Fig.3.2.1-7[3.2.1-3], and asymmetric load component of 50 MN in the total of the torus system[3.2.1-4].

Two loading modes were considered with 2.5 MN for the 18° sector as the VDE asymmeric loads acting on the blanket modules, as shown in Fig.3.2.1-8 for in-plane force mode and in Fig.3.2.1-9 for out-of-plane force mode. The vertical loads of 2.27 MN and 0.93 MN were applied at the lower vacuum vessel locations of R=6.4 m and R=9.5 m as the VDE load on the inboard and outboard divertor sector, respectively.

In addition, overall thermal loads were also applied to the in-vessel components, i.e. 250 °C uniformly on the blanket modules, 200 °C uniformly on the back plate, linear incorporation from 200 °C to 150 °C for inboard and

outboard blanket support strucrures and linear incorporation from 150 °C to 20 °C for the upper multi-layered plates of vessel gravity support.

(2)Analytical results

Structural analyses of blanket and vacuum vessel support system were performed under the several loads mentioned above, with a finite element structural code, NASTRAN[3.2.1-5].

(i) Dead weight

The overall deformation of the blanket and vacuum vessel support system under the dead weight is shown in Fig.3.2.1-10. It has a maximum deformation of ~6 mm at the lower edge of the outboard blanket(#15 blanket module), which are induced by the vacuum vessel deformations of 4.2 mm at the outboard lower region of the vacuum vessel and rotation displacement of the outboard blanket support. Figure 3.2.1-11 shows the overall Von Mises stress distribution on the blanket and vacuum vessel support system under the dead weight. The maximum stress of 64 MPa at the vacuum vessel side edge on the outboard blanket support with the multi-layered flexible plates.

(ii) Centered disruption load

The overall deformation of the blanket and vacuum vessel support system under the centered disruption load is shown in Fig.3.2.1-12. The maximum deformation of ~7 mm appeared at the upper portion of the outboard blanket(#10 blanket module) in the plasma-side direction. Figure 3.2.1-13 indicates the overall Von Mises stress distribution on the blanket and vacuum vessel support system under the centered disruption load, which has a maximum stress of 129 MPa at the back plate around the inboard midplane blanket module(#4 module). The relative large stress of ~120 MPa occurred at the module side edge on the outboard blanket support structure with multi-layered flexible plates.

(iii) VDE loads (symmetric load)

The averaged electromagnetic pressure distribution on the lower blanket modules was applied as an in-plane load on the blanket modules. The overall deformation of the blanket and vacuum vessel support system under the symmetric VDE disruption load is shown in Fig.3.2.1-14, which has a maximum deformation of ~29 mm at the lower edge of the outboard blanket(#15 module) in

the lower direction. The toroidal stiffness of the back plate, therefore, needs to be further enhanced around the lower portions. Figure 3.2.1-15 illustrates the overall Von Mises stress distribution on the blanket and vacuum vessel support system under the symmetric VDE disruption load, with a maximum stress of ~246 MPa at the back plate lower edges on the inboard and outboard blankets.

(iv) VDE loads (asymmetric load)

a) In-plane load mode

The overall deformation of the blanket and vacuum vessel support system and Von Mises stress distribution on their components under the asymmetric VDE disruption load with the in-plane load mode are shown in Fig.3.2.1-16 and Fig.3.2.1-17, respectively. The maximum deformation of ~4 mm occurred at the lower edge of the outboard blanket(#15 module), and maximum stress of ~40 MPa at the back plate lower edges on the inboard and outboard blankets.

b) Out-of-plane load mode

The overall deformation of the blanket and vacuum vessel support system and Von Mises stress distribution on their components under the asymmetric VDE disruption load with the out-of-plane load mode are shown in Fig.3.2.1-18 and Fig.3.2.1-19, respectively. The maximum deformation of ~42 mm occurred at the outboard blanket in the toroidal direction, which are induced by the deformations of ~30 mm at the vacuum vessel gravity support with the multi-layered flexible plates in the torus direction, and then maximum stress of 16 MPa occurred at the lower edge on the inboard back plate, while much larger stress of 237 MPa at the vacuum vessel side root on the multi-layered plates of the gravity support.

(v) Thermal load

The overall deformation of the blanket and vacuum vessel support system and Von Mises stress distribution on their components under the thermal load are shown in Fig.3.2.1-20 and Fig.3.2.1-21, respectively. The maximum deformation of ~52 mm occurred upward and radially at the top part of the outboard blanket(#9 module), and relative deformation between the blanket and vacuum vessel is estimated to be ~20 mm around the outboard top region. Then maximum stress of 306 MPa occurred at the blanket-side edge on the inboard blanket support structure of the multi-layered flexible plates, and large stress of

294 MPa also at the outboard blanket support structure.

(3) Mechanical assessment of blanket support system

Structural components of the blanket and vacuum vessel support system were assessed for the operation cases a)-f) described below, by the combination of results for basic loads shown above.

i) Load combinations

Primary Loads;

a) Load Case 1 : Weight Load + Centered Disruption Load.

b) Load Case 2 : Weight Load + VDE Disruption Load(Symmetric Load) + VDE Disruption Load(Asymmetric Load; In-plane).

c) Load Case 3 : Weight Load + VDE Disruption Load(Symmetric Load) + VDE Disruption Load(Asymmetric Load; Out-of-plane).

Primary & Secondary Loads;

d) Load Case 4 : Weight Load + Centered Disruption Load + Thermal Load.

e) Load Case 5 : Weight Load + VDE Disruption Load(Symmetric Load) + VDE Disruption Load(Asymmetric Load; In-plane) + Thermal Load.

f) Load Case 6 : Weight Load + VDE Disruption Load(Symmetric Load) + VDE Disruption Load(Asymmetric Load; Out-of-plane) + Thermal Load.

ii) Analytical results

The overall deformations of blanket support system and vacuum vessel and Von Mises stress distributions on their structural components are shown in Fig.3.2.1-22 to Fig.3.2.1-33 for the load cases a)-f). In addition, the Von Mises stress distributions on the inboard/outboard blanket support structures, back plate and blanket module attachment support legs are also indicated in Fig.3.2.1-34 to Fig.3.2.1-51.

The stress evaluation was conducted based on the standard of ASME Sec. III[3.2.1-5], for the stresses on the structural components due to several load cases, which has a design criteria on the stress limitation as follows:

$$\text{Primary Stress, } Pm + Pb < 1.5*Sm$$

$$\text{Primary + Secondary Stress, } Pm + Pb + Q < 3*Sm$$

where, Sm is an allowable stress limit of general primary-membrane stress intensity, and Sm values at 150 °C to 250 °C of type 316 stainless steel are indicated as follows;

Sm = 142 MPa at 150 °C
= 132 MPa at 200 °C
= 125 MPa at 250 °C

Maximum stresses in the inboard/outboard blanket support structures were assessed for the load case 1 to case 6 as follows:

Case 1 : Smax = 194 MPa in Outboard < 1.5*Sm (= 198 MPa, at 200 °C)
Case 2 : Smax = 231 MPa in Inboard > 1.5*Sm (= 198 MPa)
Case 3 : Smax = 257 MPa in Inboard > 1.5*Sm (= 198 MPa)
Case 4 : Smax = 420 MPa in Inboard > 3*Sm (=396MPa)
Case 5 : Smax = 313 MPa in Inboard < 3*Sm (=396MPa)
Case 6 : Smax = 327 MPa in Inboard < 3*Sm (=396MPa)

Though primary stresses on the blanket support structures were beyond the allowable stress limit in the load case 2 and case 3, the stress under the load case 1 was enough below the allowable limit. Primary and secondary stresses on the blanket support structures under the load case and case 6 were within the allowable stress limits.

Maximum stresses in the back plate were also evaluated for the load case 1 to case 6;

Case 1 : Smax = 131 MPa < 1.5*Sm (= 198 MPa, at 200 °C)
Case 2 : Smax = 312 MPa > 1.5*Sm (= 198 MPa)
Case 3 : Smax = 278 MPa > 1.5*Sm (= 198 MPa)
Case 4 : Smax = 181 MPa < 3*Sm (=396MPa)
Case 5 : Smax = 342 MPa < 3*Sm (=396MPa)
Case 6 : Smax = 327 MPa < 3*Sm (=396MPa)

Similary, the stresses of the blanket module attachment support legs were also evaluated as follows:

Case 1 : Smax = 127 MPa < 1.5*Sm (= 188 MPa, at 250 °C)
Case 2 : Smax = 87 MPa < 1.5*Sm (= 188 MPa)
Case 3 : Smax = 92 MPa < 1.5*Sm (= 188 MPa)
Case 4 : Smax = 218 MPa < 3*Sm (=376MPa)
Case 5 : Smax = 123 MPa < 3*Sm (=376MPa)

Case 6 : Smax = 123 MPa < 3*Sm (=376MPa)

The stresses on the blanket module attachment support leg were sufficiently below the allowable stress limits for all the load cases, however, primary membrane stress on the attachment of #4 blanket module is estimated to be about 120 MPa in the load case 1, which is marginal to Sm value of SS316 at 250 °C. Then, the thickness of the attachment may need to increase up to 80 mm for the #4 module, taking into stress concentration on the poloidal edge in the attachment. As for other module attachments, 70 mm thickness would be reasonable.

From the stress assessment results, followings were drawn.

-Primary stresses on both the blanket support structure and back plate were beyond the allowable stress limits n the load case of weight load and VDE disruption load, while the primary and secondary stress on their components within the stress limits.

-Stresses on the blanket module attachment support leg were sufficiently below the allowable limits for all the load cases, including the marginal membrane stress on the #4 module in the load case 1. The attachment thickness on the #4 module may need to be increased from 70 mm to about 80 mm.

(4) Concluding remarks

Three-dimensional structural analyses of the blanket support system and vacuum vessel were conducted with 18° sector FEM model including the blanket modules, module attachment support legs, back plate, inboard/outboard support structures and vacuum vessel, all components of which were modeled with shell elements. In the analysis, following loads were considered: weights of the components, centered disruption load to the blanket modules, VDE disruption loads to the blanket modules and thermal loads with the temperatures of 250 °C in the modules, 200 °C in the back plate and 150 °C in the vacuum vessel, uniformly.

Then, maximum stress induced on the blanket support structures and back plate were assessed under the several load combination of the above loads.

From the study, following conclusions were drawn.

-Primary stresses on both the blanket support structure and back plate were beyond the allowable stress limits in the load case of weight load and VDE disruption load, while the primary and secondary stress on their components

within the stress limits.

-Stresses on the blanket module attachment support leg were sufficiently below the allowable limits for all the load cases, including the membrane stress on the #4 module in the load case 1. The attachment leg thickness on the #4 module may need to be increased from 70 mm to about 80 mm.

-Either inboard and outboard lower parts of the back plate are required to be reinforced by increasing thickness or mounting a toroidal ring support and poloidal ribs. The blanket support structures are also further optimized by the reinforcements.

Reference

[3.2.1-1] ITER INTERM DESIGN REPORT, Design Description Document 1.5, IAEA, to be published.

[3.2.1-2] G.Johnson, Vacuum Vessel Working Meeting(Oct.30-Nov.2)-Summary, JCT-Garching, Nov.6,1995.

[3.2.1-3] ITER INTERM DESIGN REPORT, Design Description Document 1.6, IAEA, to be published.

[3.2.1-4] D.Williamson, BLANKET SYSTEM BACK PLATE AND SUPPORTS-RESPONSE TO DISTRIBUTION AND SEISMIC LOADS, Nov.20, 1995, JCT-Garching.

[3.2.1-5] The MacNeal-Schwendler Corporation, MSC/NASTRAN Version 66A User's Manual, Nov.(1989).

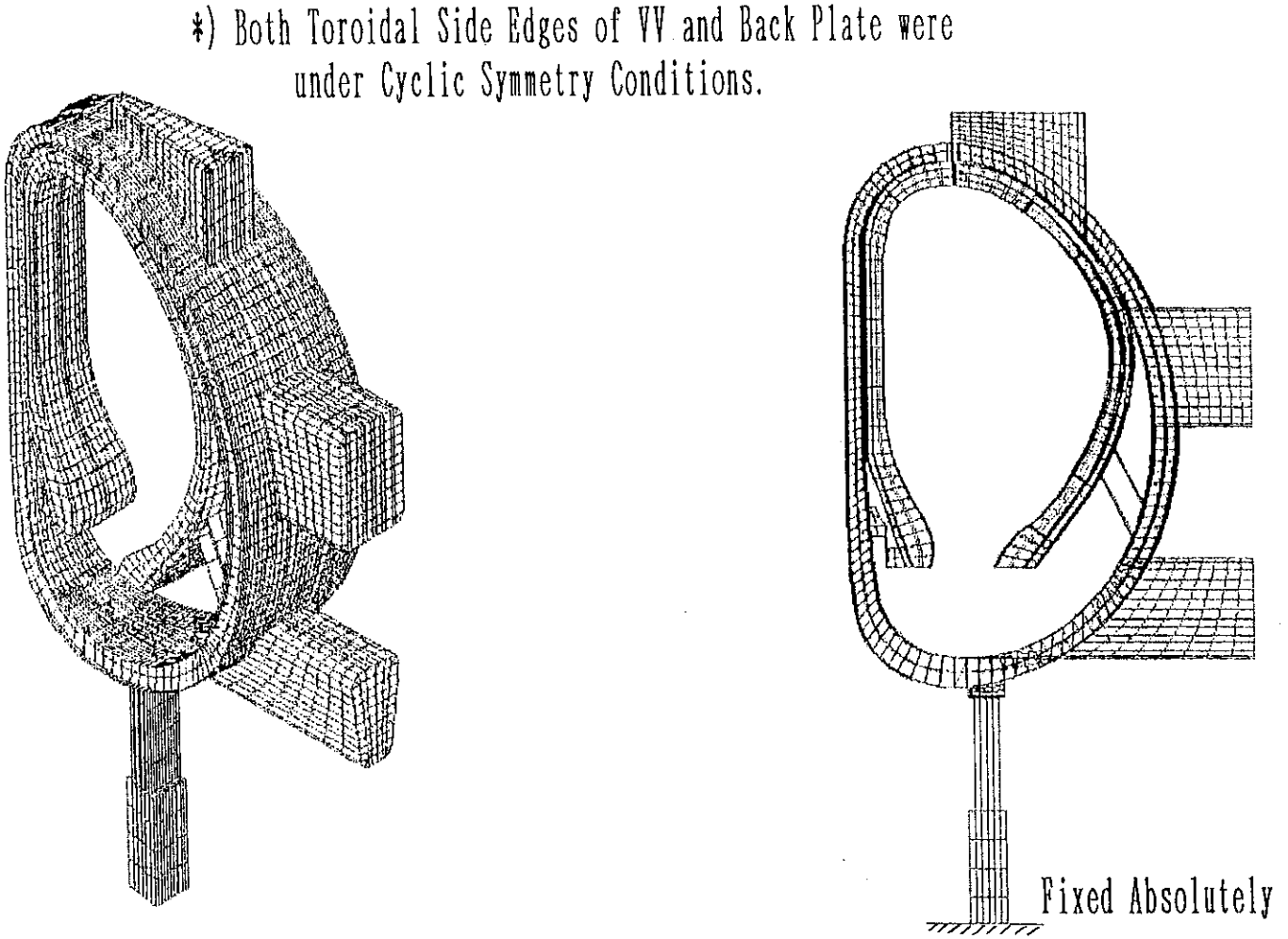

Fig. 3.2.1 – 1 FEM Model with 18° sector toroidally, consisting of Blanket Modules, Back Plate, Blanket support Structures and Vacuum Vessel.

Fig. 3.2.1－2 Details of Blanket Modules and Back Plate.

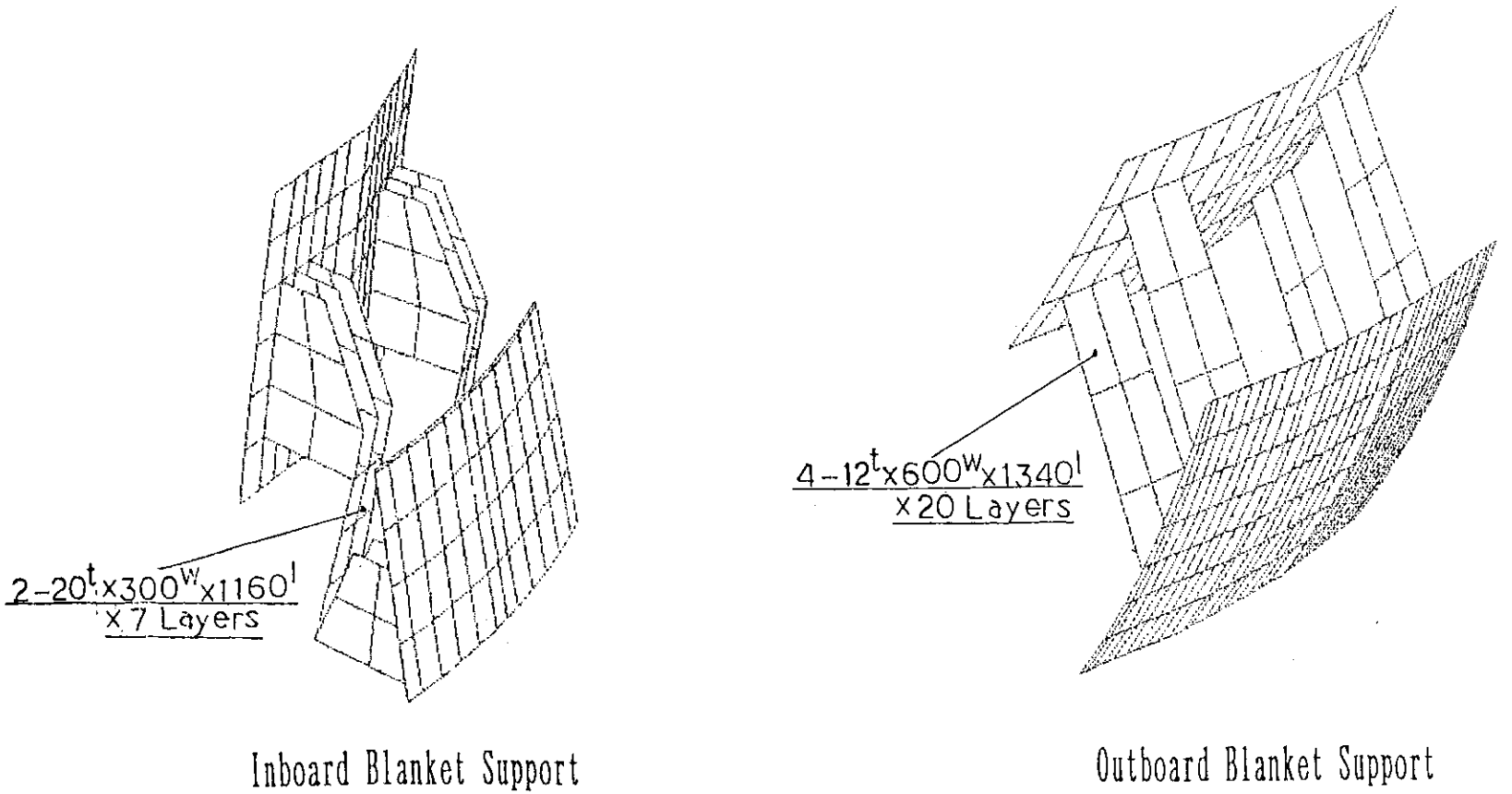

Fig. 3.2.1 – 3 Details of Inboard and Outboard Blanket Support Structure Models, with Multi Layered Flexible Plates Proposed by VV Gr in Garching JCT.

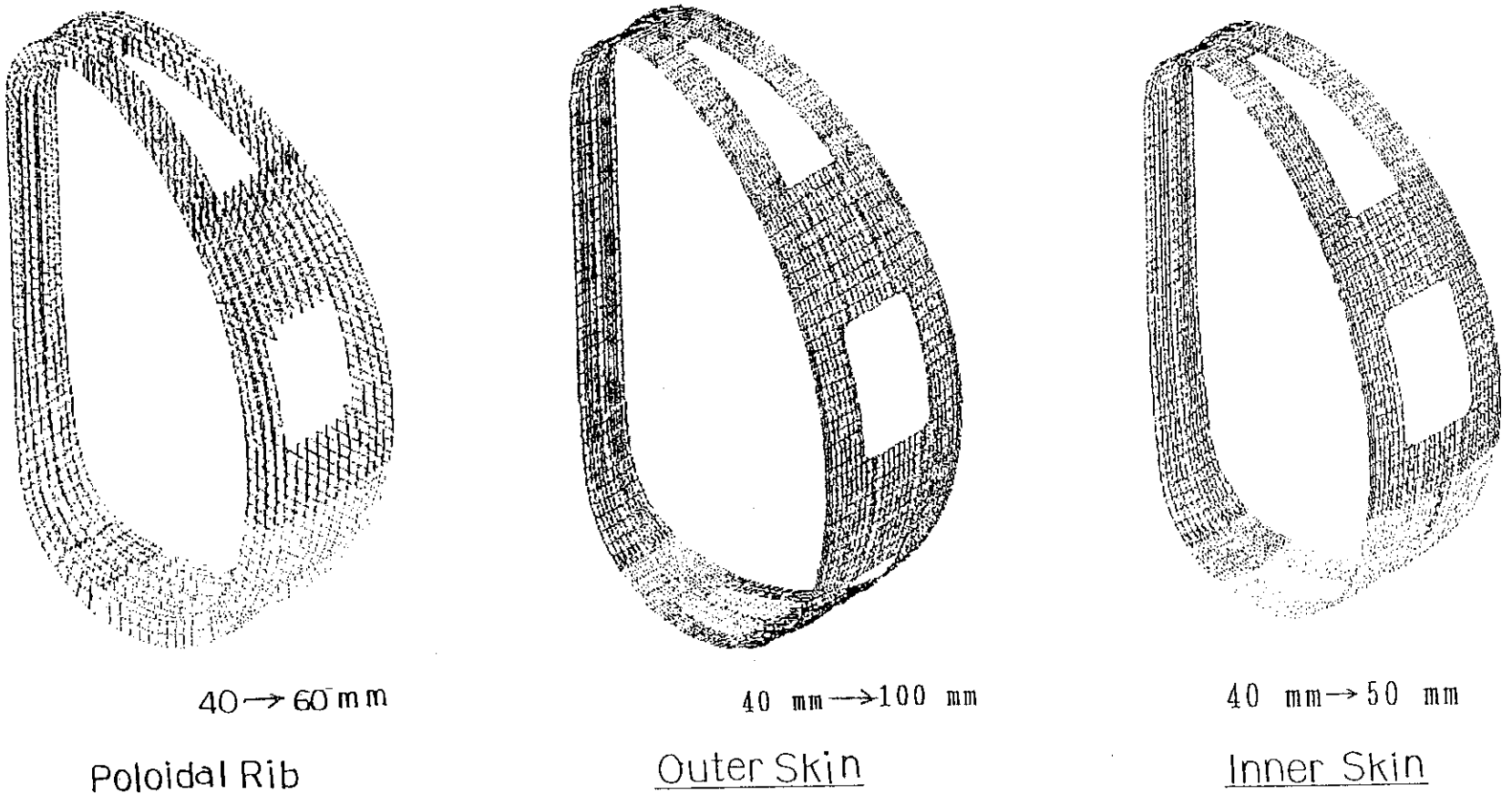

Fig. 3.2.1 – 4 Modified Reinforcements on VV Structural Components

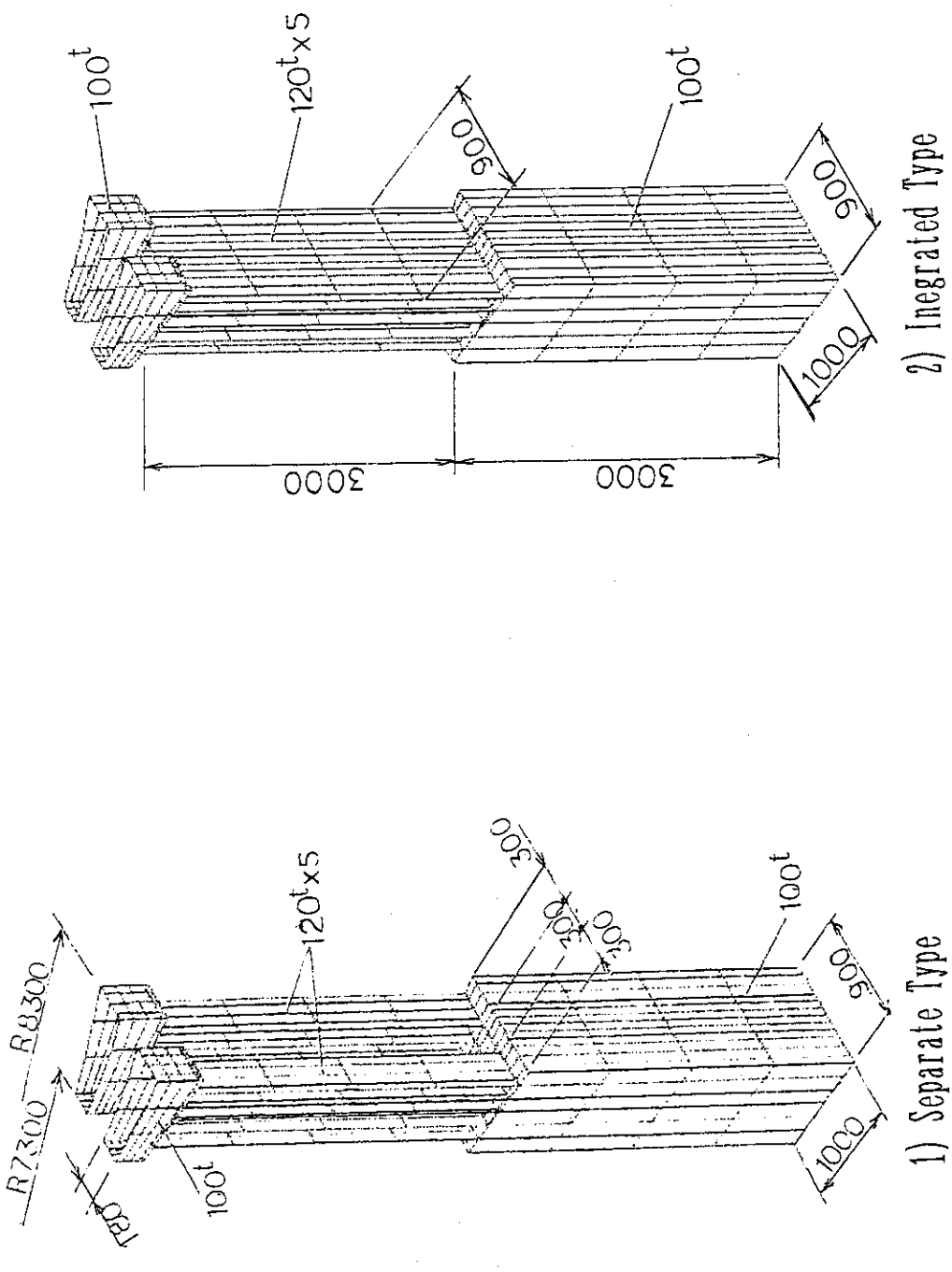

Fig. 3.2.1 – 5 Details of VV Support Leg,
with Multi Layered Flexible Plates of 3 m Length,
and Box – Type Rigid Support Leg of 3 m Length.

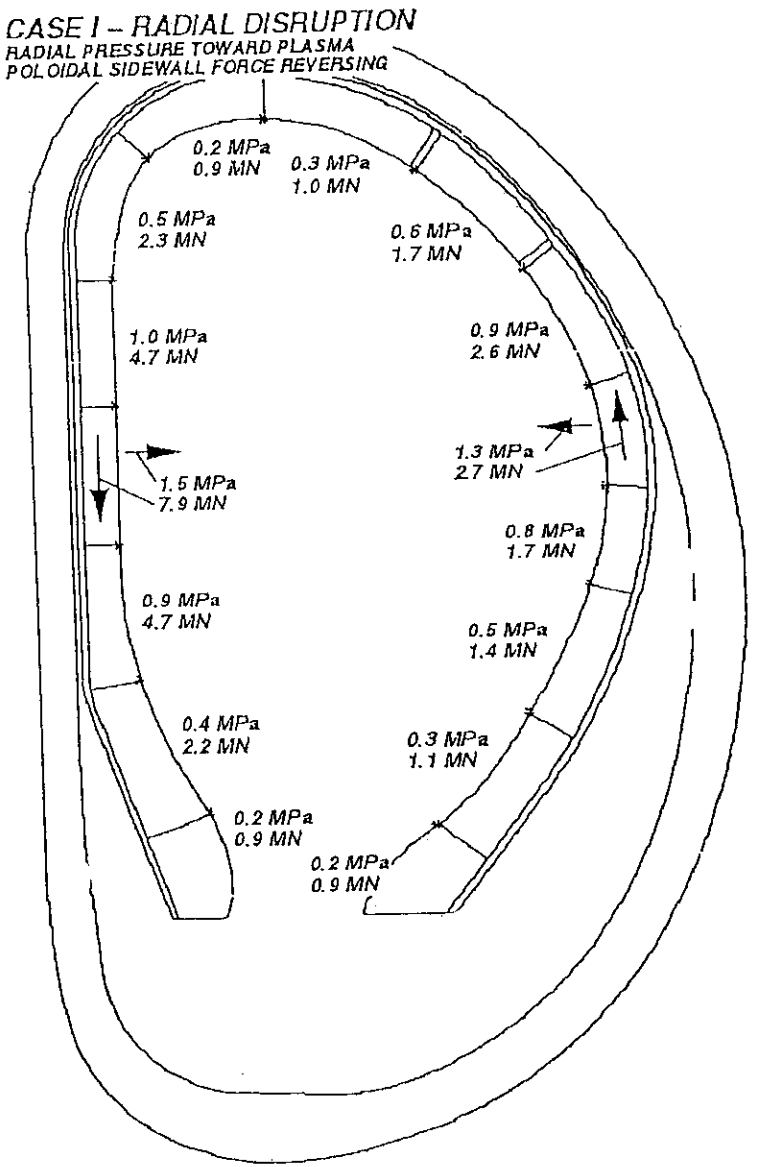

Fig. 3.2.1 – 6
Blanket System Disruption Loads (Radial Disruption)

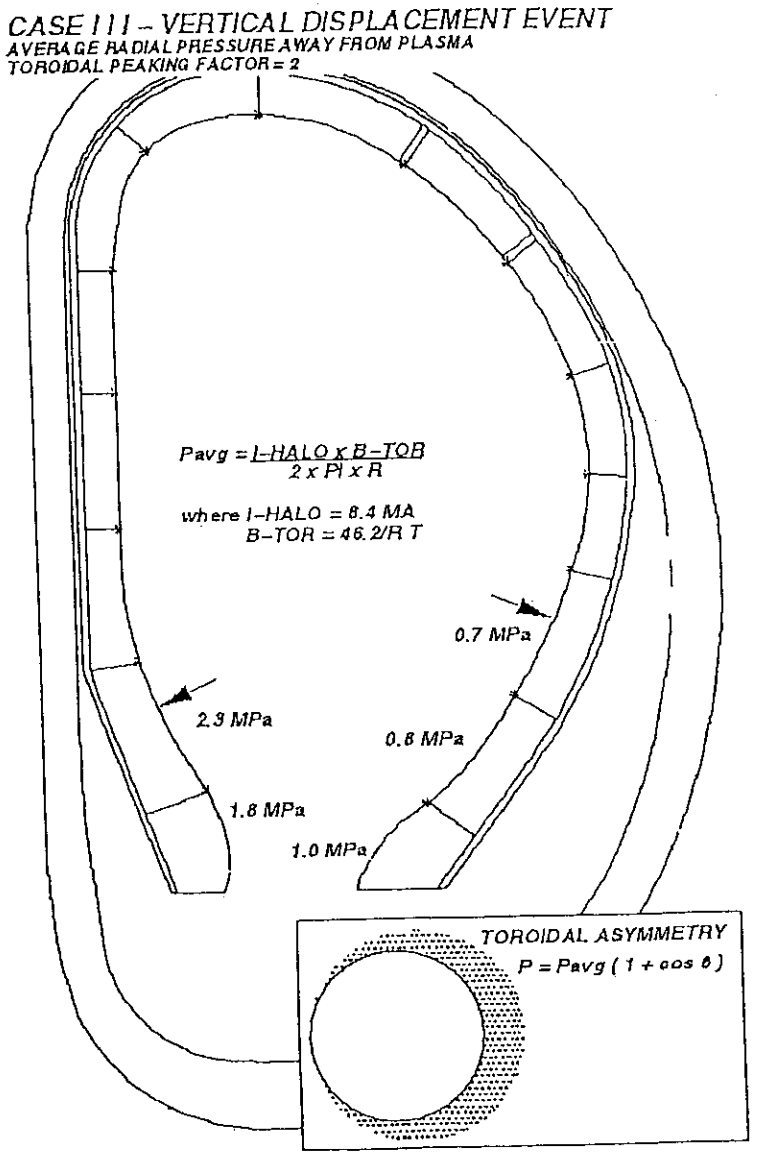

Fig. 3.2.1 – 7
Blanket System VDE Loads (Symmetric Load Component)

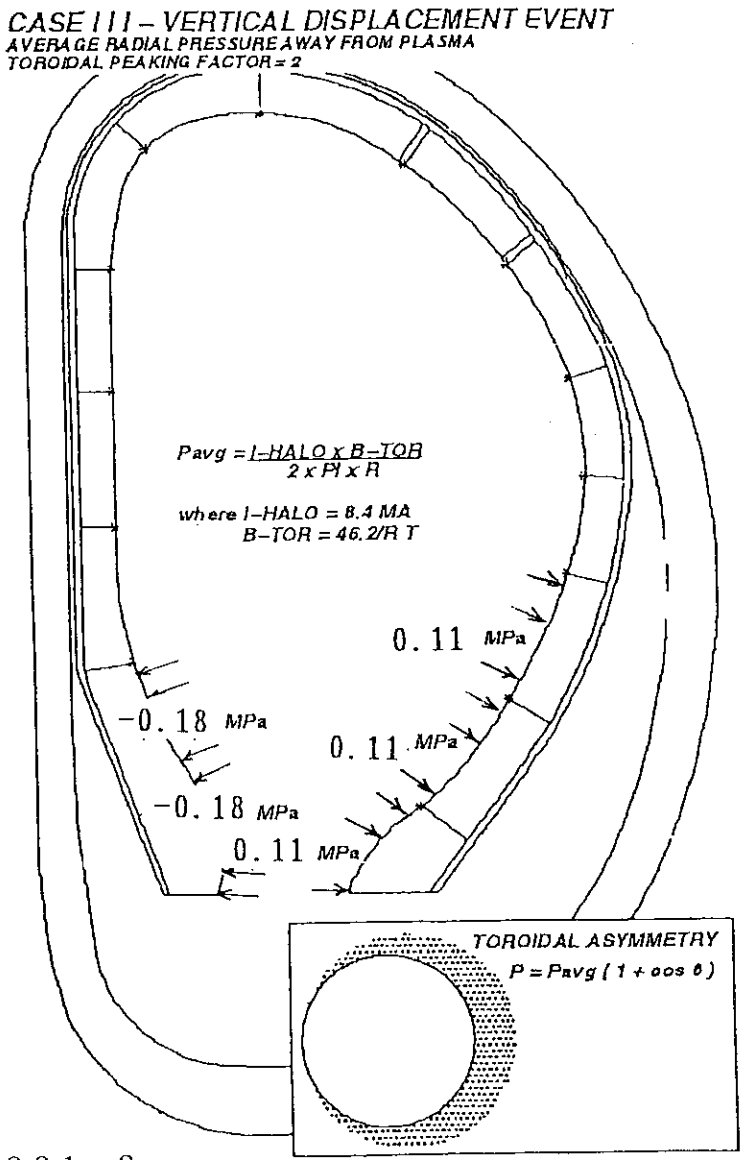

Fig. 3.2.1 – 8
Blanket System VDE Loads (Asymmetric Horizontal Component : Case1 – – – In – plane Force)

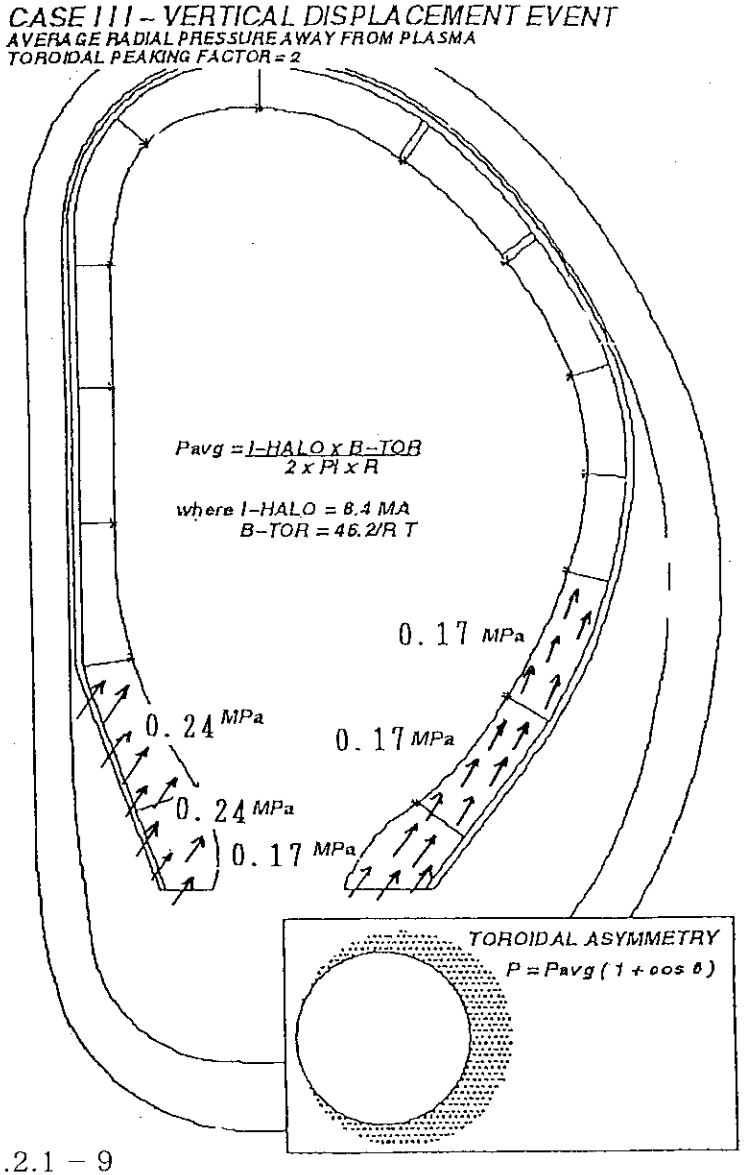

Fig. 3.2.1 – 9
Blanket System VDE Loads (Asymmetric Horizontal Component : Case2 – – – Out – of – plane Force)

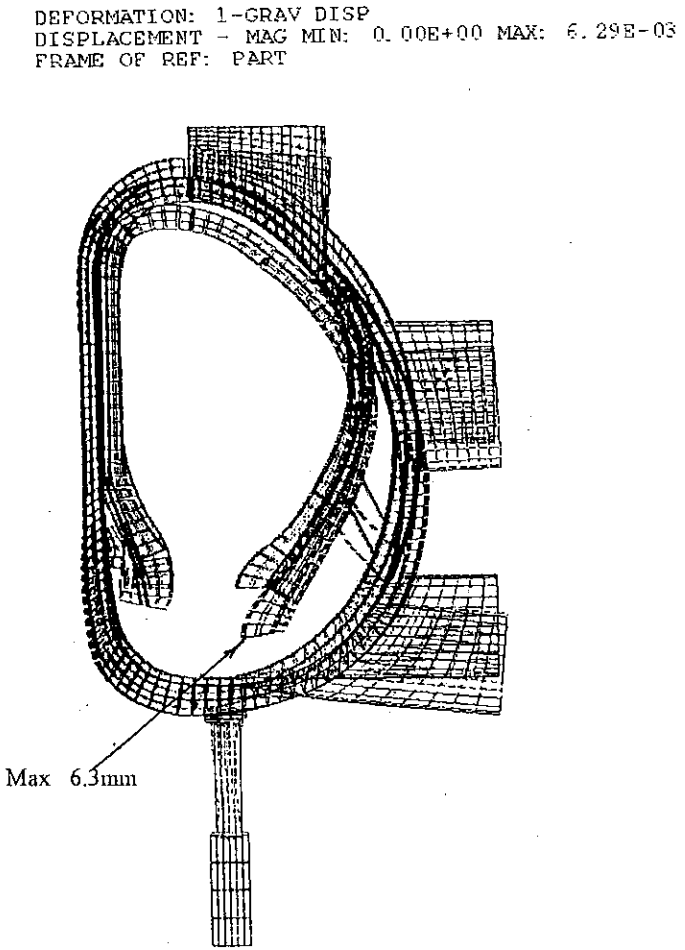

Fig. 3.2.1 – 10 Deformations of Vacuum Vessel and Blanket under their Dead Weight.

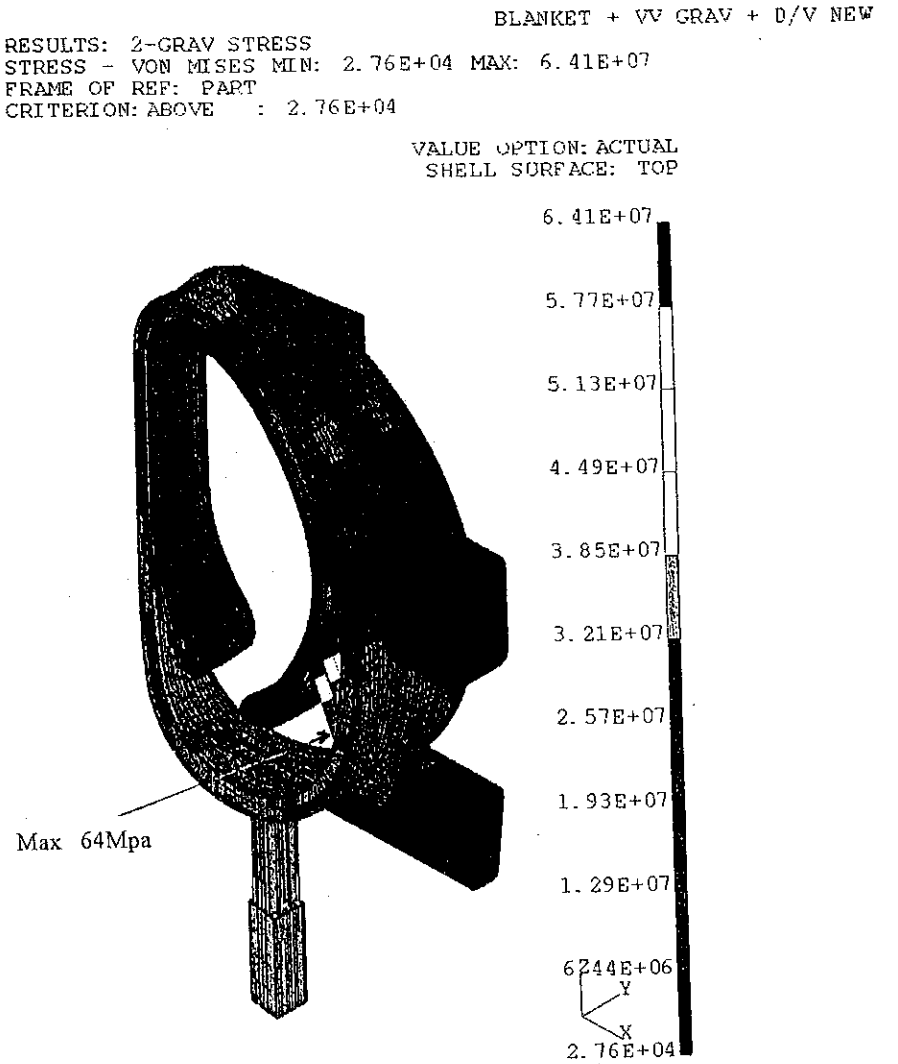

Fig. 3.2.1 – 11
Von Mises Stress Distribution on Vessel and Blanket under Dead Weights.

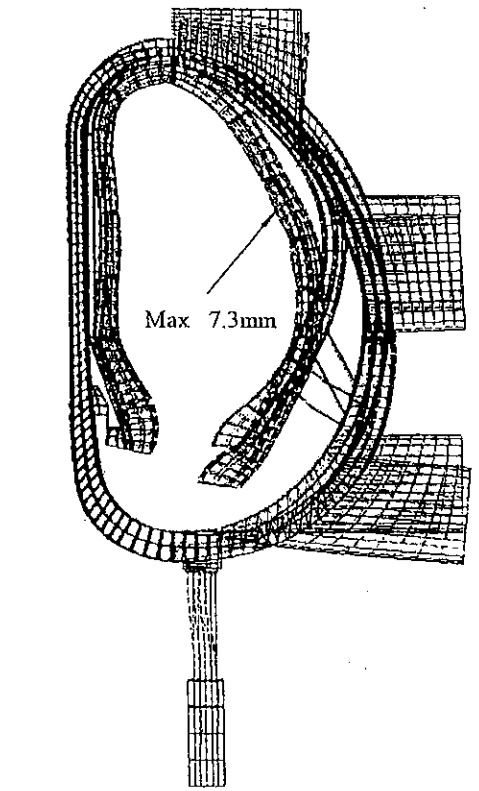

Fig. 3.2.1 – 12
Overall Deformation of Blanket and VV Support System under the Centered Disruption Load.

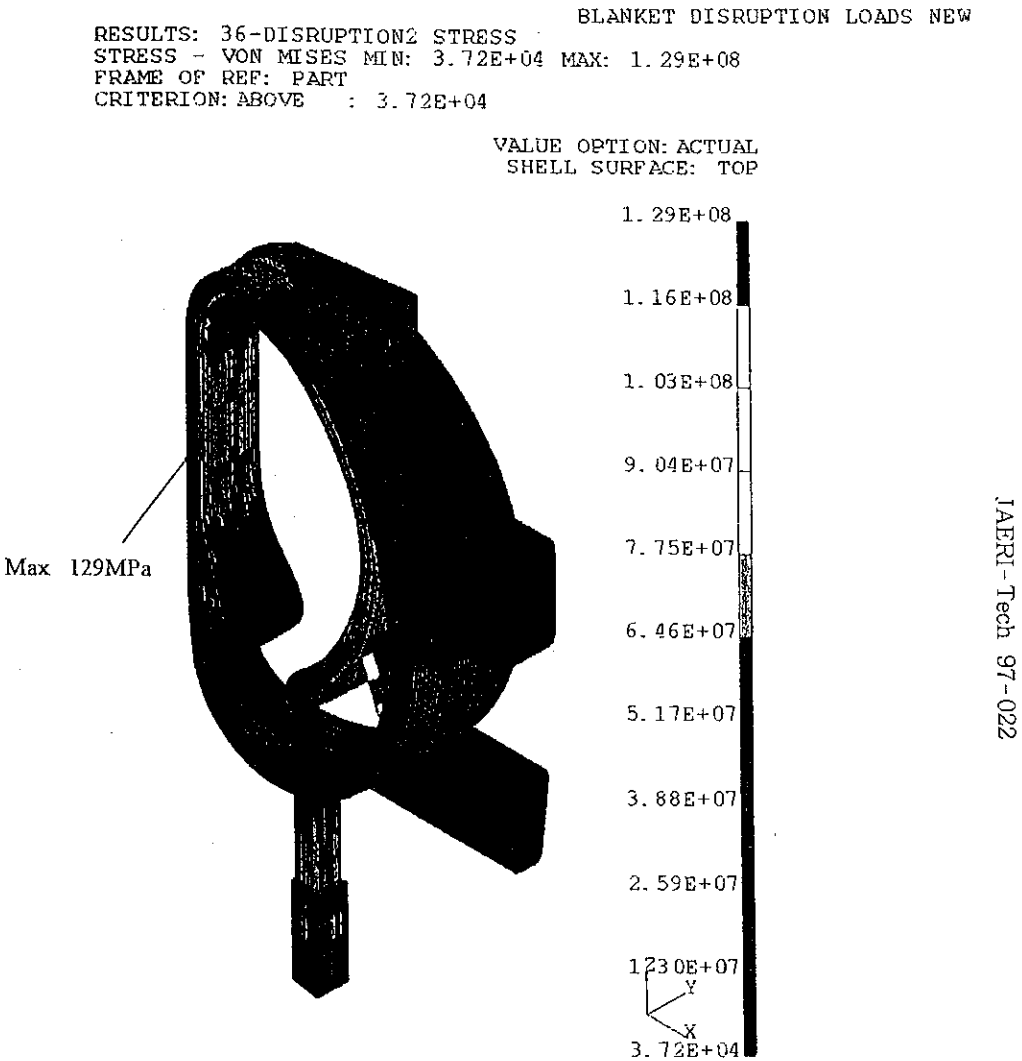

Fig. 3.2.1 – 13
Overall Von Mises Stress Distribution on Blanket and VV Support System under the Centered Disruption Load.

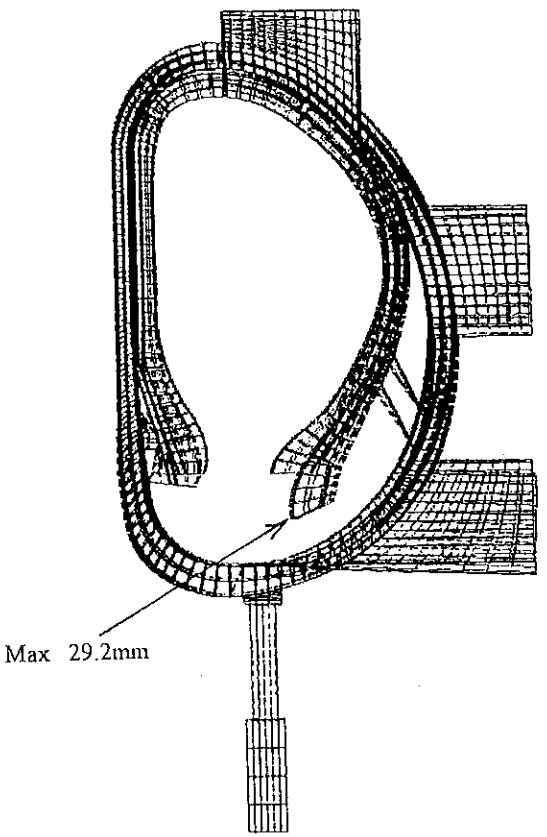

Fig. 3.2.1 - 14
Deformations of Vacuum Vessel and Blanket under VDE Disruption Loads (Symmetric Load Component).

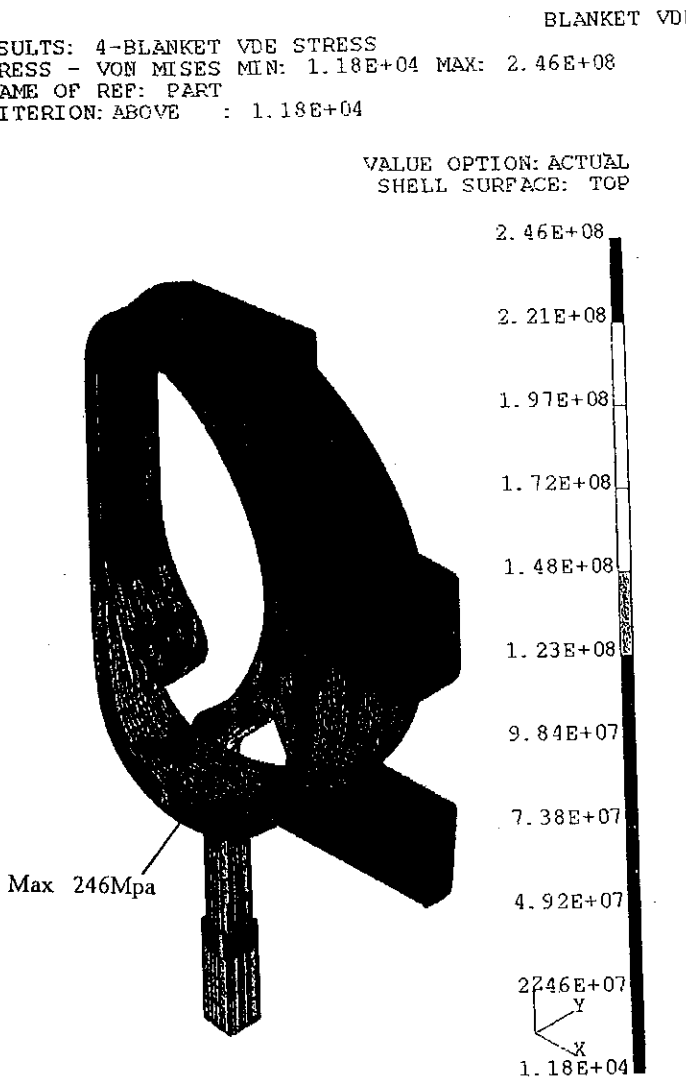

Fig. 3.2.1 - 15
Von Mises Stress Distribution on Vessel and Blanket under VDE Disruption Loads (Symmetric Load Component).

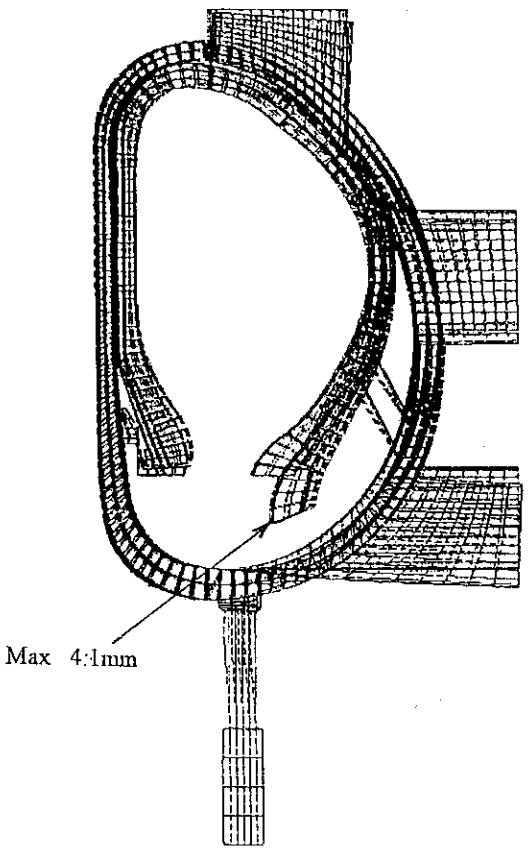

Fig. 3.2.1 – 16
Deformations of Vacuum Vessel and Blanket under VDE Disruption Loads (Asymmetric Horizontal Component : Case1 – – In – plane Force).

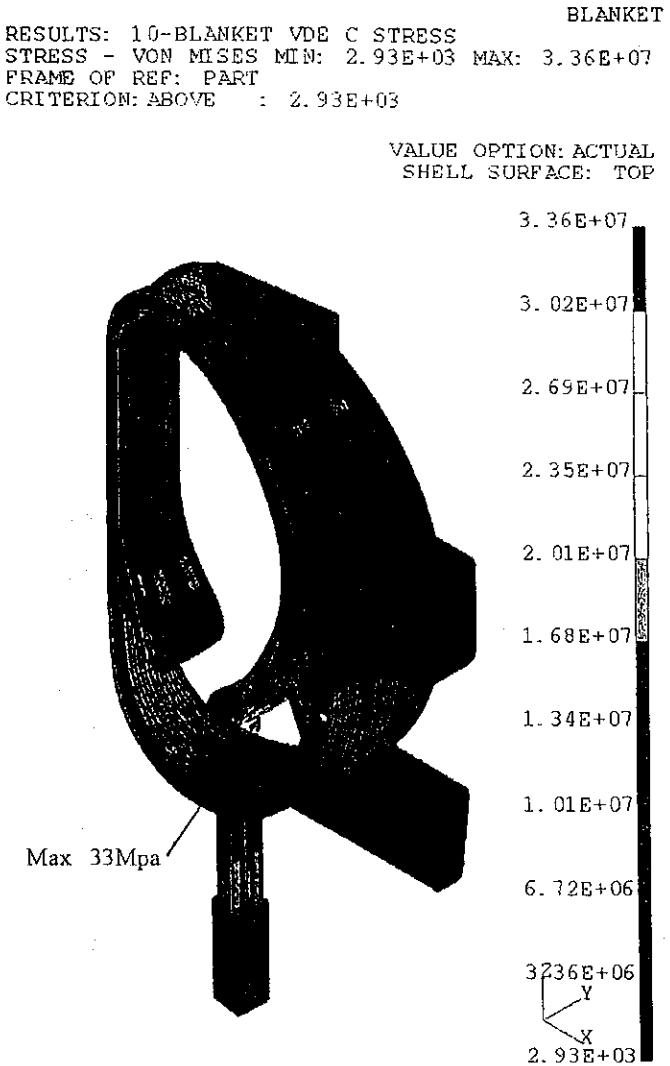

Fig. 3.2.1 – 17
Von Mises Stress Distribution on Vessel and Blanket under VDE Disruption Loads (Asymmetric Horizontal Component : Case1 – – In – plane Force).

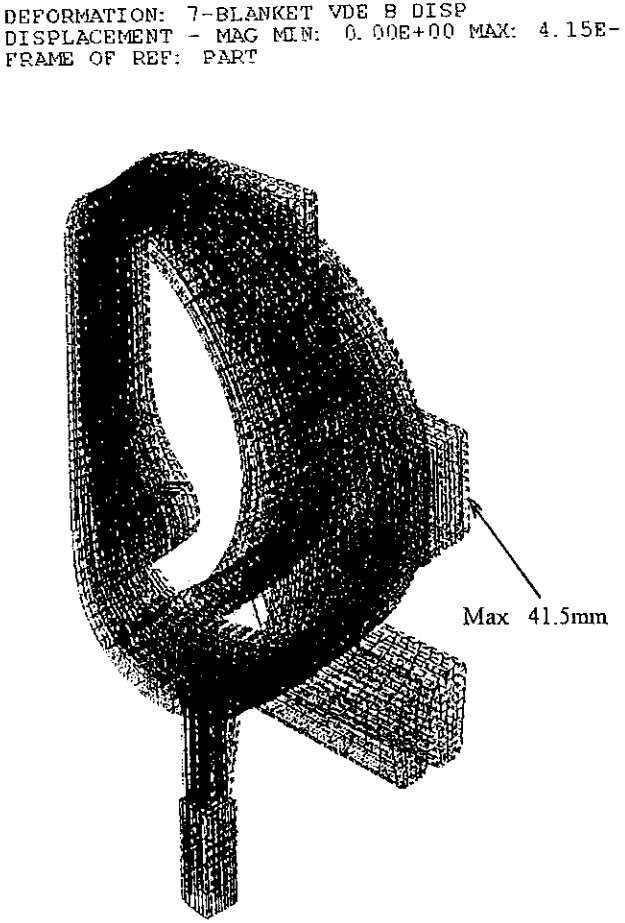

Fig. 3.2.1 - 18
Deformations of Vacuum Vessel and Blanket under VDE Disruption Loads (Asymmetric Horizontal Component : Case2 - - Out - of - plane Force).

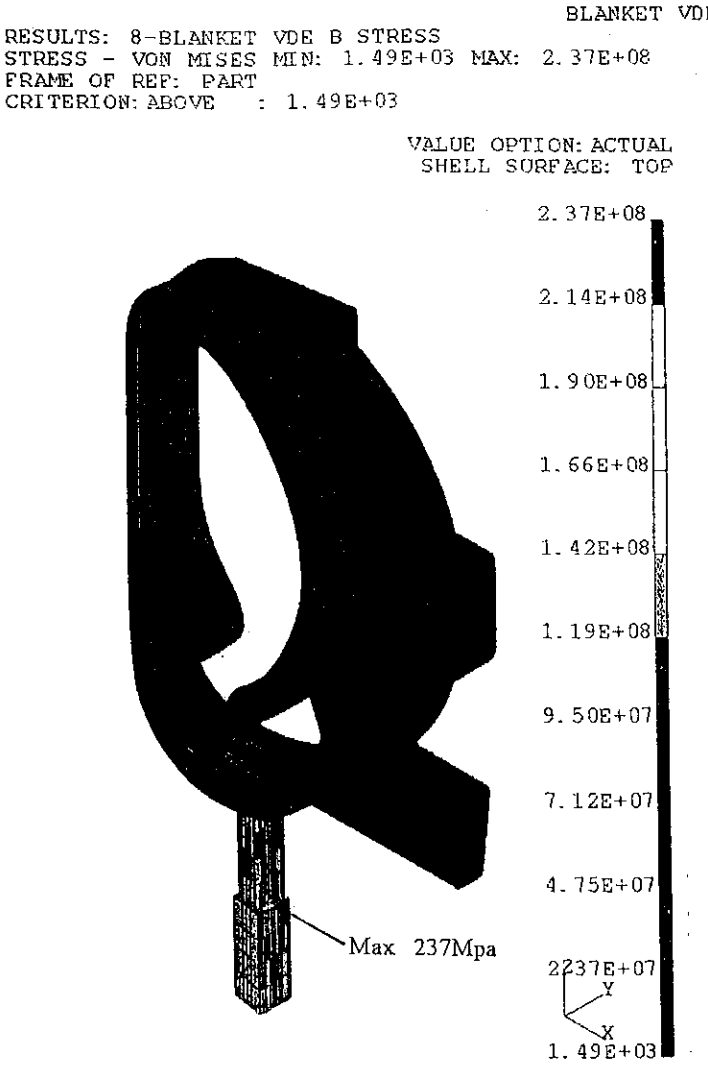

Fig. 3.2.1 - 19
Von Mises Stress Distribution on Vessel and Blanket under VDE Disruption Loads (Asymmetric Component : Case2 - - Out - of - plane Force).

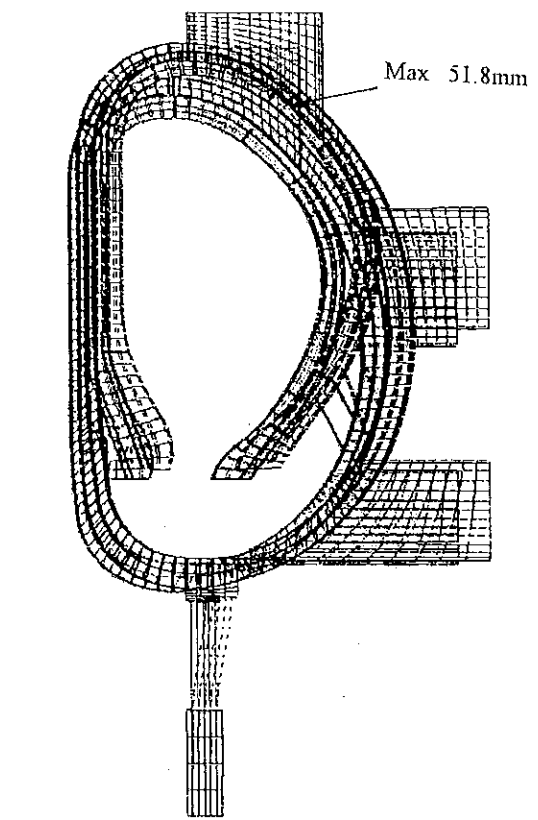

Fig. 3.2.1 – 20
Deformations of Vacuum Vessel and Blanket under Thermal Loads.(Vessel and Blanket Temperatures are set to be 150℃ and 250℃)

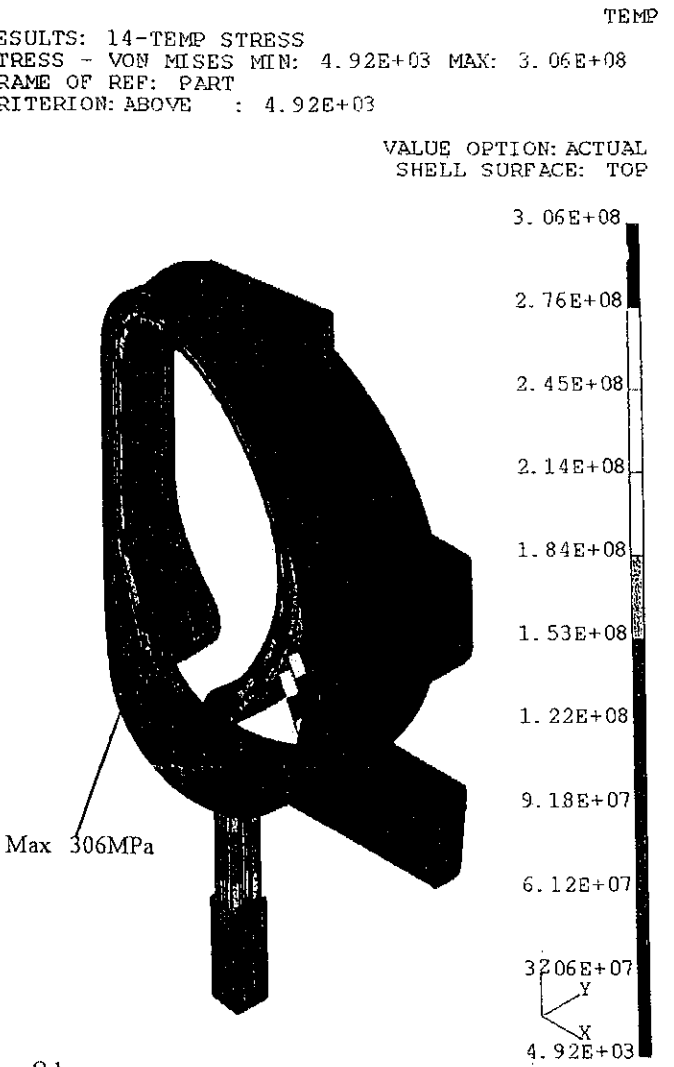

Fig. 3.2.1 – 21
Von Mises Stress Distribution on Vessel and Blanket under Thermal Loads.(Vessel and Blanket Temperatures are set to be 150℃ and 250℃)

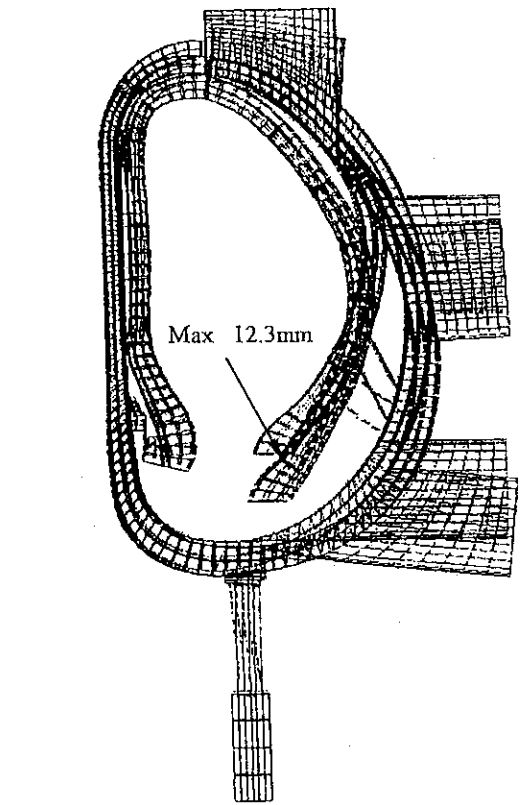

Fig. 3.2.1 – 22
Overall Deformation of Blanket Support System and VV under Weight Load + Centered Disruption Load (Case – 1).

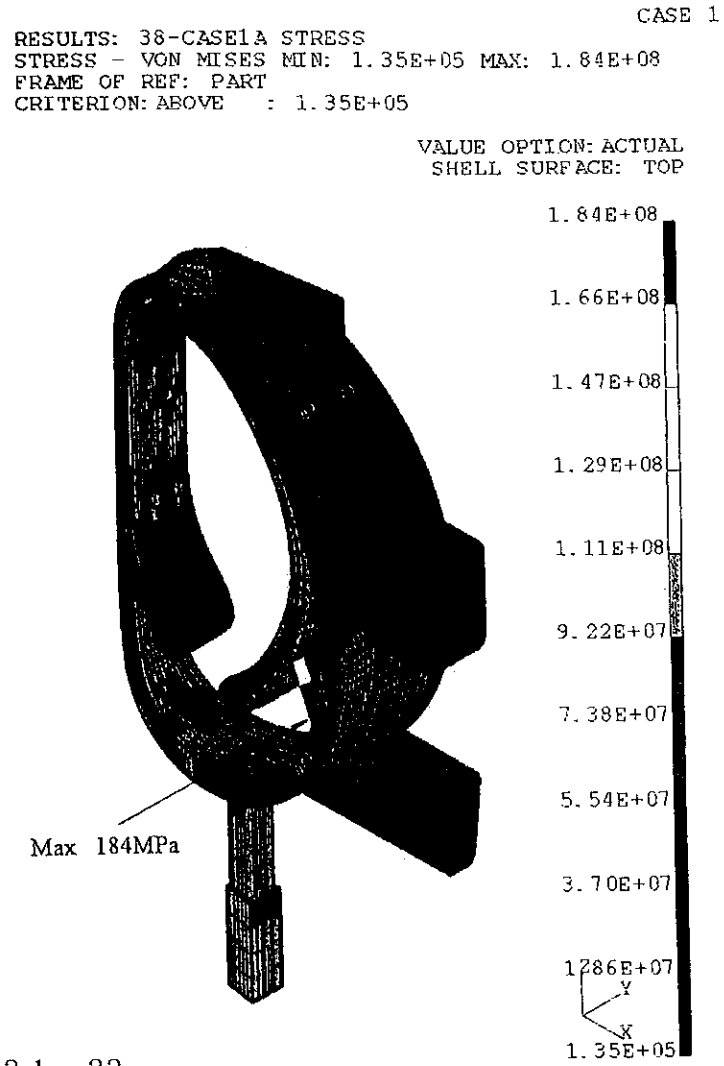

Fig. 3.2.1 – 23
Von Mises Stress Distribution on Blanket Support System and VV under Weight Load + Centered Disruption Load (Case – 1).

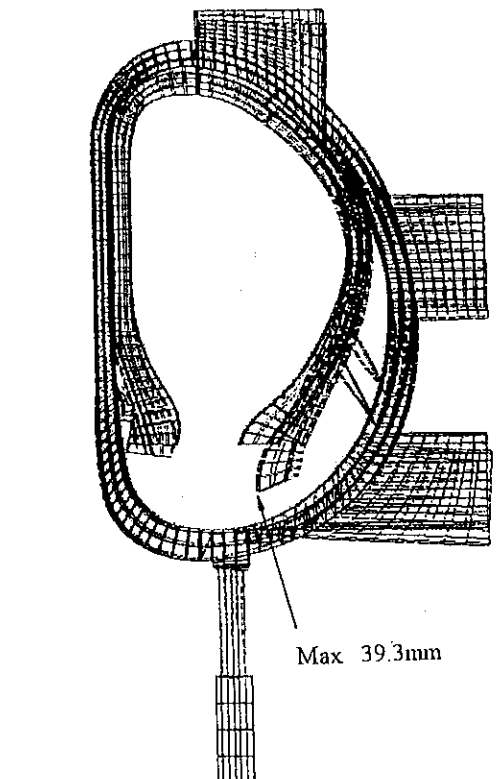

Fig. 3.2.1 - 24
Overall Deformation of Blanket Support System and VV under Weight Load + VDE Disruption (Symmetric Load)
+ VDE Disruption (Asymmetric Load ; In - plane) (Case - 2).

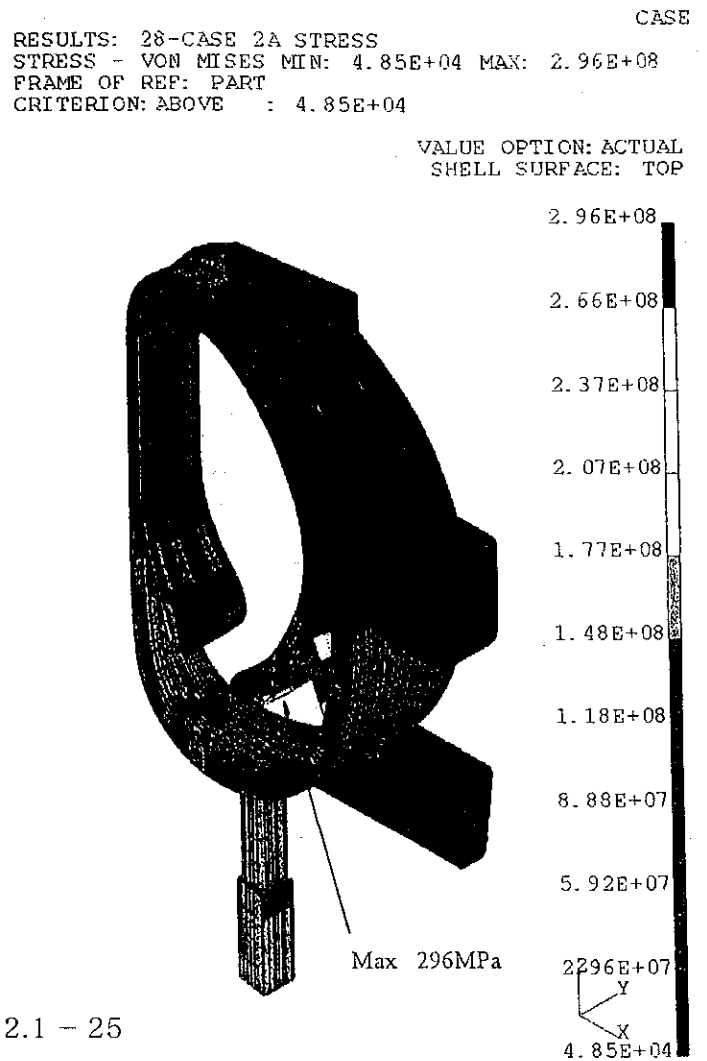

Fig. 3.2.1 - 25
Von Mises Stress Distribution on Blanket Support System and VV under Weight Load + VDE Disruption (Symmetric Load)
+ VDE Disruption (Asymmetric Load ; In - plane) (Case - 2).

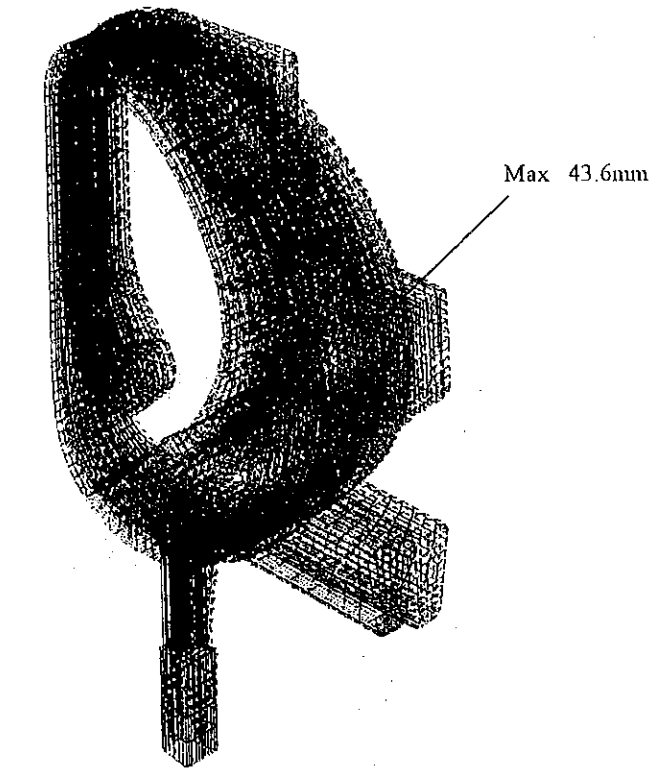

Fig. 3.2.1 – 26
Overall Deformation of Blanket Support System and VV under Weight Load + VDE Disruption (Symmetric Load)
+ VDE Disruption (Asymmetric Load ; Out – of – plane) (Case – 3)

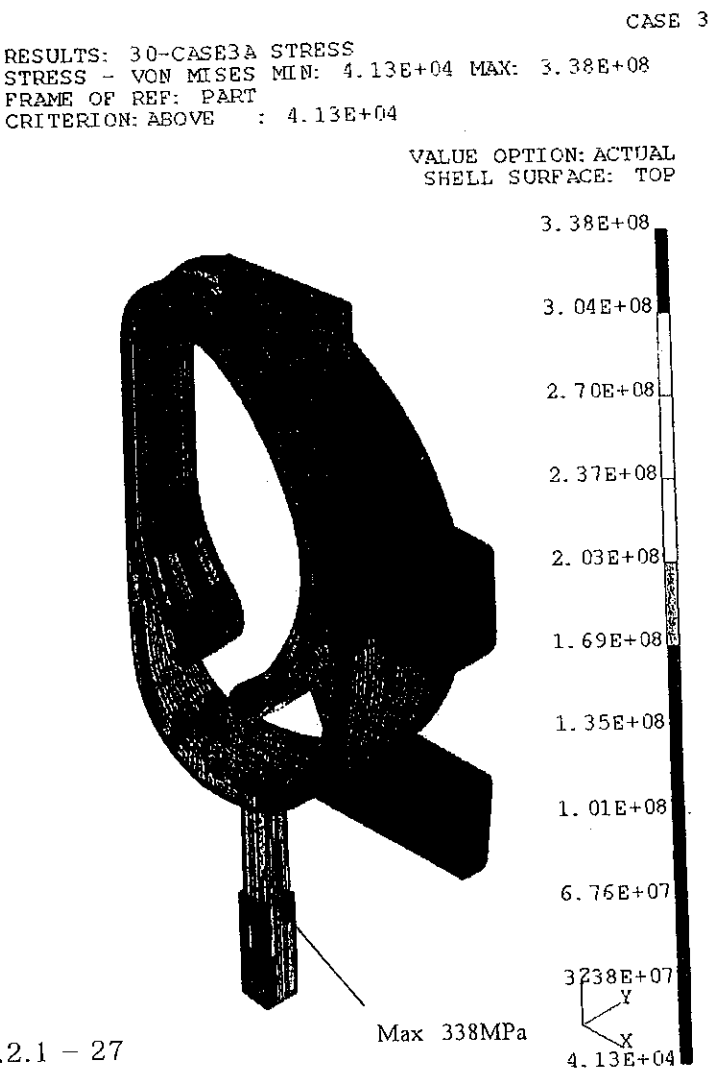

Fig. 3.2.1 – 27
Von Mises Stress Distribution on Blanket Support System and VV under Weight Load + VDE Disruption (Symmetric Load)
+ VDE Disruption (Asymmetric Load ; Out – of – plane) (Case – 3).

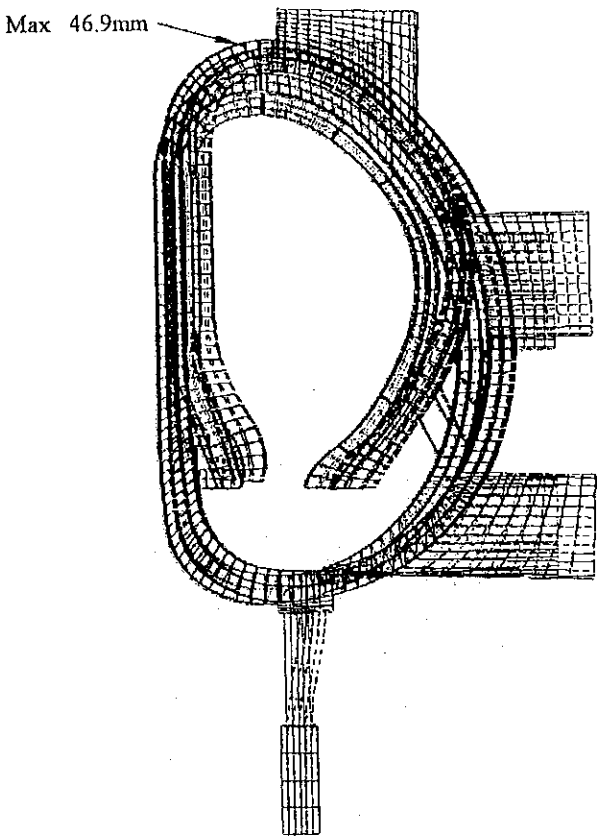

Fig. 3.2.1 – 28
Overall Deformation of Blanket Support System and VV under Weight Load + Centered Disruption Load + Thermal Load (Case – 4).

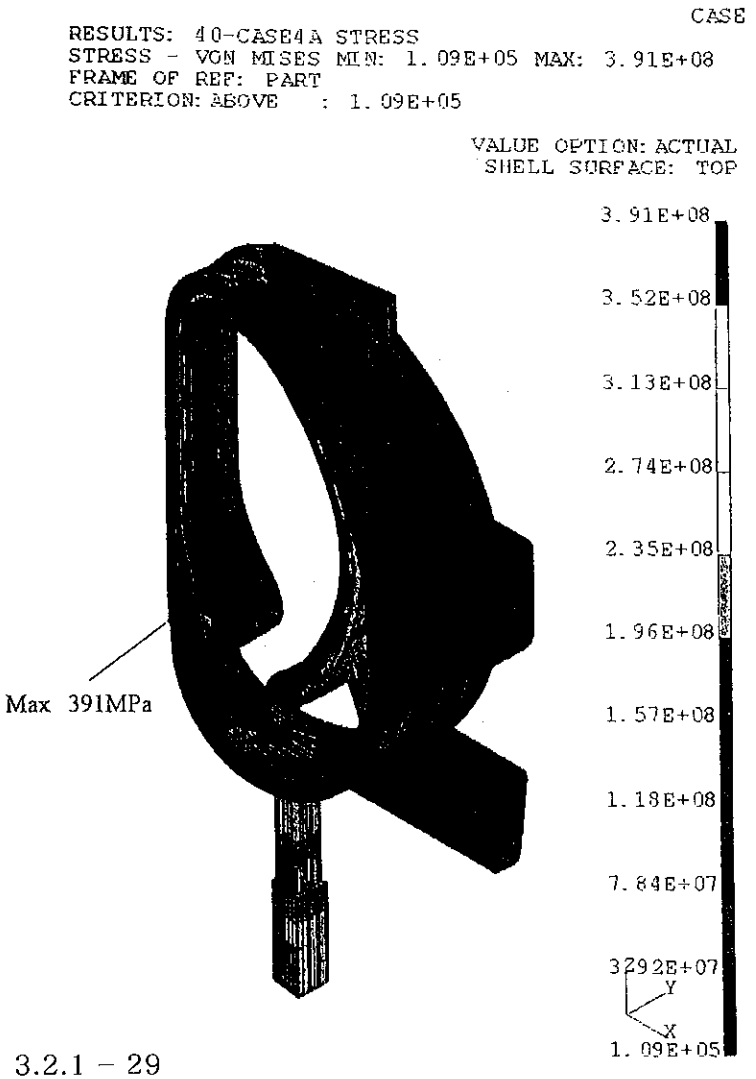

Fig. 3.2.1 – 29
Von Mises Stress Distribution on Blanket Support System and VV under Weight Load + Centered Disruption Load + Thermal Load (Case – 4).

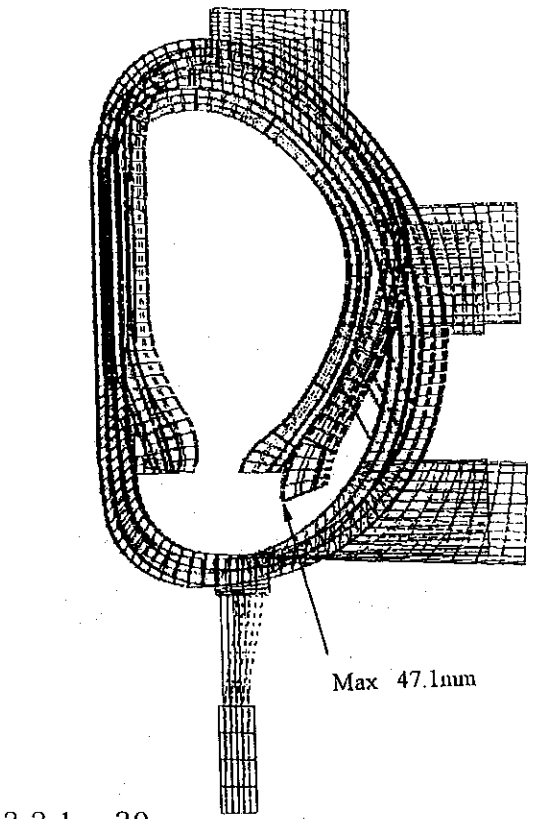

Fig. 3.2.1 – 30
Overall Deformation of Blanket Support System and VV under Weight Load + VDE Disruption (Symmetric Load)
+ VDE Disruption (Asymmetric Load ; In – plane)
+ Thermal Load (Case – 5).

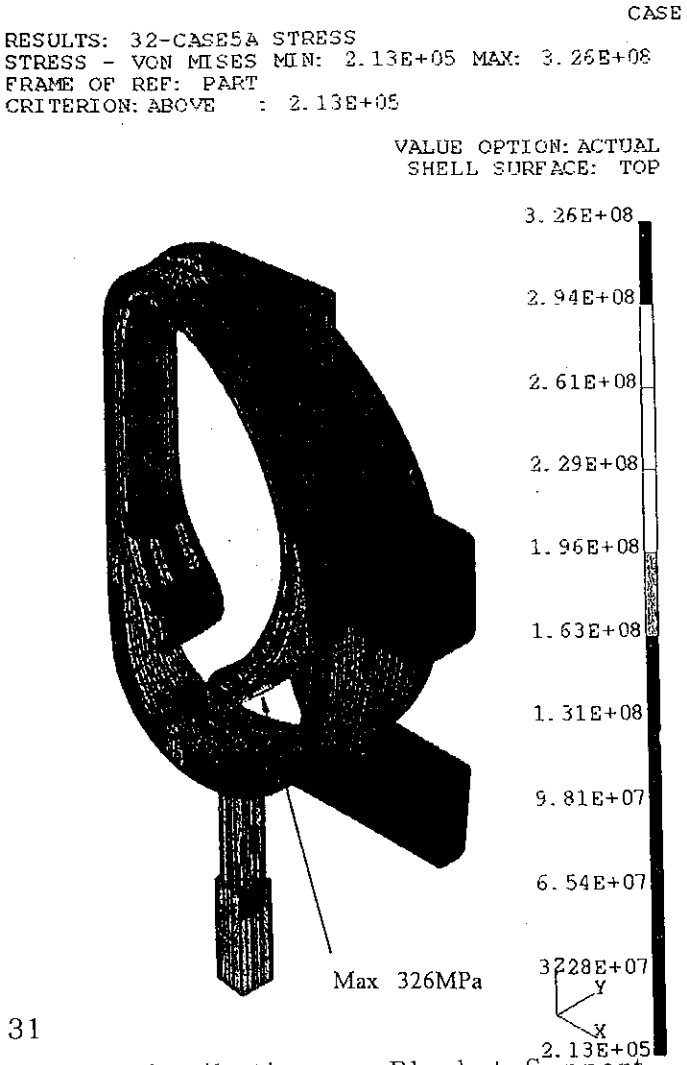

Fig. 3.2.1 – 31
Von Mises Stress Distribution on Blanket Support System and VV under Weight Load + VDE Disruption (Symmetric Load)
+ VDE Disruption (Asymmetric Load ; In – plane)
+ Thermal Load (Case – 5).

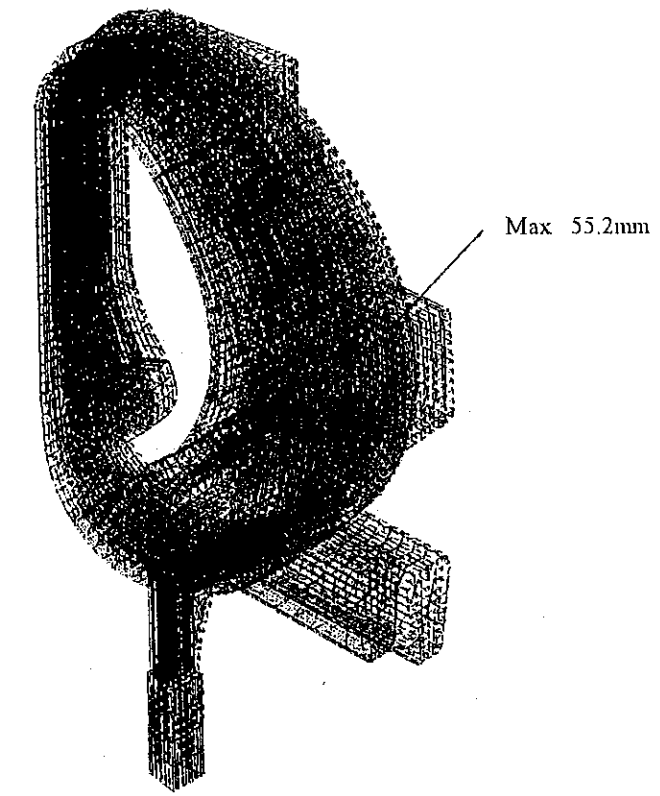

Fig. 3.2.1 – 32
Overall Deformation of Blanket Support System and VV under Weight Load + VDE Disruption (Symmetric Load)
+ VDE Disruption (Asymmetric Load ; Out – of – plane)
+ Thermal Load (Case – 6).

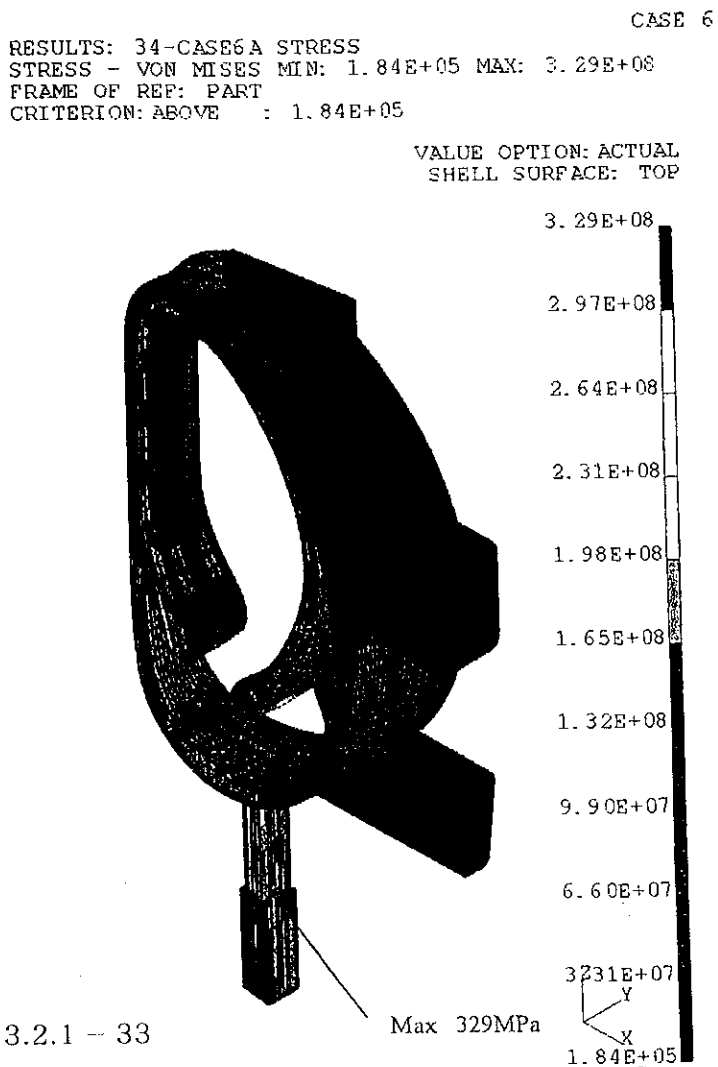

Fig. 3.2.1 – 33
Von Mises Stress Distribution on Blanket Support System and VV under Weight Load + VDE Disruption (Symmetric Load)
+ VDE Disruption (Asymmetric Load ; Out – of – plane)
+ Thermal Load (Case – 6).

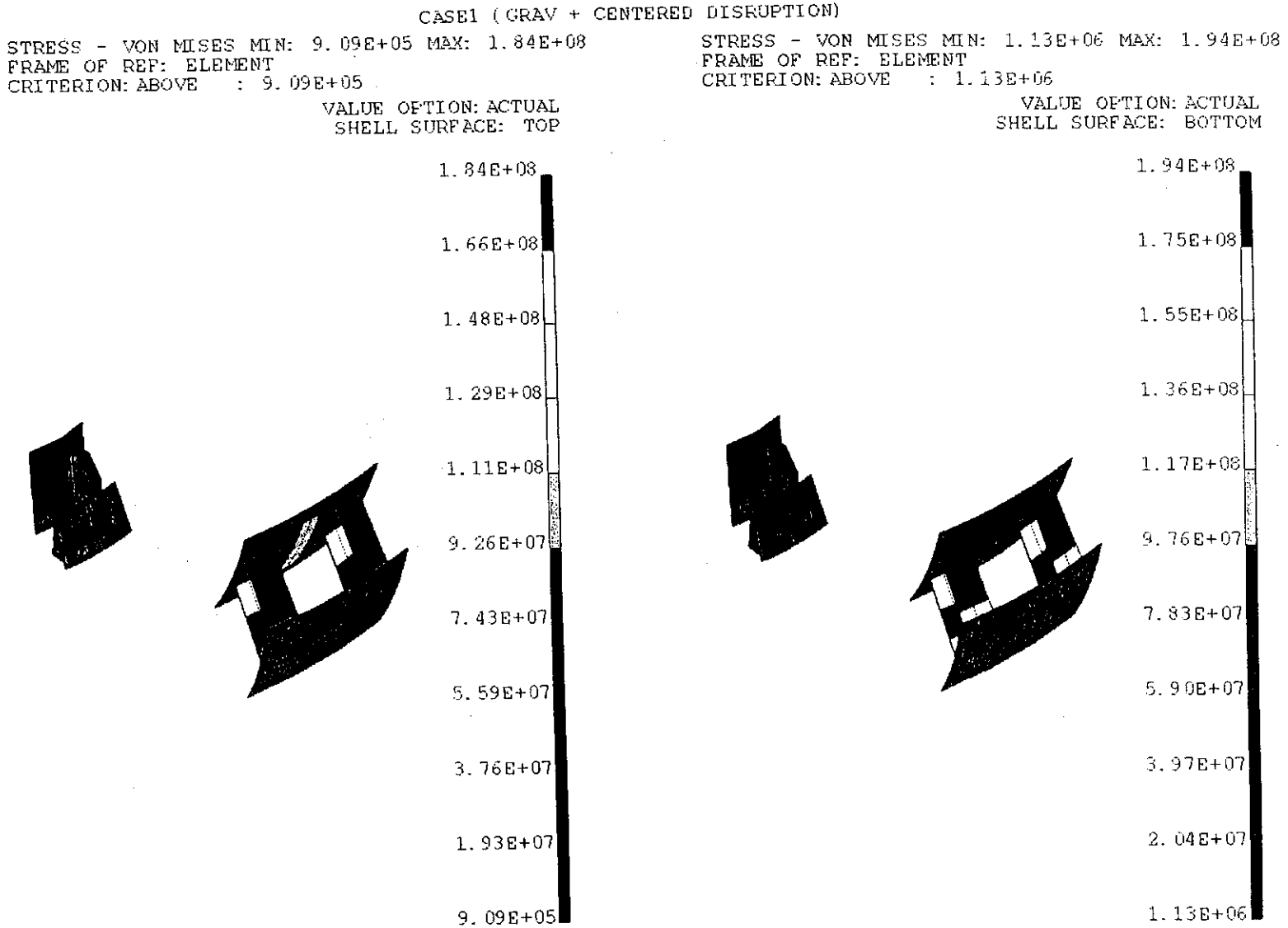

Fig. 3.2.1 – 34 Von Mises Stress Distribution on Blanket Support Structures under Weight Load + Centered Disruption Load (Case – 1).

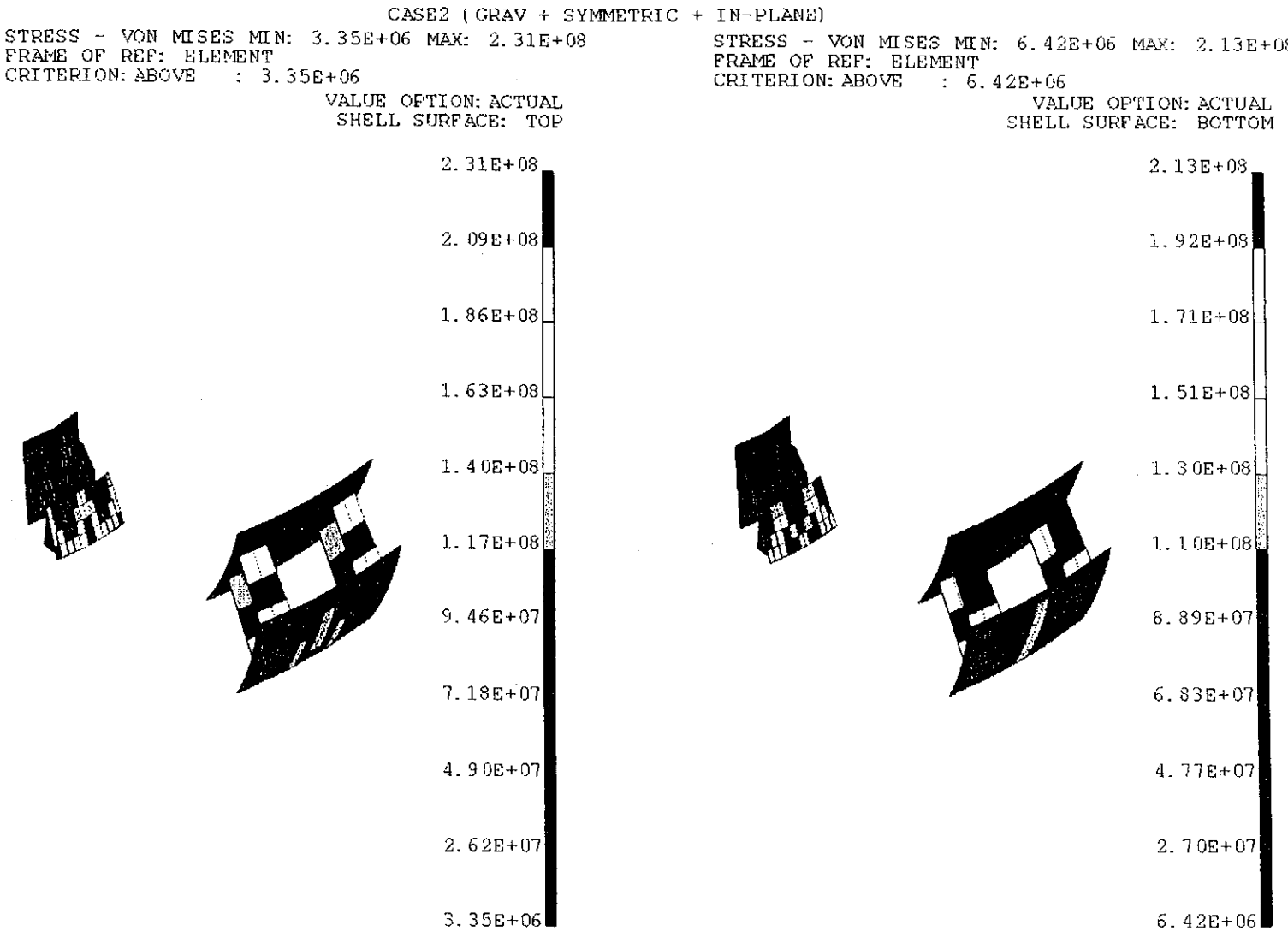

Fig. 3.2.1 – 35 Von Mises Stress Distribution on Blanket Support Structures under Weight Load + VDE Disruption (Symmetric Load) + VDE Disruption (Asymmetric Load ; In – plane) (Case – 2).

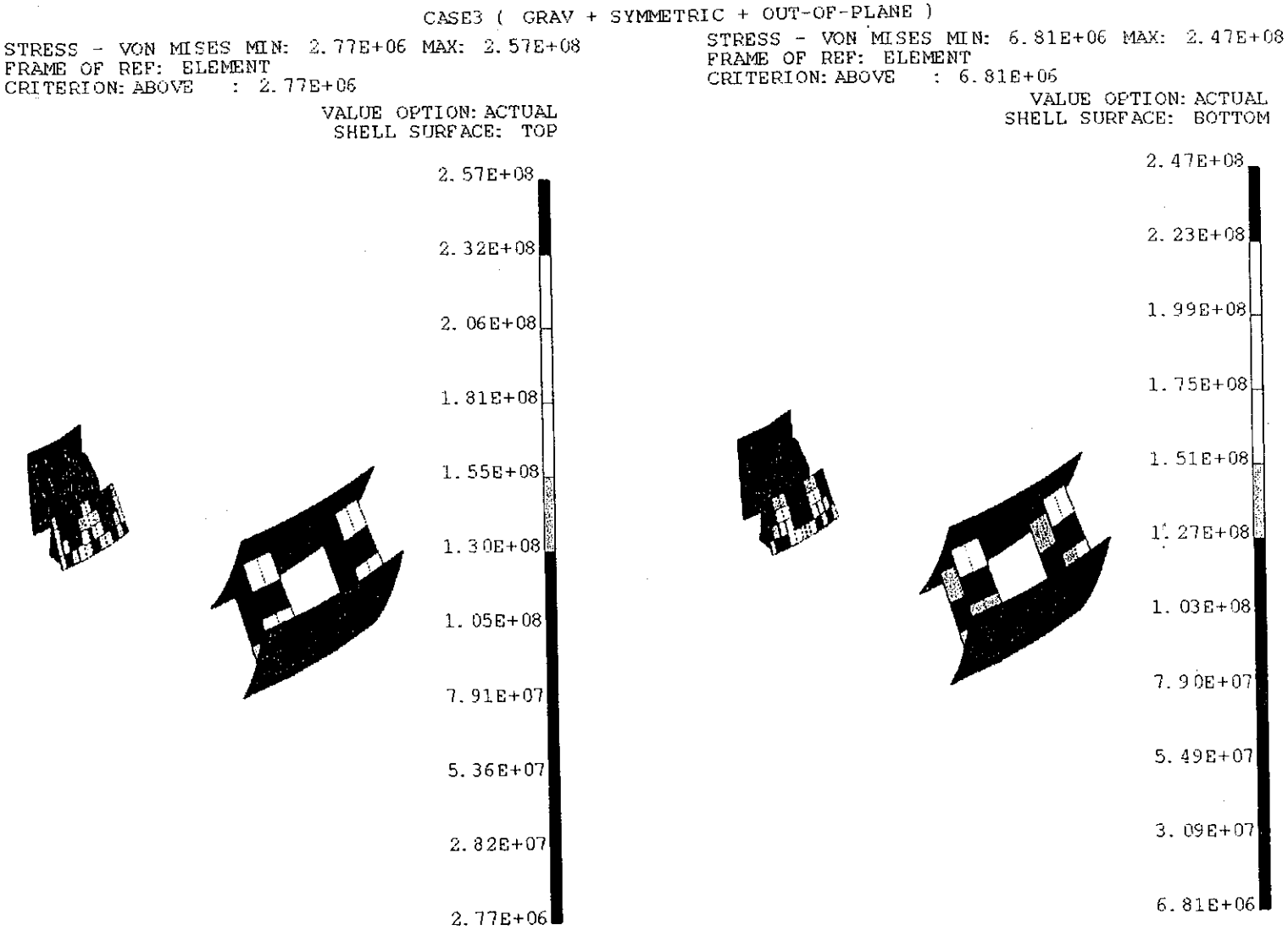

Fig. 3.2.1 – 36 Von Mises Stress Distribution on Blanket Support Structures under Weight Load + VDE Disruption (Symmetric Load) + VDE Disruption (Asymmetric Load ; Out – of – plane) (Case – 3).

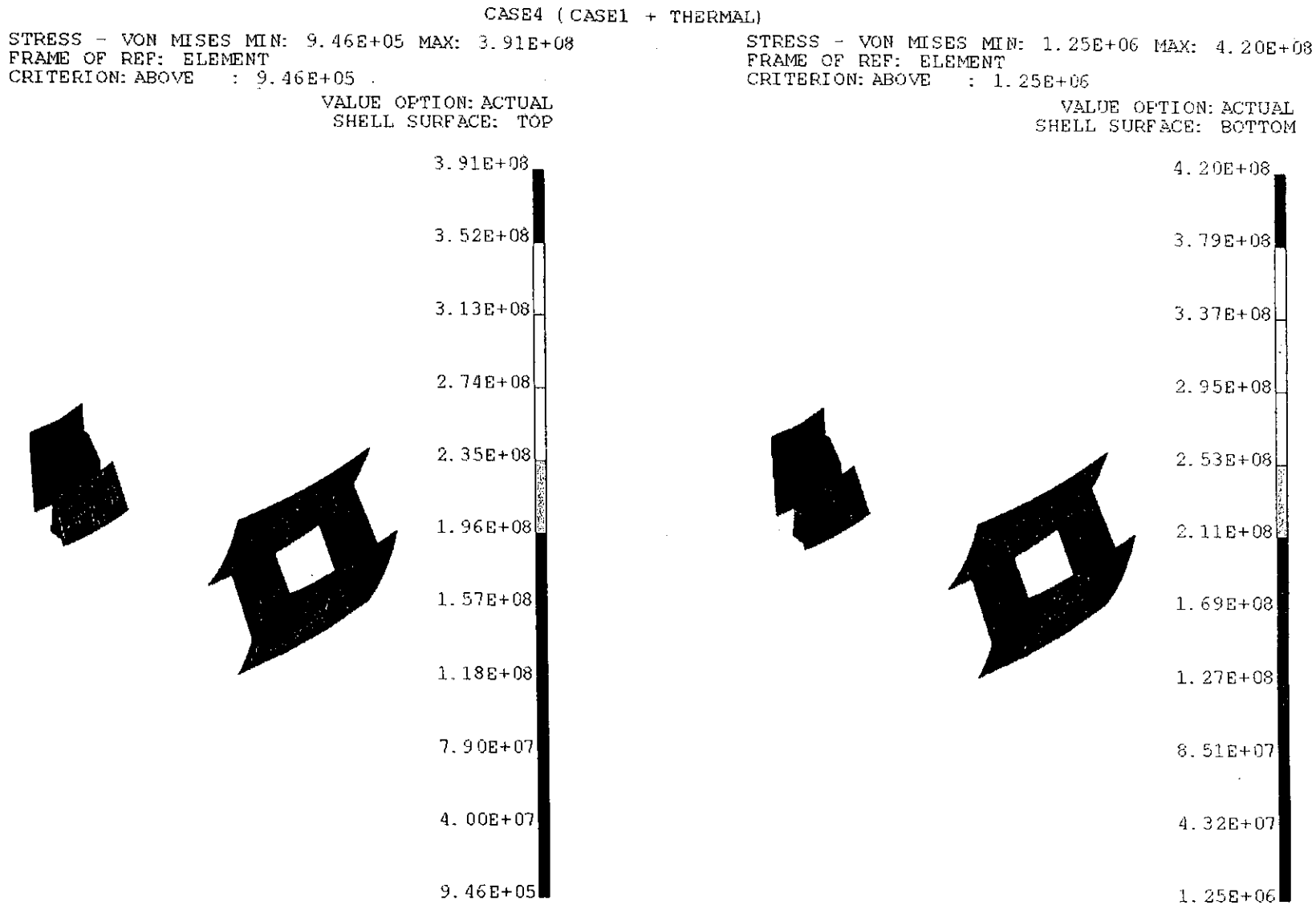

Fig. 3.2.1 – 37 Von Mises Stress Distribution on Blanket Support Structures under Weight Load + Centered Disruption Load + Thermal Load (Case – 4).

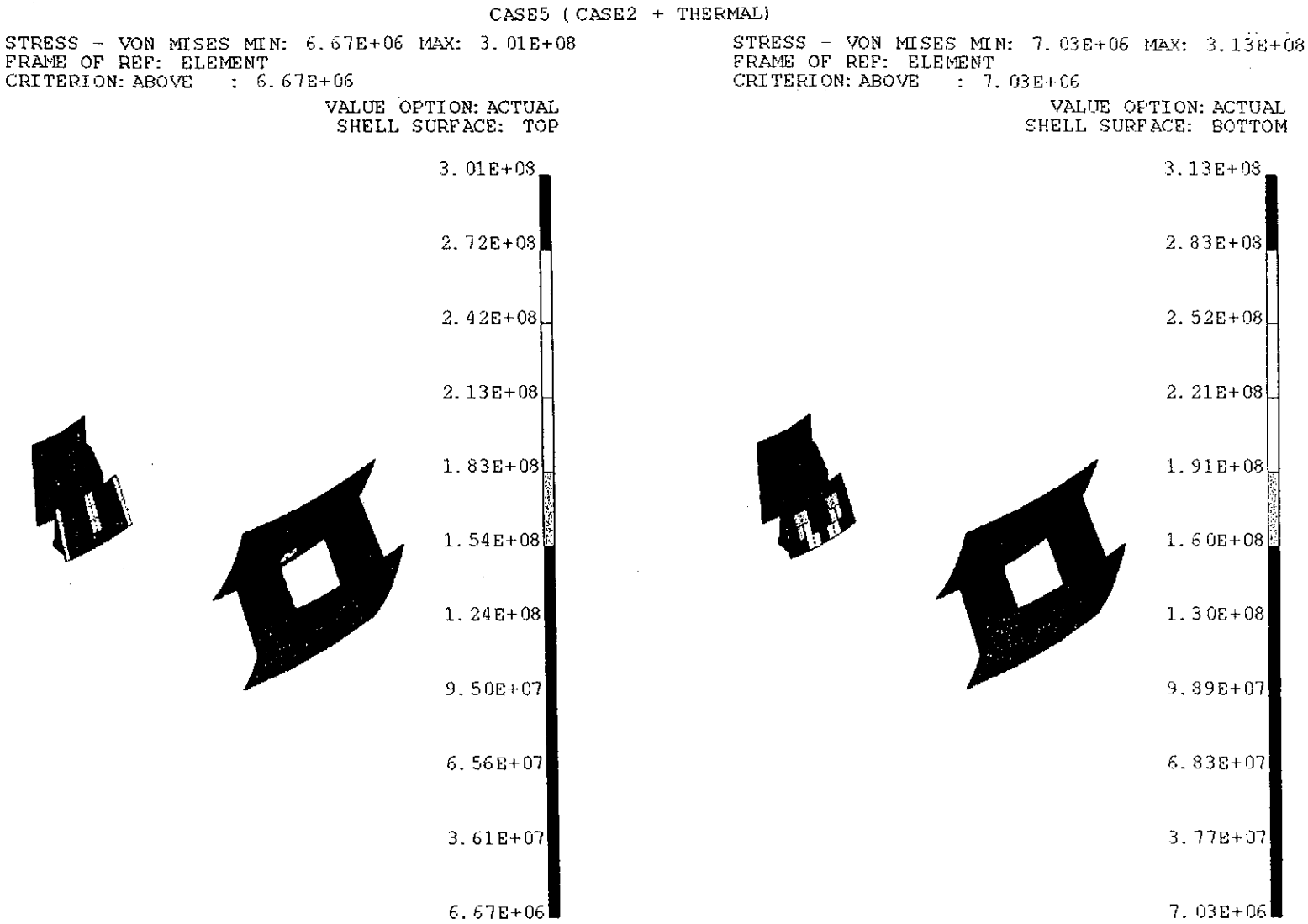

Fig. 3.2.1 - 38 Von Mises Stress Distribution on Blanket Support Structures under Weight Load + VDE Disruption (Symmetric Load) + VDE Disruption (Asymmetric Load ; In - plane) + Thermal Load (Case - 5).

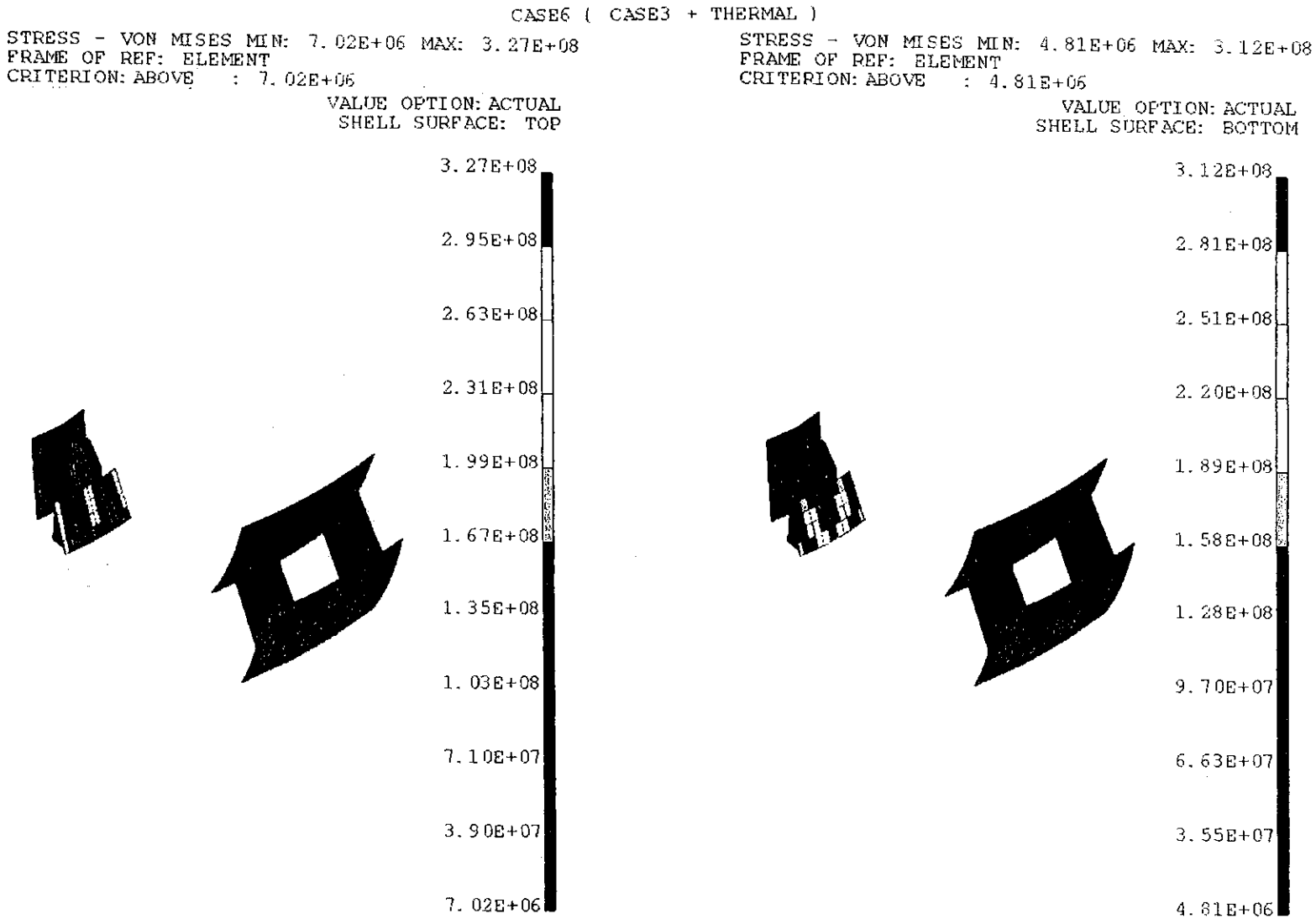

Fig. 3.2.1 – 39 Von Mises Stress Distribution on Blanket Support Structures under Weight Load + VDE Disruption (Symmetric Load) + VDE Disruption (Asymmetric Load ; Out – of – plane) + Thermal Load (Case – 6).

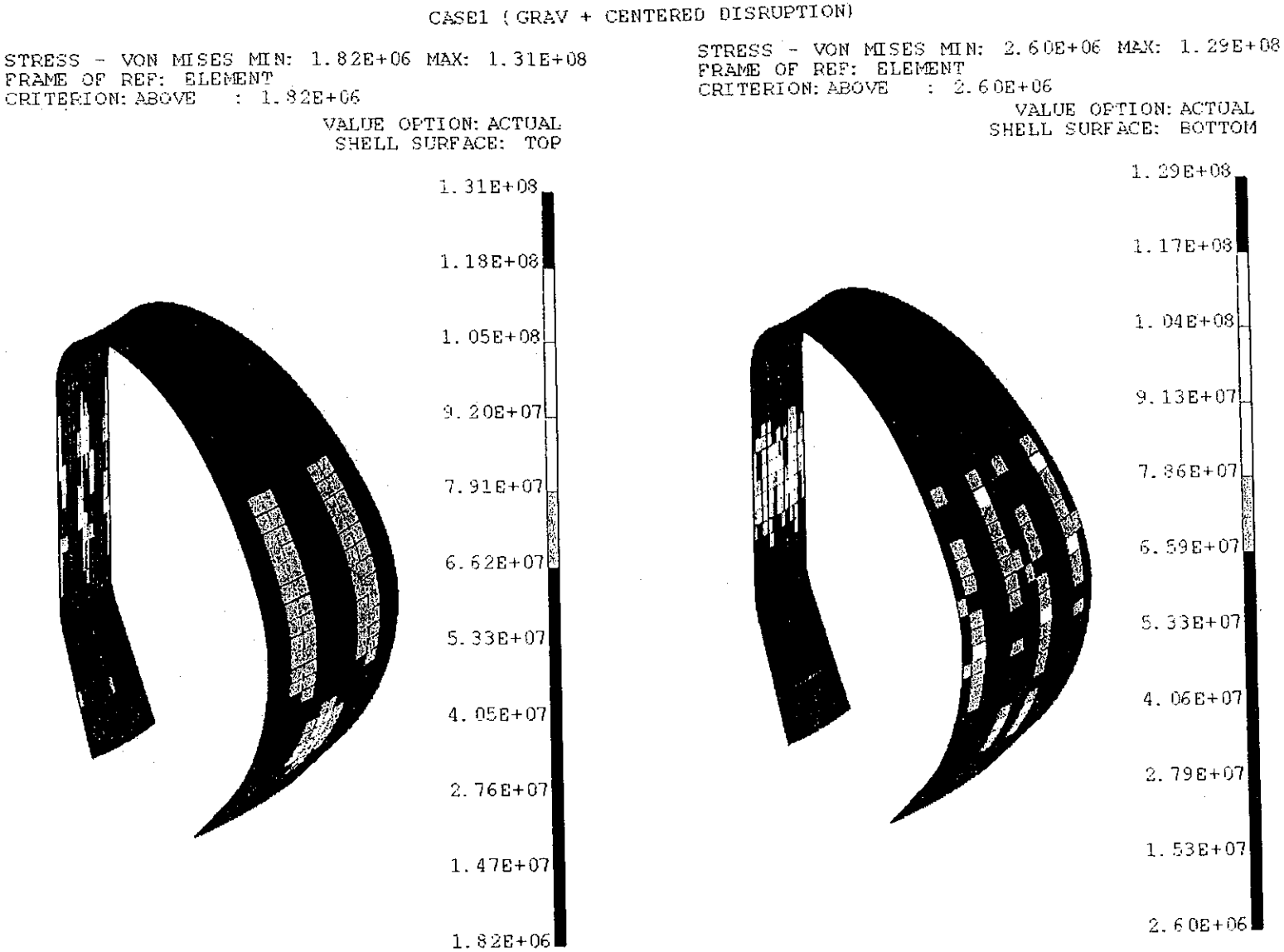

Fig. 3.2.1 – 40 Von Mises Stress Distribution on Back Plate under Weight Load + Centered Disruption Load (Case – 1).

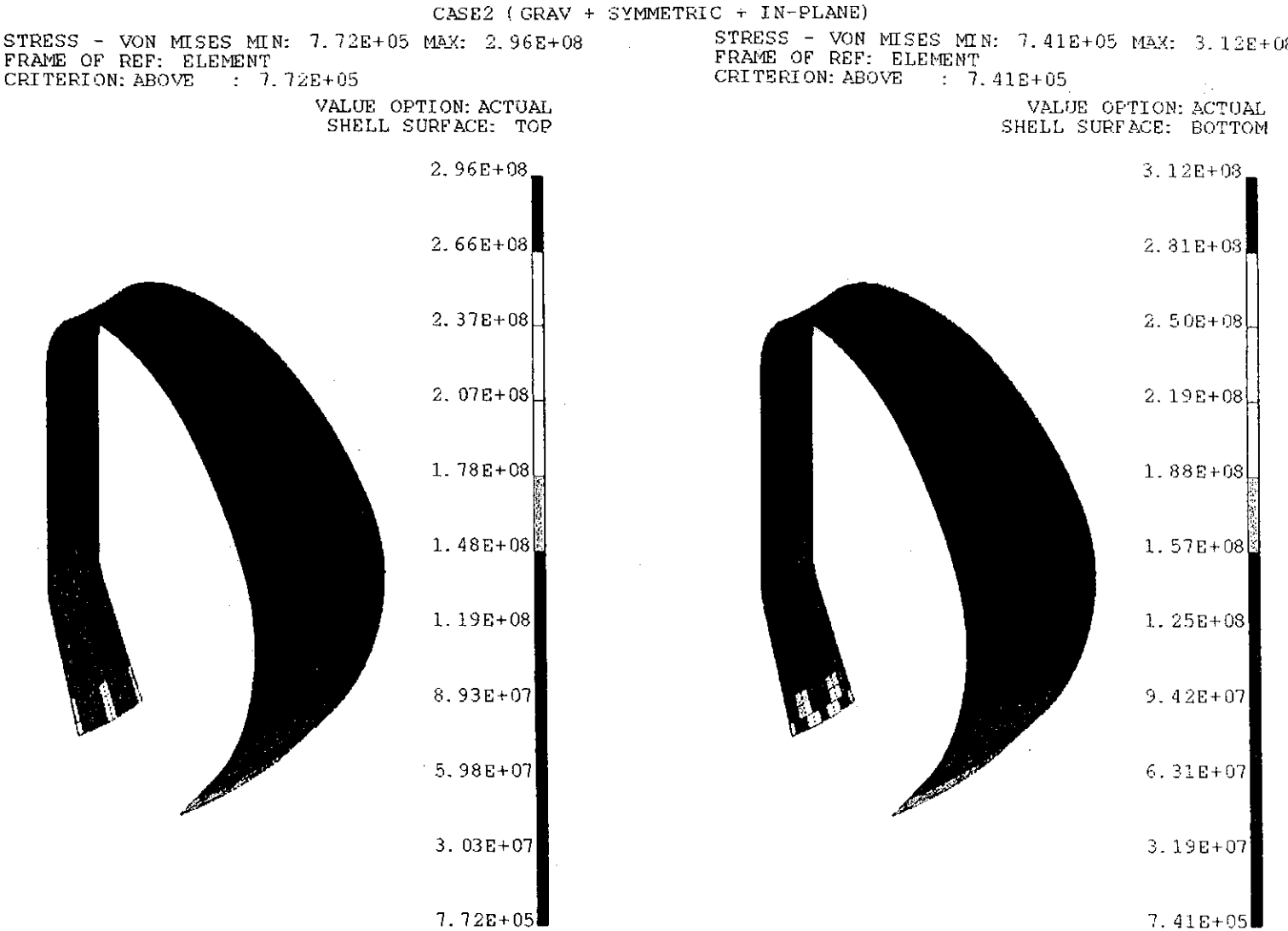

Fig. 3.2.1 – 41 Von Mises Stress Distribution on Back Plate under Weight Load + VDE Disruption (Symmetric Load) + VDE Disruption (Asymmetric Load ; In – plane) (Case – 2).

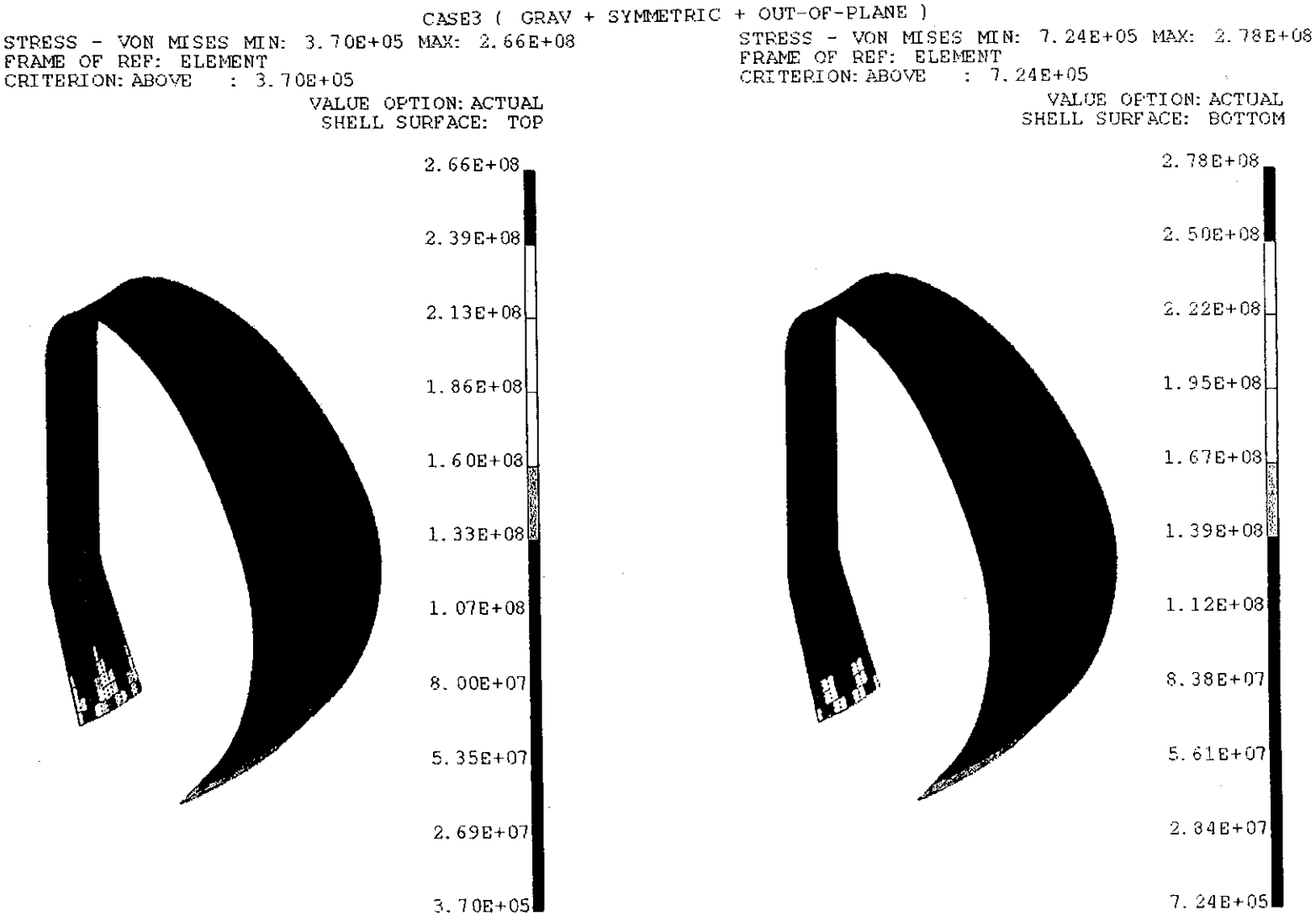

Fig. 3.2.1 – 42 Von Mises Stress Distribution on Back Plate under Weight Load + VDE Disruption (Symmetric Load) + VDE Disruption (Asymmetric Load ; Out – of – plane) (Case – 3).

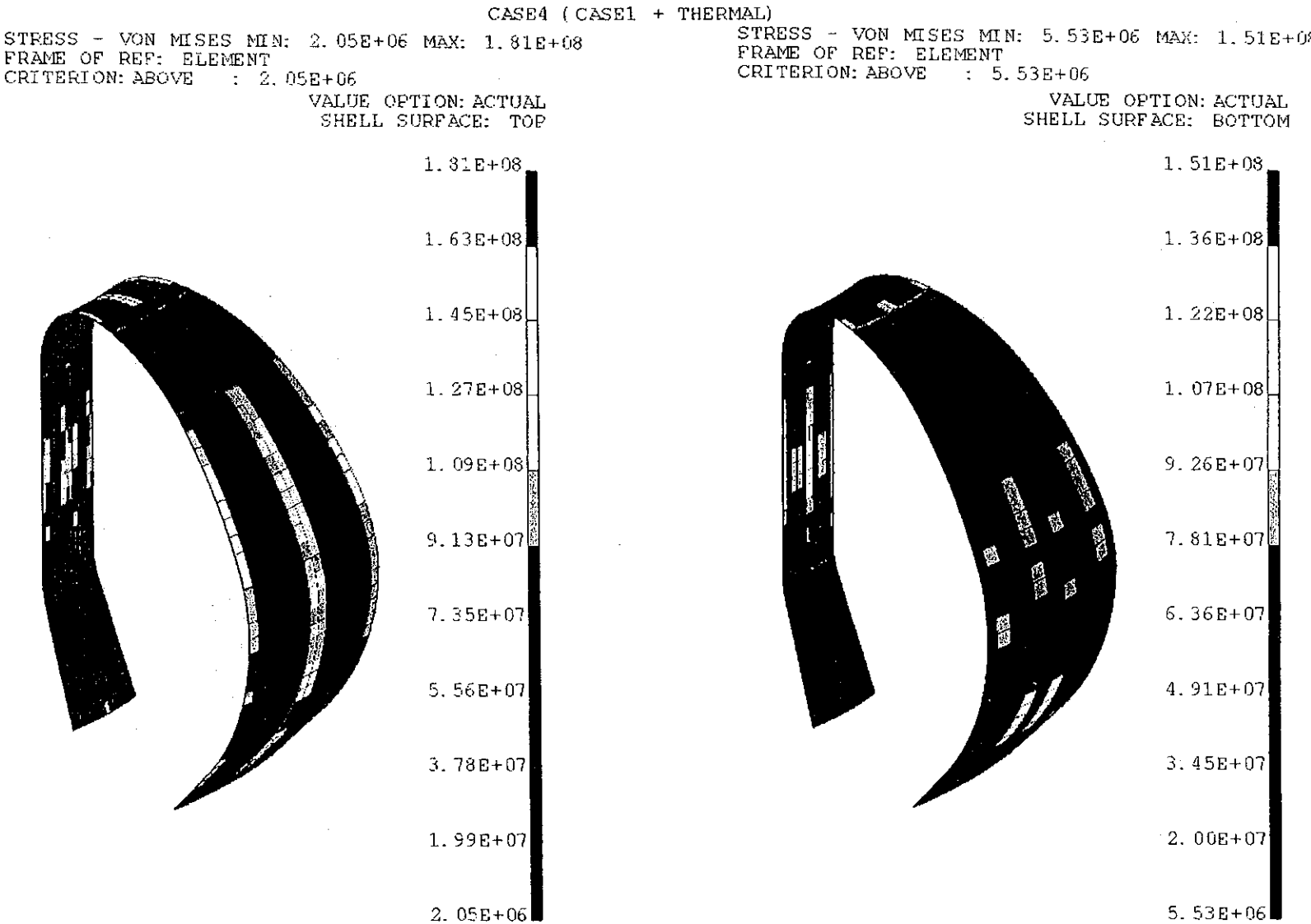

Fig. 3.2.1 – 43 Von Mises Stress Distribution on Back Plate under Weight Load + Centered Disruption Load + Thermal Load (Case – 4).

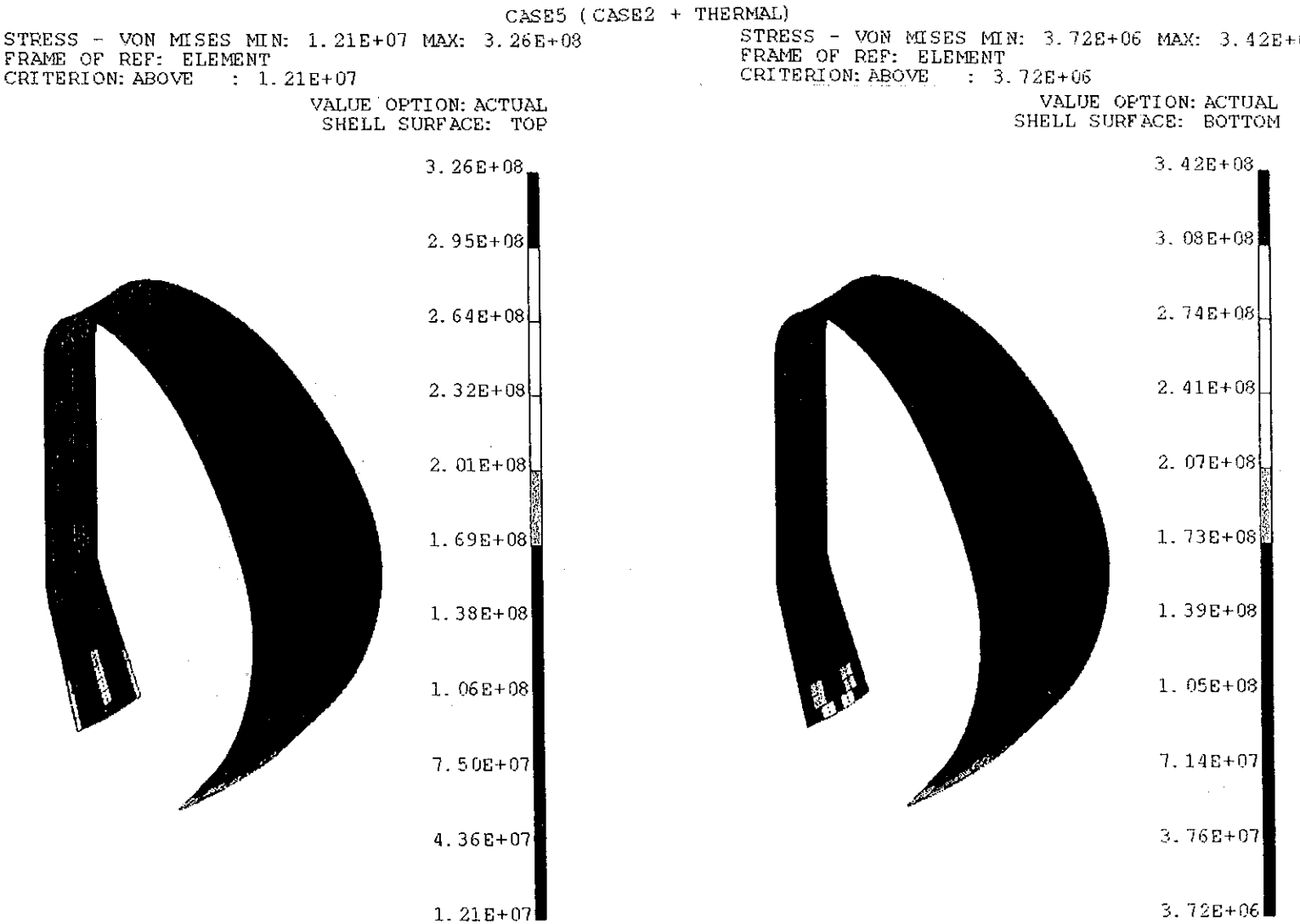

Fig. 3.2.1 - 44 Von Mises Stress Distribution on Back Plate under Weight Load + VDE Disruption (Symmetric Load) + VDE Disruption (Asymmetric Load ; In - plane) + Thermal Load (Case - 5).

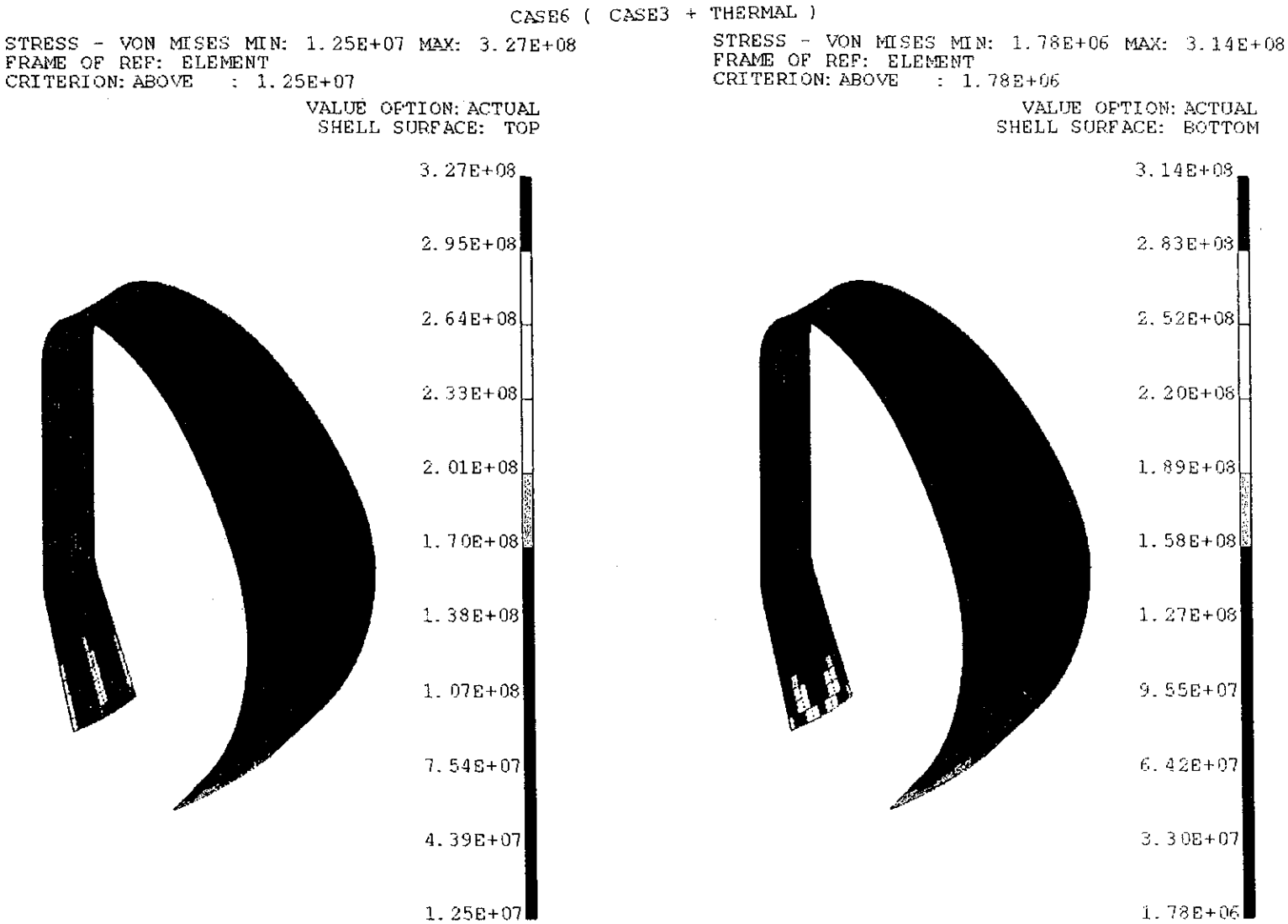

Fig. 3.2.1 – 45 Von Mises Stress Distribution on Back Plate under Weight Load + VDE Disruption (Symmetric Load) + VDE Disruption (Asymmetric Load ; Out – of – plane) + Thermal Load (Case – 6).

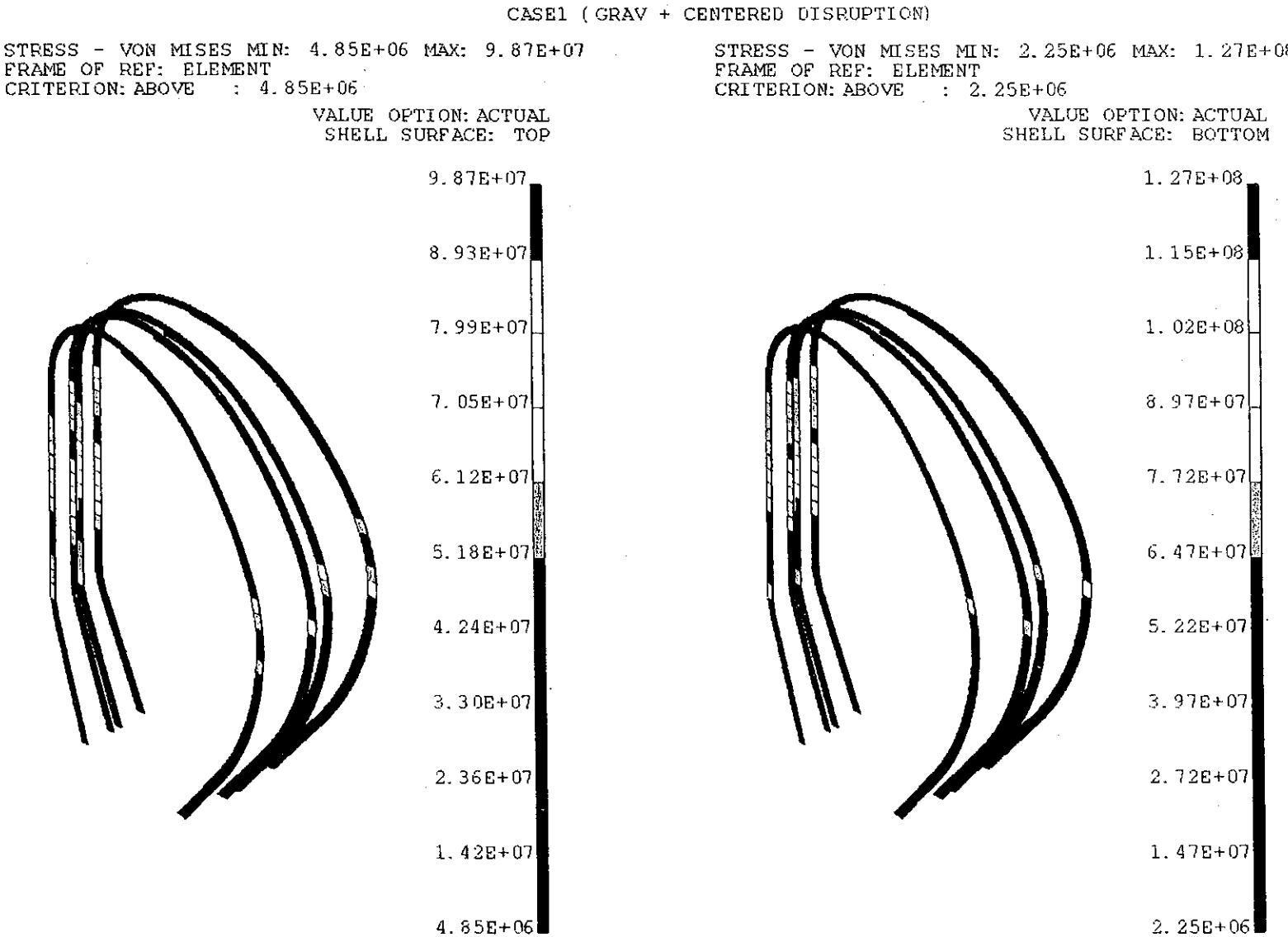

Fig. 3.2.1 – 46 Von Mises Stress Distribution on Blanket Support Legs under Weight Load + Centered Disruption Load (Case – 1).

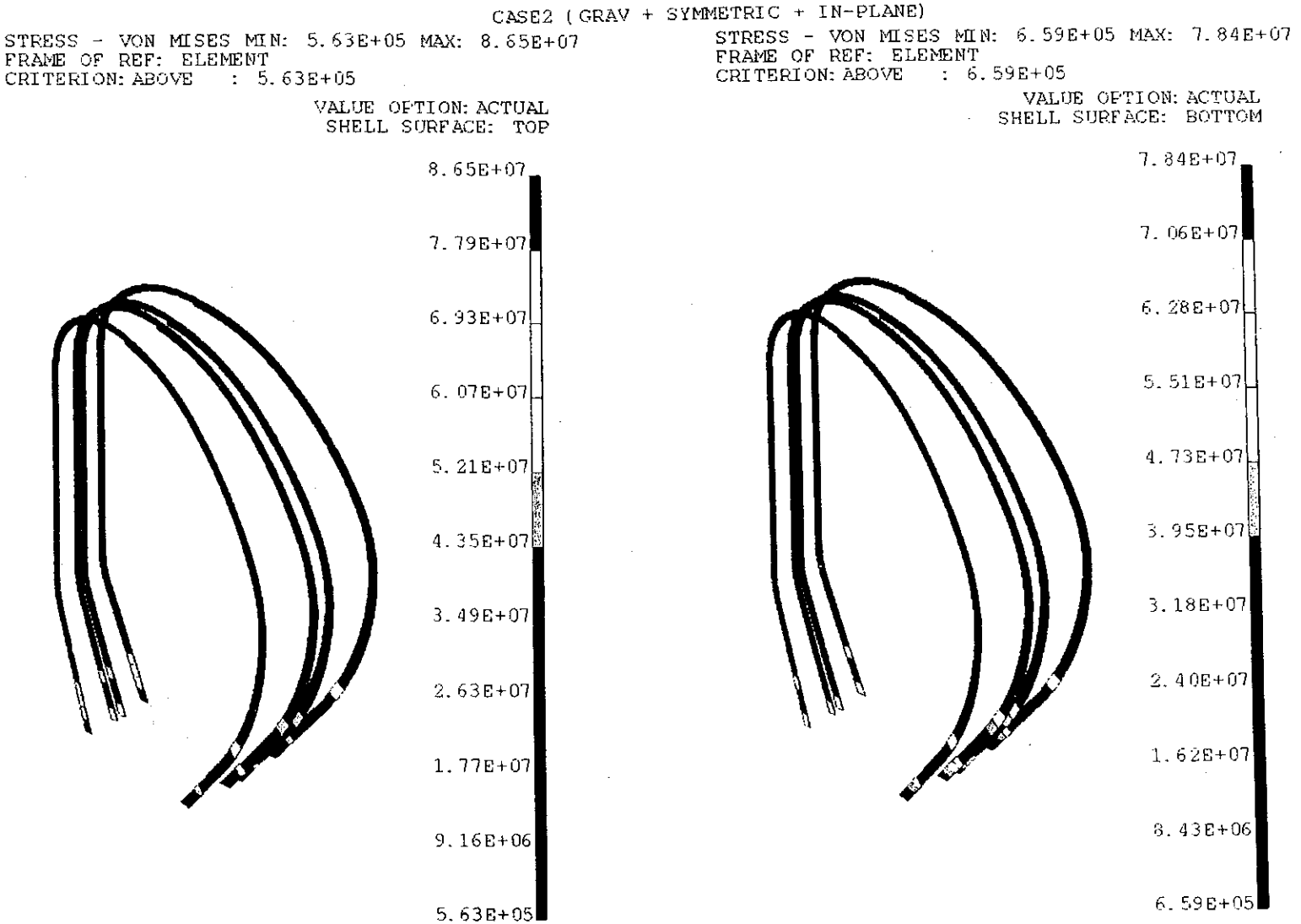

Fig. 3.2.1 – 47 Von Mises Stress Distribution on Blanket Support Legs under Weight Load + VDE Disruption (Symmetric Load) + VDE Disruption (Asymmetric Load ; In – plane) (Case – 2).

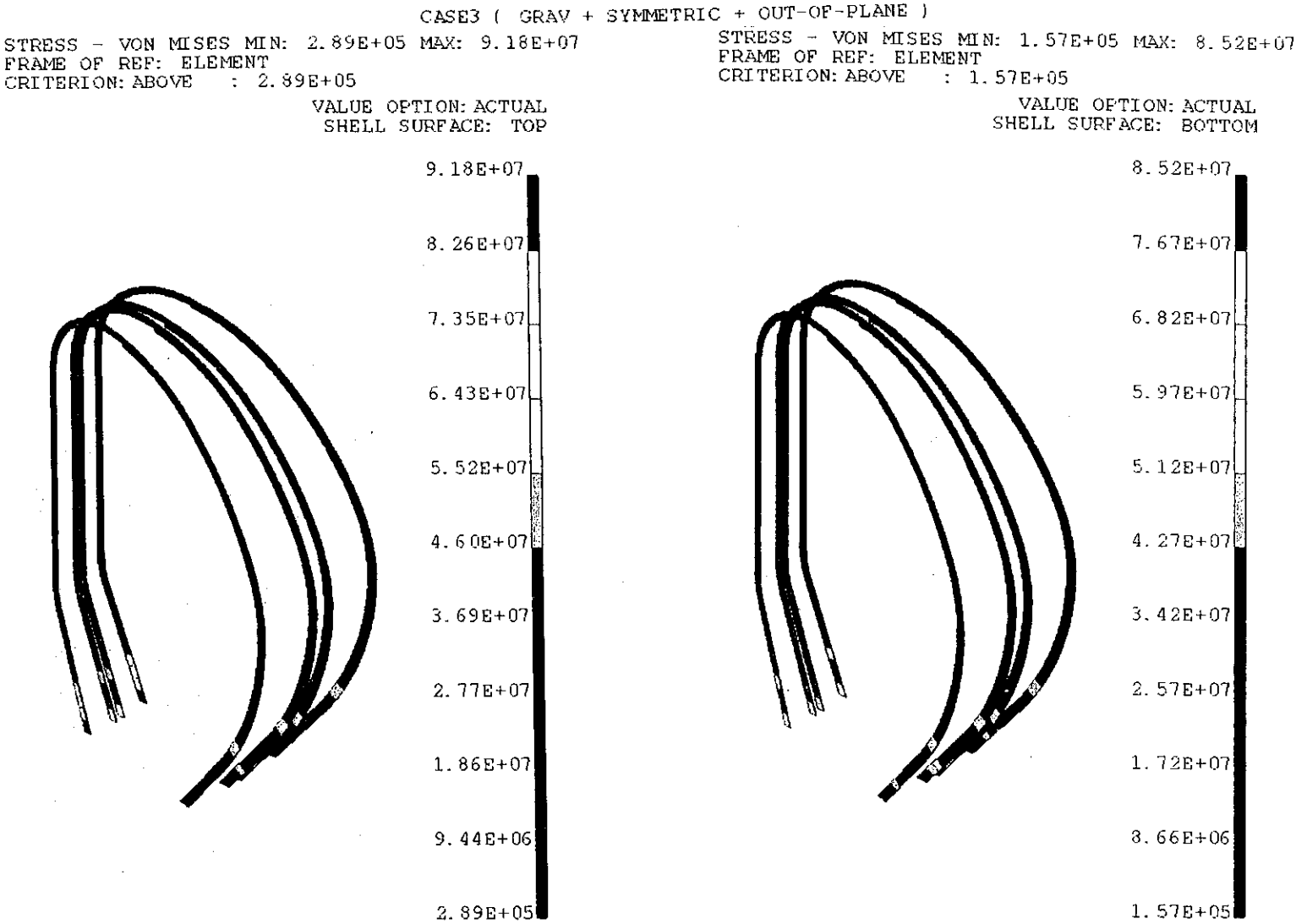

Fig. 3.2.1 – 48 Von Mises Stress Distribution on Blanket Support Legs underWeight Load + VDE Disruption (Symmetric Load) + VDE Disruption (Asymmetric Load ; Out – of – plane) (Case – 3).

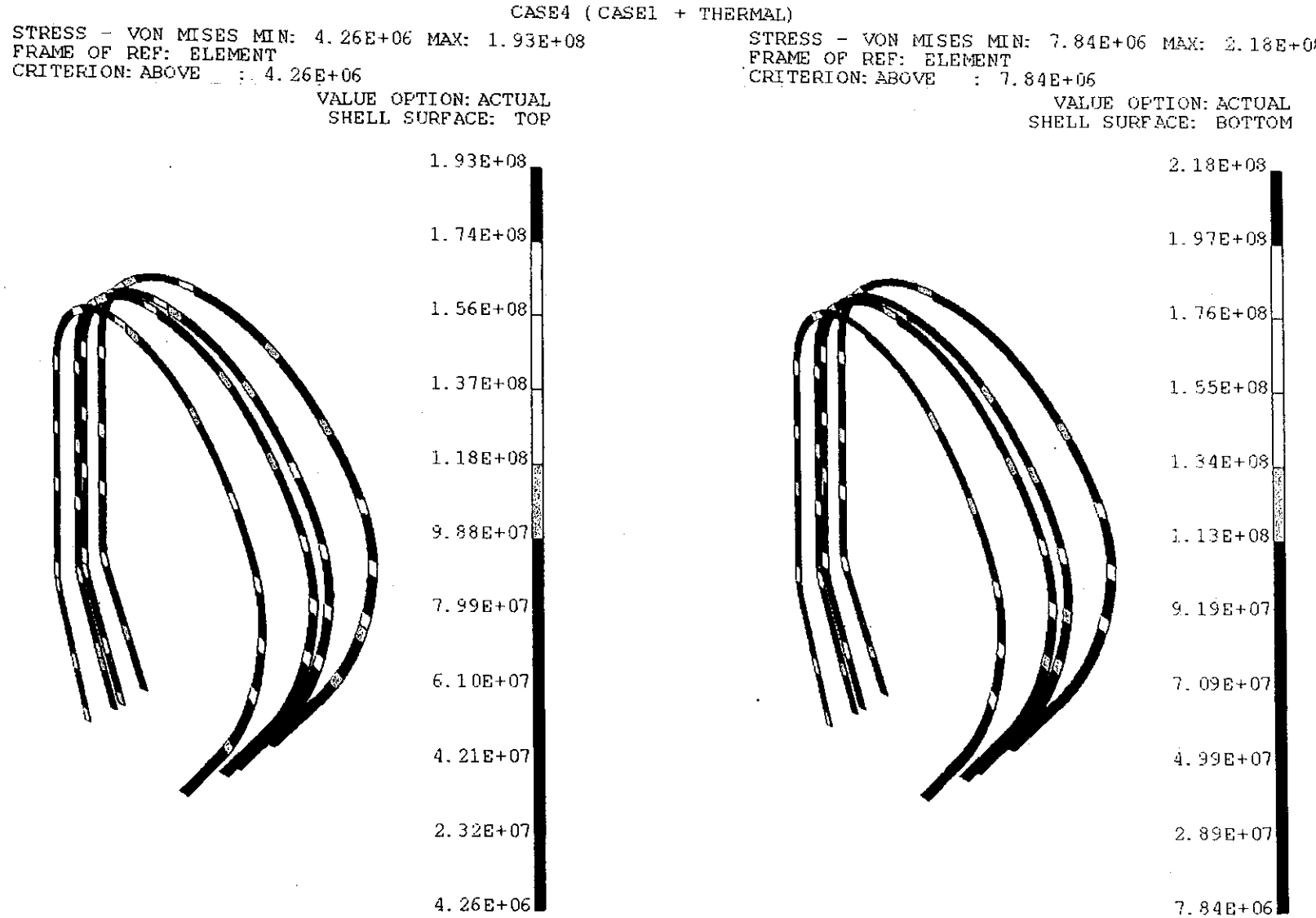

Fig. 3.2.1 - 49 Von Mises Stress Distribution on Blanket Support Legs under Weight Load + Centered Disruption Load + Thermal Load (Case - 4).

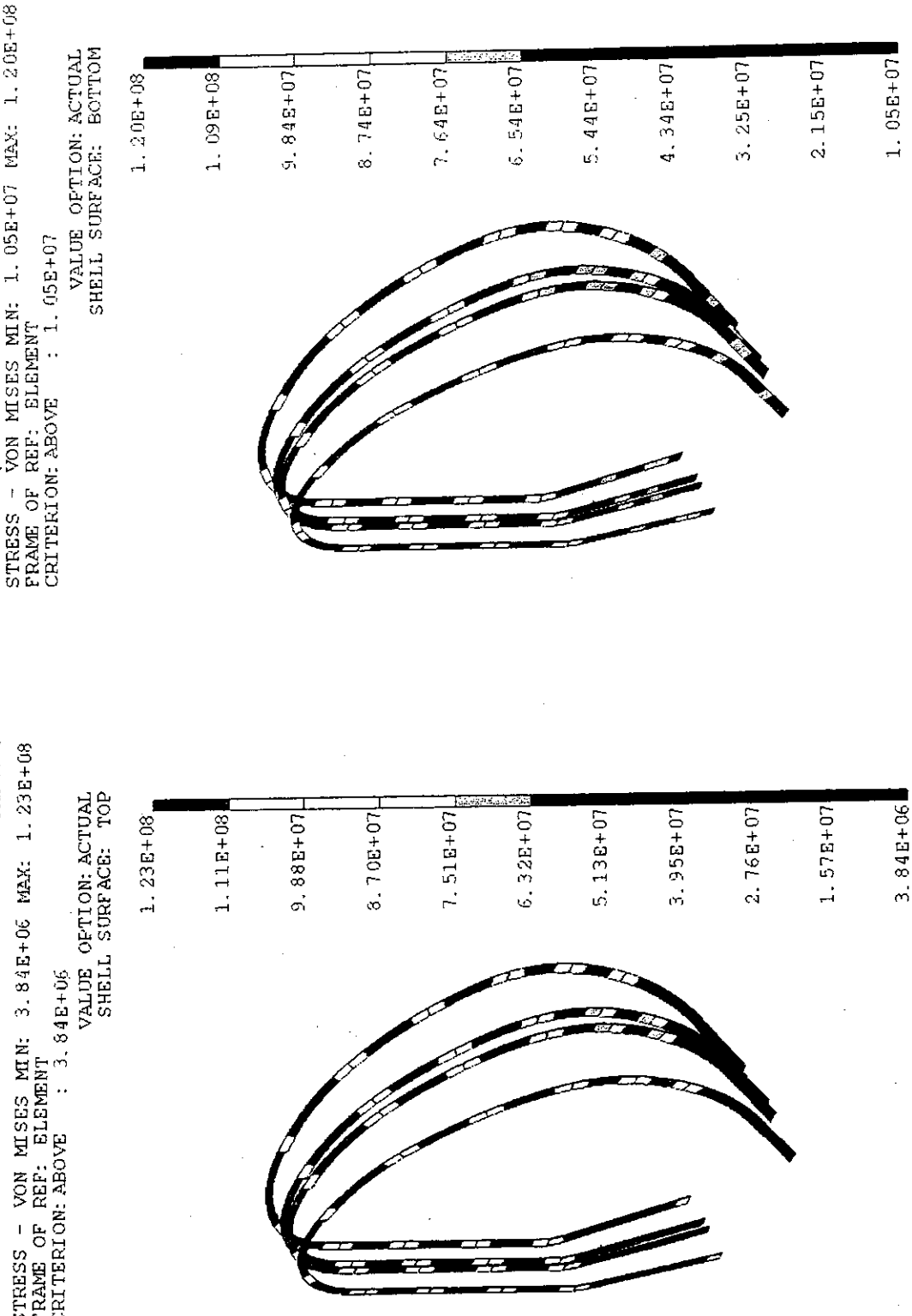

Fig. 3.2.1 – 50 Von Mises Stress Distribution on Blanket Support Legs under Weight Load + VDE Disruption (Symmetric Load) + VDE Disruption (Asymmetric Load ; In – plane) + Thermal Load (Case – 5).

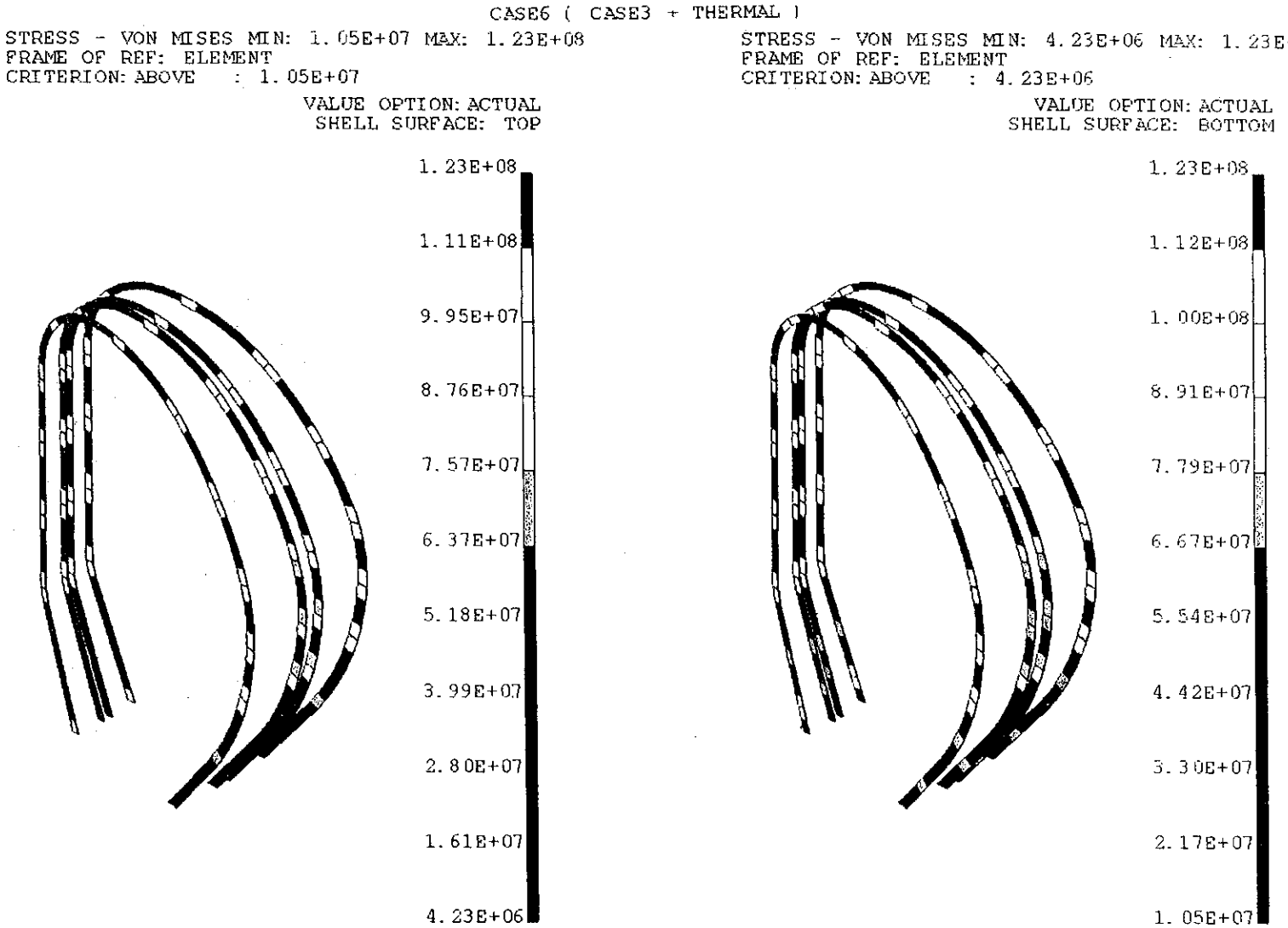

Fig. 3.2.1 – 51 Von Mises Stress Distribution on Blanket Support Legs under Weight Load + VDE Disruption (Symmetric Load) + VDE Disruption (Asymmetric Load ; Out – of – plane) + Thermal Load (Case – 6).

Table 3.2.1 – 1 Materials and Thickness of Structural Components

Components	Thickness	Material
Vacuum Vessel		SS316
Inner Skin	40 mm	
Outer Skin	40 mm	
Poloidal Rib	40 mm	
Upper Port	80 mm(H= 80 mm)	
Mid Port	80 mm(H=200 mm)	
Divertor Port	80 mm(H=200 mm)	
Support Base Plates	100 mm	
Flexible Support Leg(l=3m)	5x120 mm	
Box Support Leg(l=3m)	100 mm	
Blanket Module		SS316
First Wall	100 mm	
Side Wall	100 mm	
End Wall	100 mm	
Top/Bott. Plates	100 mm	
Support Leg	70 mm	
Back Plates		SS316
Inboard	100 mm	
Outboard	100 mm	
Base at Blanket Support	200 mm	
Blanket Support Structure		SS316
Inboard	2- 7 Layers-20 mm	
Outboard	4-20 Layers-12 mm	

3.2.2 Thermal and stress analyses of blanket module

Transient thermal and stress analyses of a blanket module have been performed with a mid-plane cross-section model of #4 blanket. The cross-section and a finite element model including one half of blanket module and corresponding back plate are shown in Figs. 3.2.2.1 and 3.2.2.2, respectively. The calculation code used is ABAQUS. Material properties of Be, DSCu and SS316LN are indicated in Tables 3.2.2.1-3.2.2.3 [3.2.2.1].

Thermal analysis conditions are summarized in Fig. 3.2.2.3. Surface heat flux from plasma to the first wall is 0.5 MW/m^2 with decrease corresponding to its angle facing to plasma at blanket corner as shown in Fig. 3.2.2.4. Volumetric heating rates in Be, DSCu and SS316 are indicated in Figs. 3.2.2.5-3.2.2.7 which are calculated by neutronics analysis. An initial temperature of the blanket and back plate is taken to be 125 °C in this analysis. A step-wise start up is assumed for plasma operation.

Temperature responses at various points in the module and back plate are described in Fig. 3.2.2.8. Temperature distributions at 6 sec, 48 sec and 768 sec after the start up and in steady state are indicated in Figs. 3.2.2.9-3.2.2.12. Maximum temperatures in steady state are 285 °C in Be, 241 °C in DSCu, and 251 °C in SS near first wall.

Restraint condition for stress analysis is shown in Fig. 3.2.2.13. Generalized plain strain is taken into account for out-of-plane condition. Mechanical properties of Be, DSCu and SS316LN are summarized in Tables 3.2.2.1-3.2.2.3. For Be, equivalent Young's moduli are evaluated, i.e. about 1/100 of those of pure Be, referring slits or grooves formed on Be surface as indicated in Fig. 3.2.2.14. As for DSCu, allowable stresses are estimated based on tensile and yield strengths as indicated in Table 3.2.2.4. Also, a fatigue curve of DSCu is estimated as shown in Fig. 3.2.2.15 based on R&D results on DSCu with heat treatment as same as DSCu/SS HIP conditions.

Stress distribution due to coolant pressure, 3 MPa, is shown in Fig. 3.2.2.16. Maximum stresses due to coolant pressure in DSCu and SS are sufficiently low such as 7 MPa and 12 MPa, respectively. Thermal stress responses and distributions at times corresponding to Figs. 3.2.2.9-3.2.2.12 are shown in Figs. 3.2.2.17-3.2.2.21. Maximum stress (Tresca stress) in DSCu is 187 MPa at first wall corner at 50 seconds after the start up. As for SS, maximum stress is 380 MPa at inner surface of coolant channel in the last row at steady state.

Results of stress evaluations following MITI 501, that is almost same as ASME Section III, are summarized in Table 3.2.2.5. For DSCu, stresses at about 50 seconds after the start up are evaluated. The evaluation line for DSCu is A-A' shown in Fig. 3.2.2.19 including the point A of the maximum stress. Both of the membrane + bending stress intensity and the cumulative fatigue damage due to peak stress are below allowable limits. Also for SS in the shielding block, stresses along the line B-B' in Fig. 3.2.2.21 at steady state are evaluated resulting in satisfying the criteria of the membrane + bending stress intensity and the cumulative fatigue damage. The membrane + bending stress intensity at point C of SS coolant tube at steady state evaluated along the line C-C' in Fig. 3.2.2.21 exceeds 3Sm. Therefore, simplified elasto-plastic evaluation is applied to this point according to MITI 501. The resulted peak stress intensity at the point C is 243 MPa for which allowable number of cycles is 3×10^5. Thus the cumulative fatigue damage against the number of operation cycles of 1×10^4 during the BPP is 0.03 that is well below the allowable limit.

Distortion due to coolant pressure and thermal loads at steady state is indicated in Fig. 3.2.2.22. In this result, the radial distortion of the torus structure of the back plate is not taken into account. The first wall deforms 0.66 mm toward plasma relative to the back plate. Toroidal distortion of the blanket side wall is very small such as 0.55 mm.

Reference

[3.2.2.1] ITER Design Description Document, 1.7

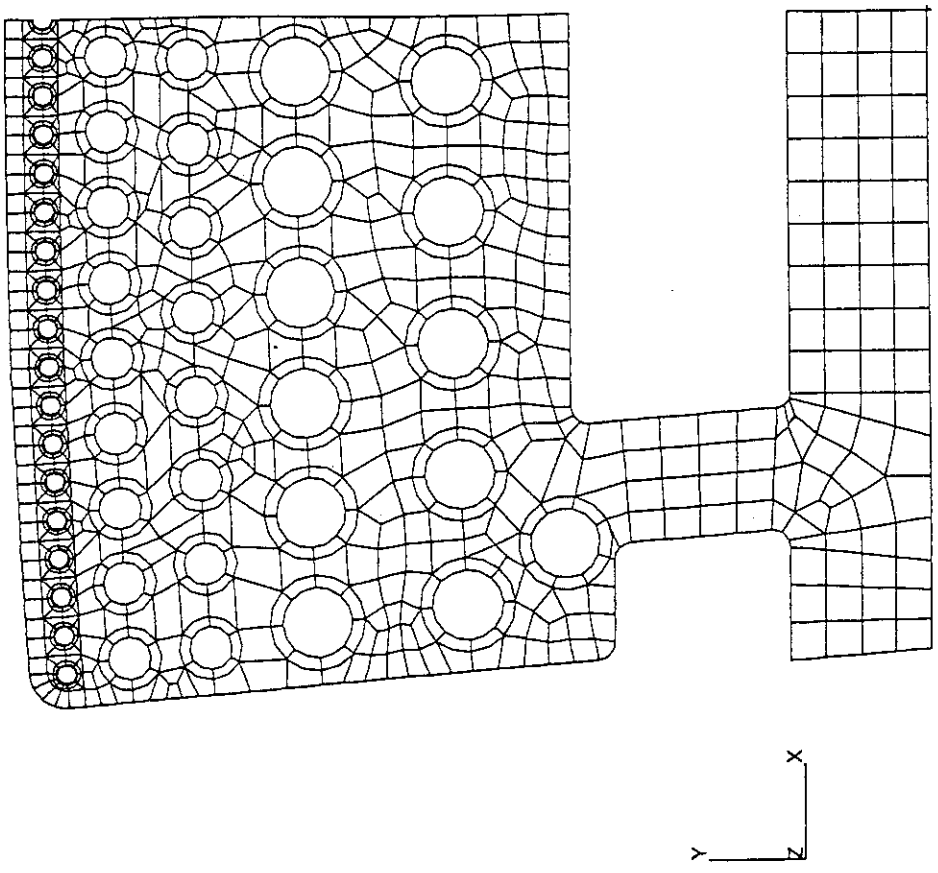

Fig. 3.2.2.2 Finite element model

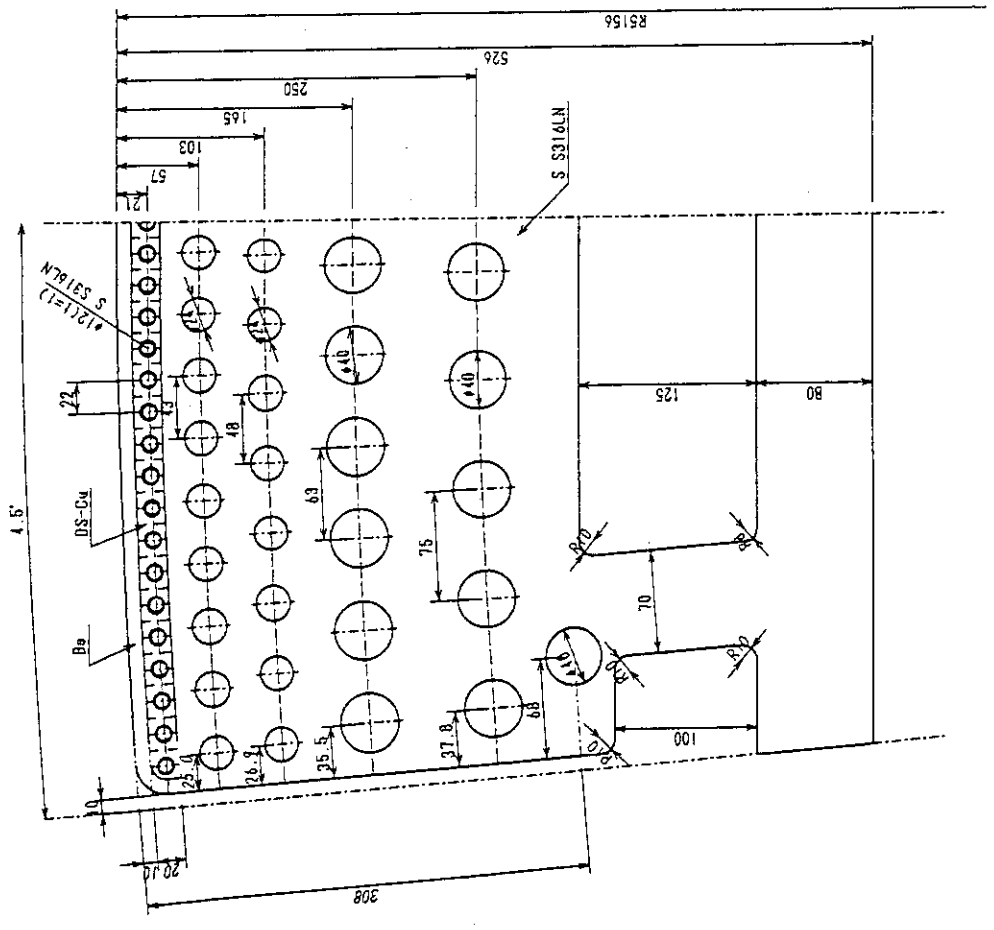

Fig. 3.2.2.1 Shape of Inboard BLanket Module

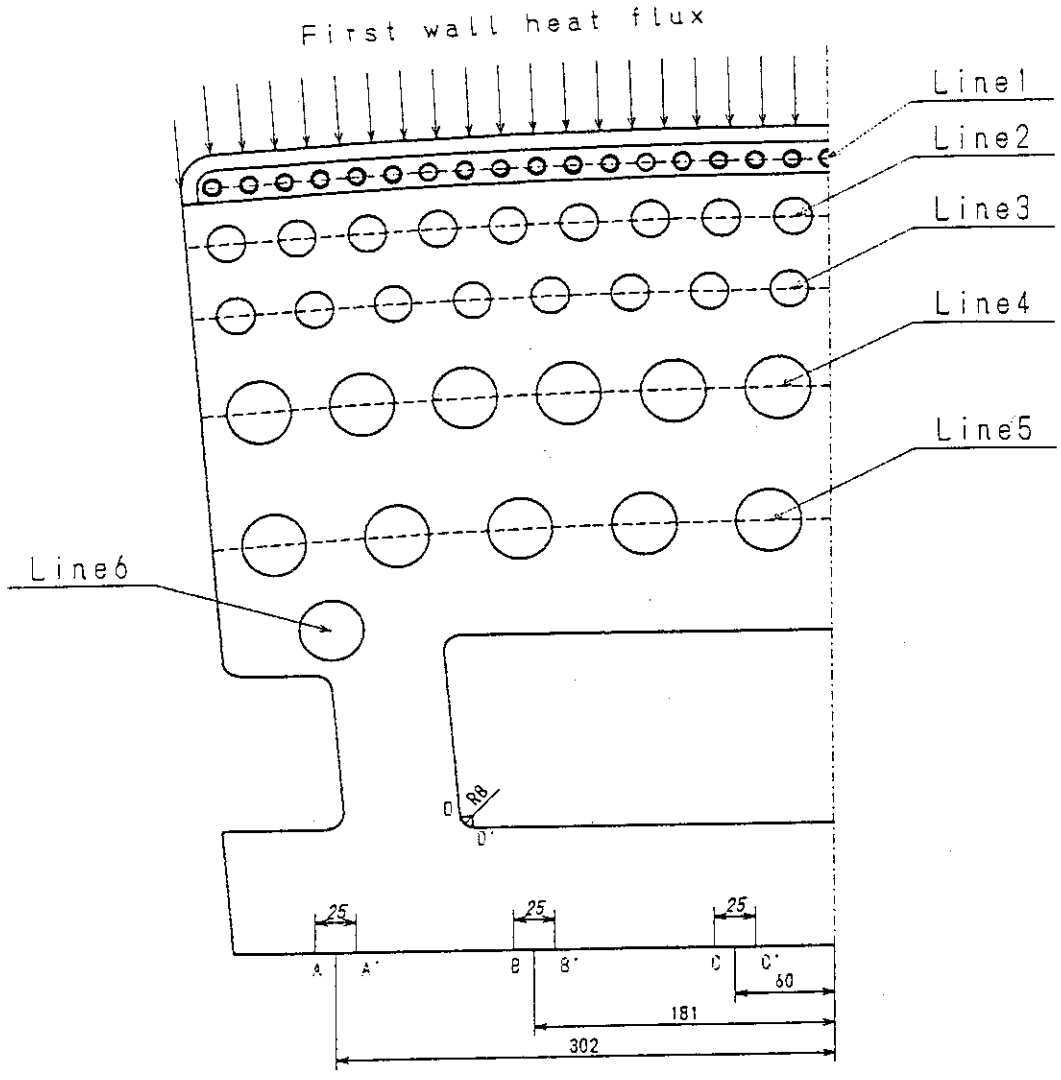

Initial temperature	125 ℃	
First wall heat flux	0.5 MW/m^2 (corner section:Fig. 3.2.4	
Volumetric heating rate	Figs. 3.2.5 - 3.2.7	
Coolant temperature	Coolant tube	150 ℃
	Boundary AA' ~DD'	150 ℃
Coolant tube pressure	3.0 MPa	
Heat transfer coefficient	Line1	32300 W/m^{2}K
	Line2	19400 W/m^{2}K
	Line3	21300 W/m^{2}K
	Line4	10700 W/m^{2}K
	Line5	10700 W/m^{2}K
	Line6	10700 W/m^{2}K
	Boundary AA' ~CC'	14800 W/m^{2}K
	Boundary DD'	12900 W/m^{2}K

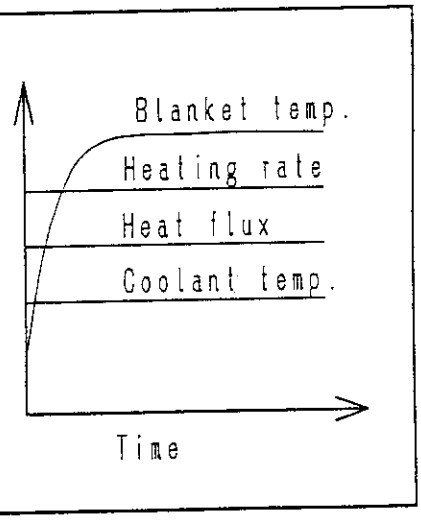

Fig. 3.2.2.3 Thermal boundary condition

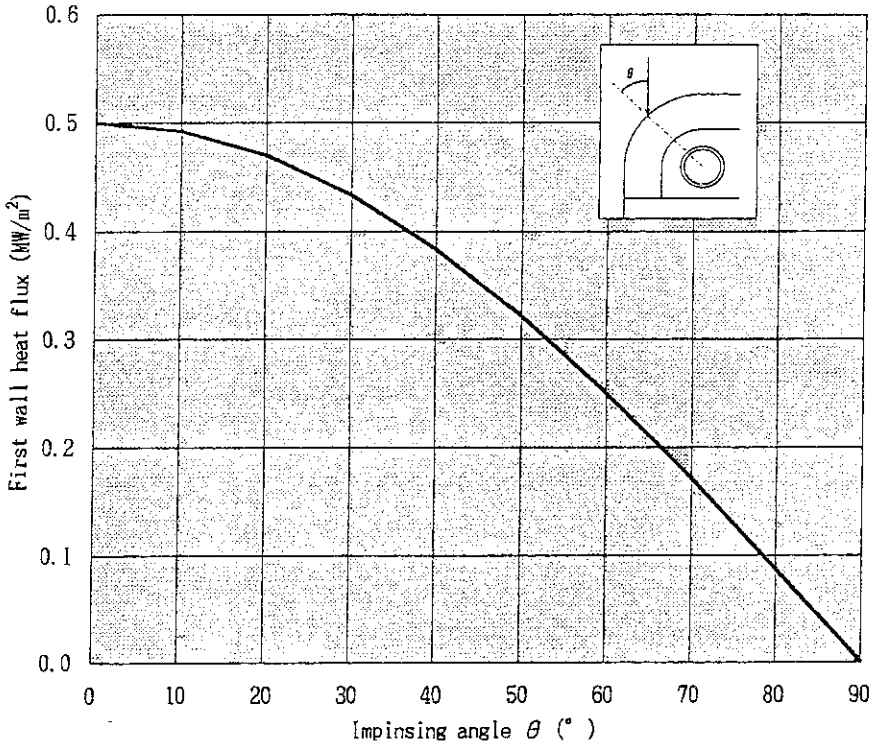

Fig. 3.2.2.4 Relationships between Impinsing angle and First wall heat flux

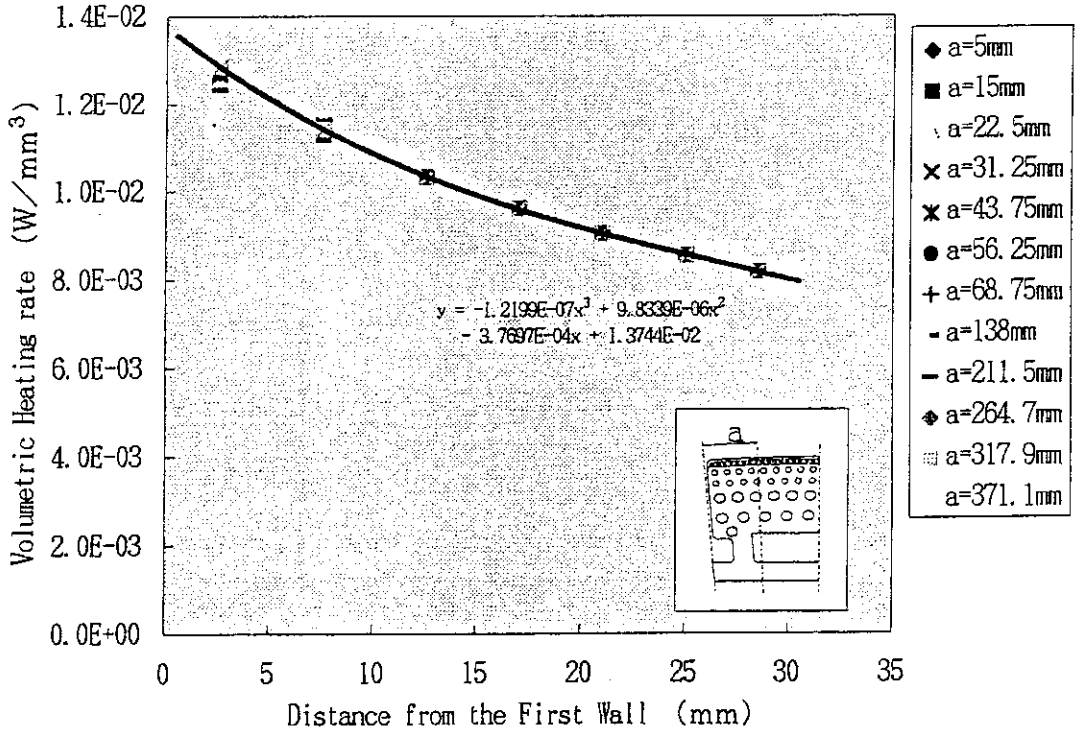

Fig. 3.2.2.5 Relationships between the Distance from the First Wall and Volumetric Heating rate for Berillium

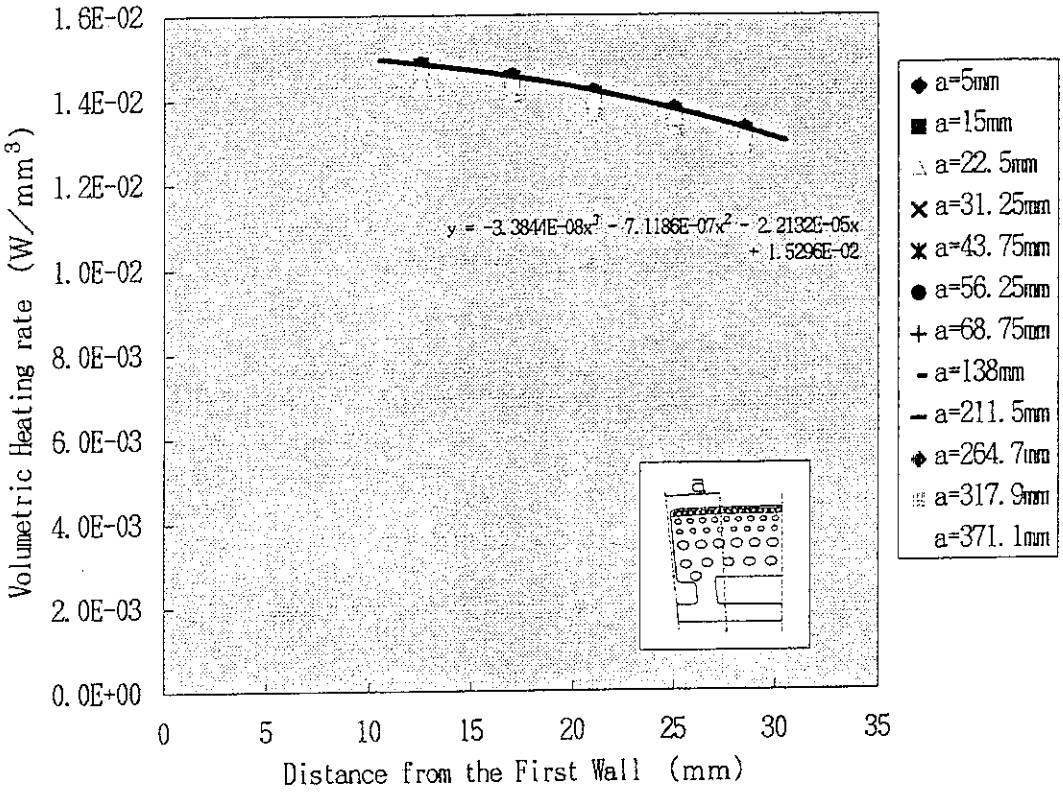

Fig. 3.2.2.6 Relationships between the Distance from the First Wall and Volumetric Heating rate for DS - Cu

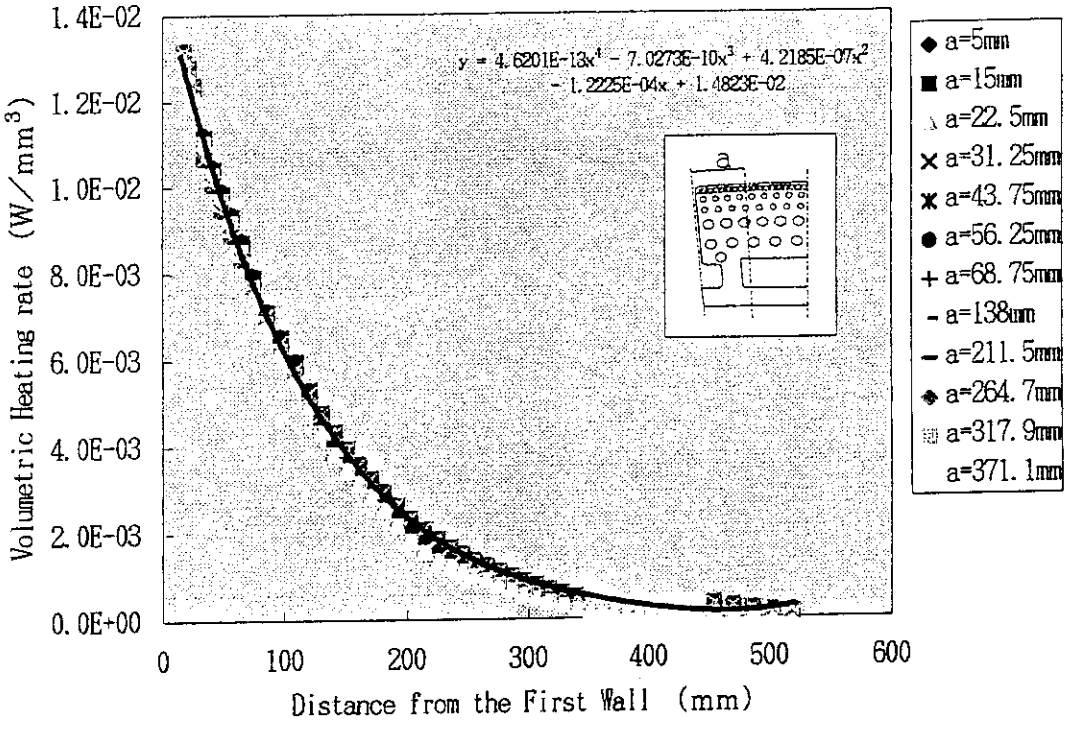

Fig. 3.2.2.7 Relationships between the Distance from the First Wall and Volumetric Heating rate for 316LN

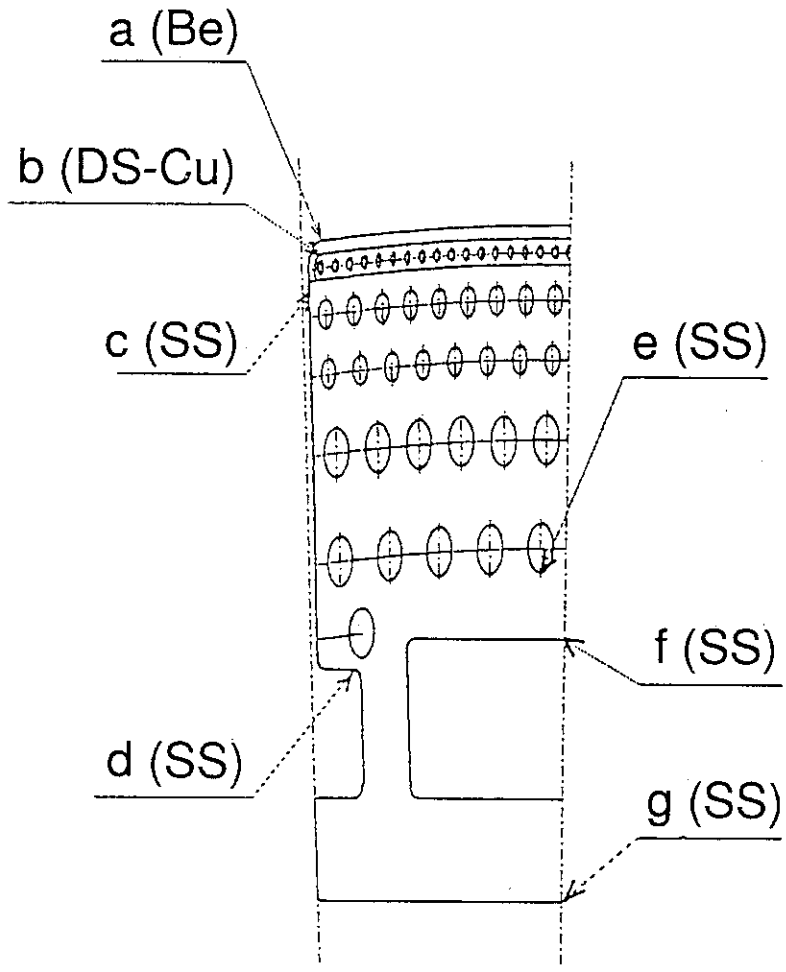

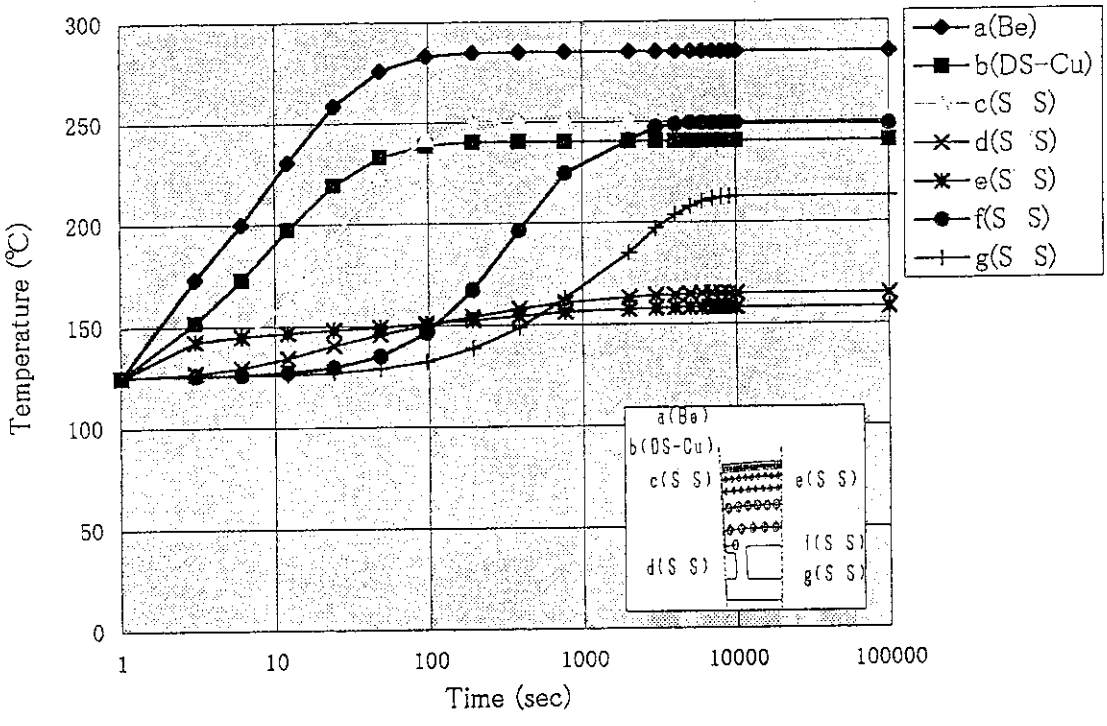

Fig. 3.2.2.8 Relationships between the time and temperature

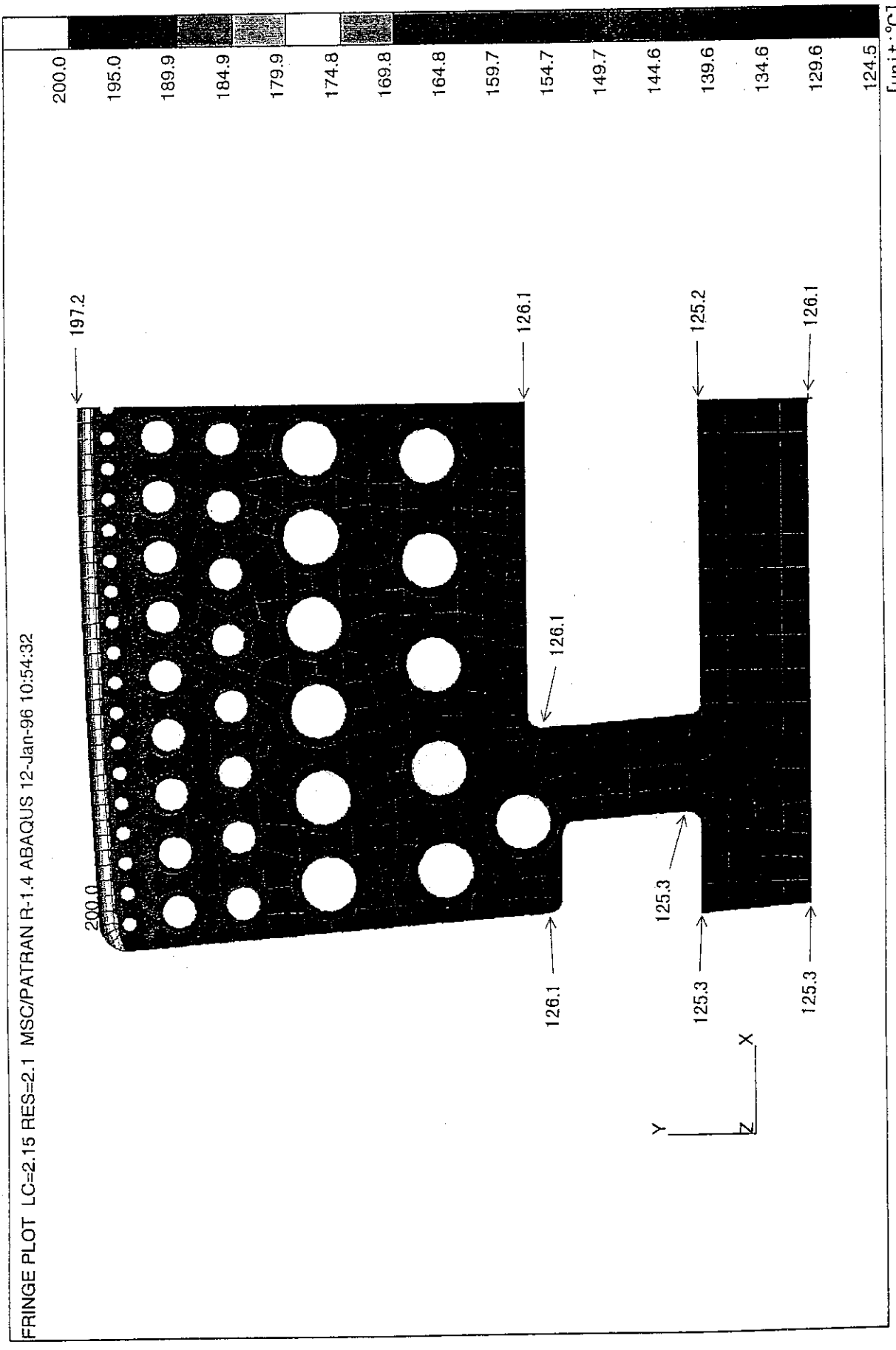

Fig. 3.2.2.9 Temperature distribution (after 6sec)

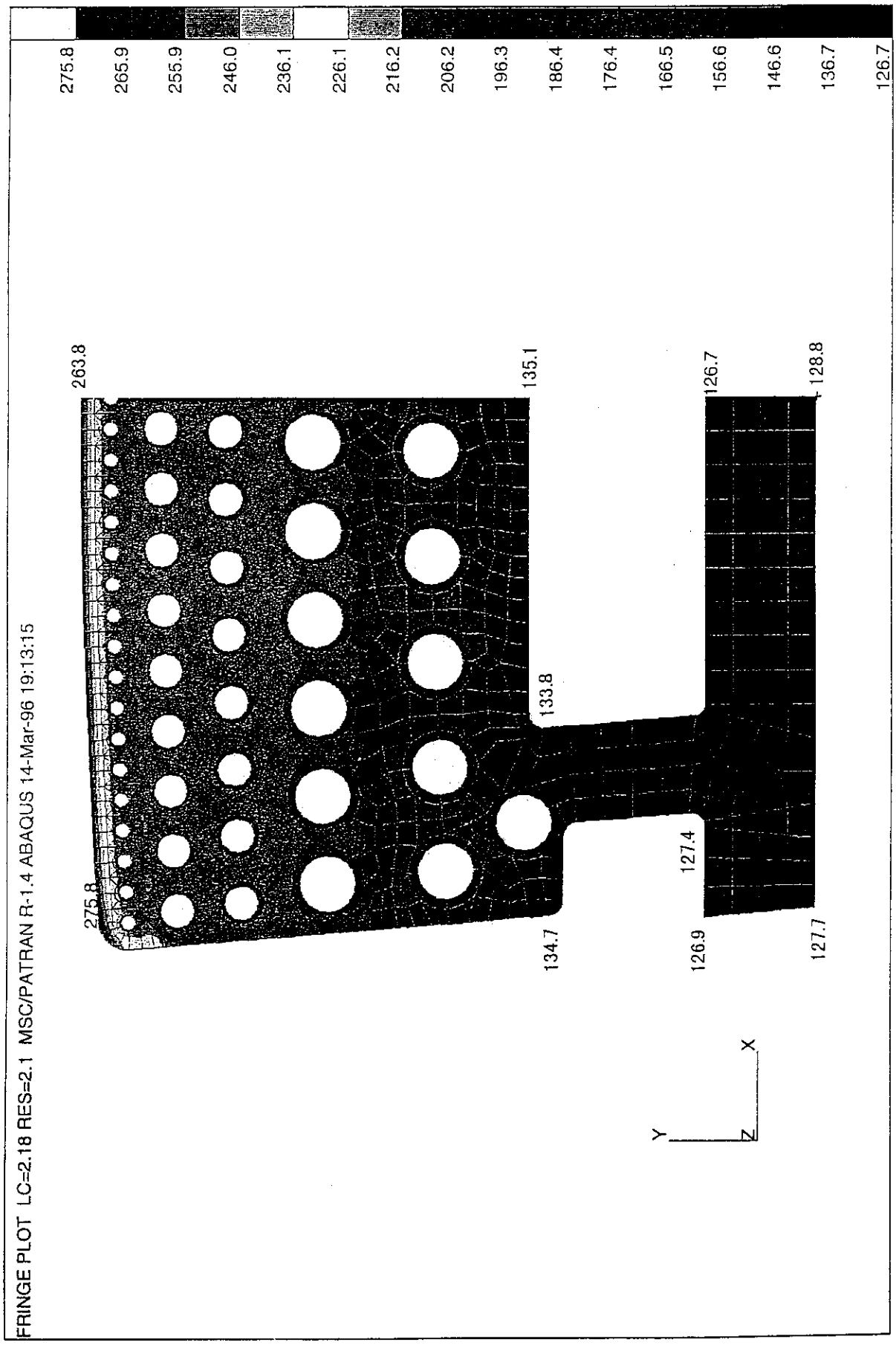

Fig. 3.2.2.10 Temperature distribution (after 48sec)

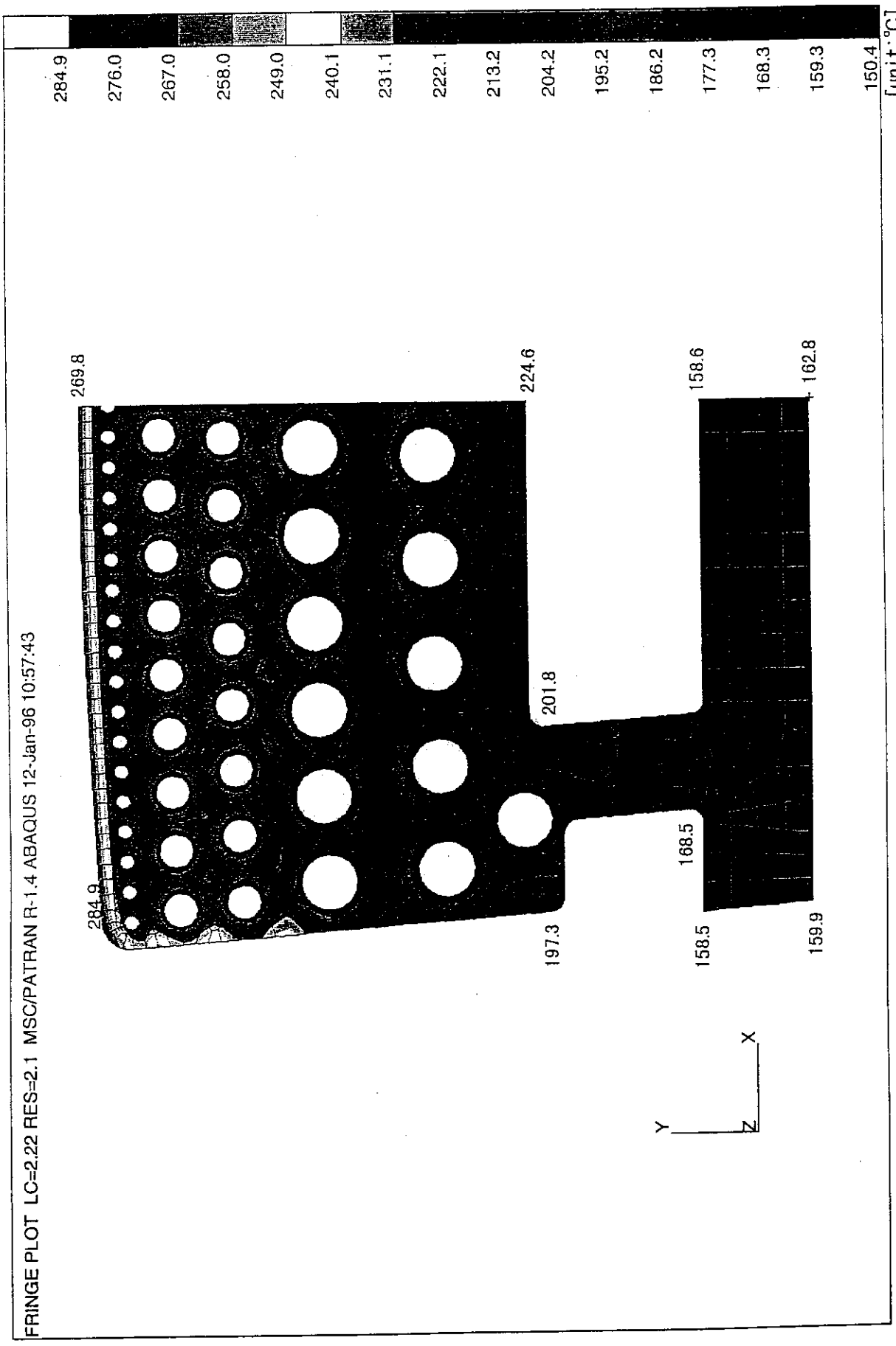

Fig. 3.2.2.11 Temperature distribution (after 768sec)

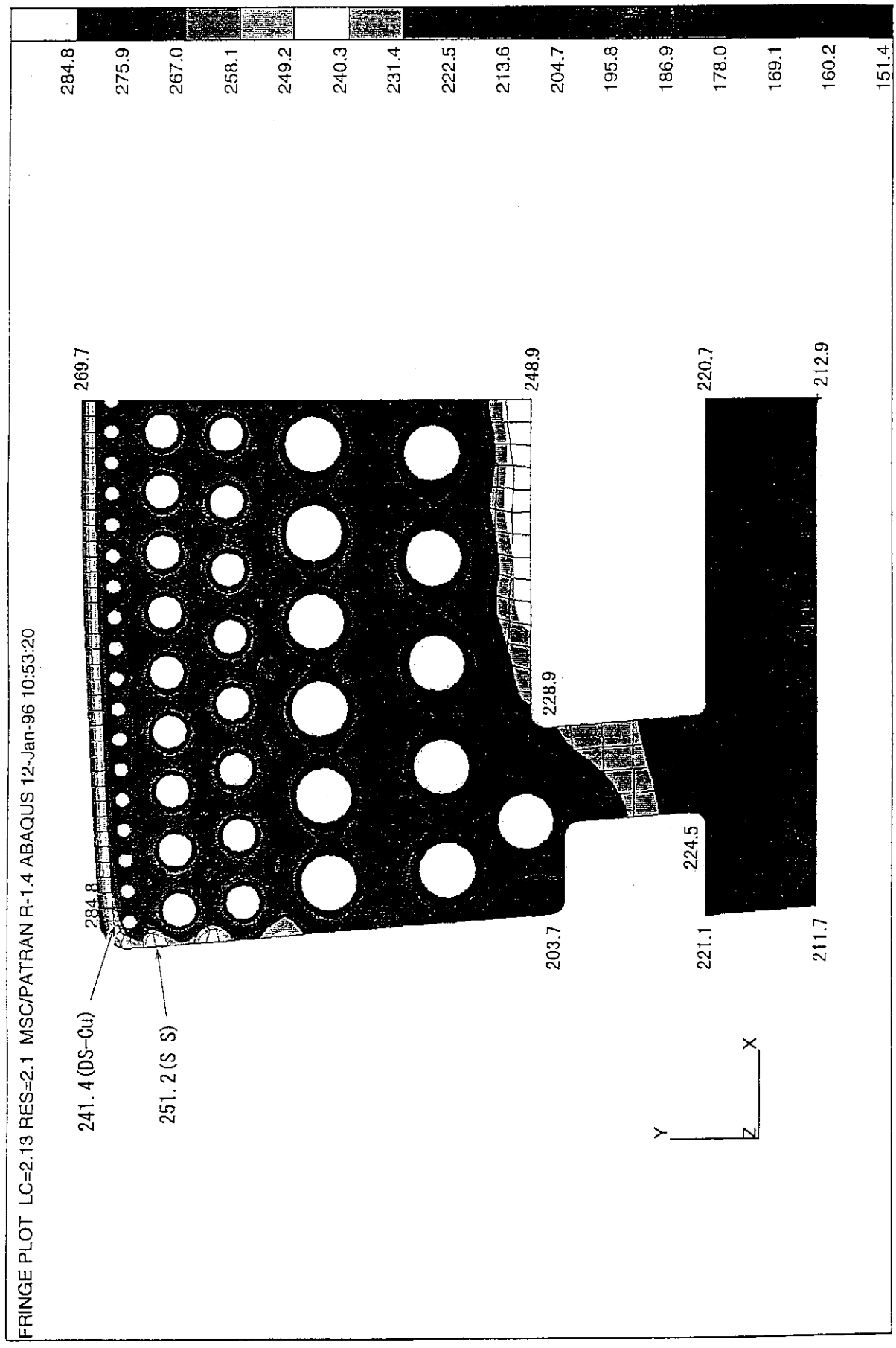

Fig. 3.2.2.12 Temperature distribution (Steady State)

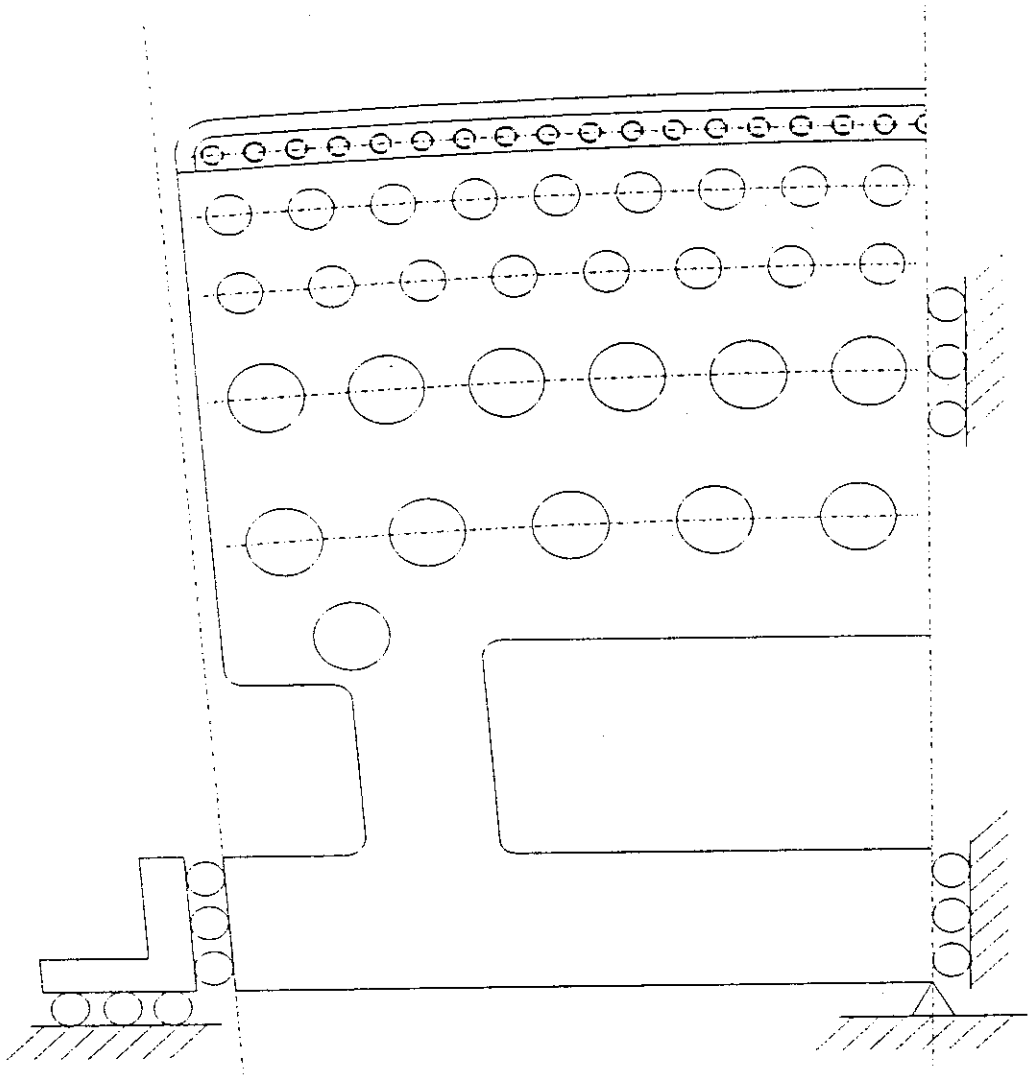

Fig. 3.2.2.13 Restraint condition

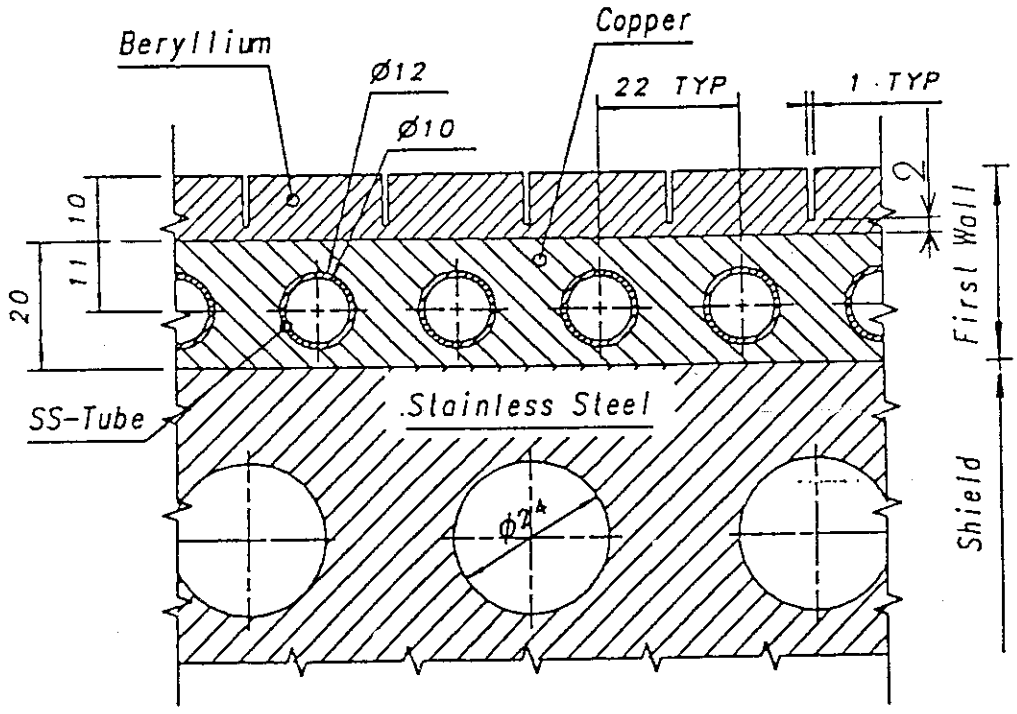

a) Primary First wall cross-section

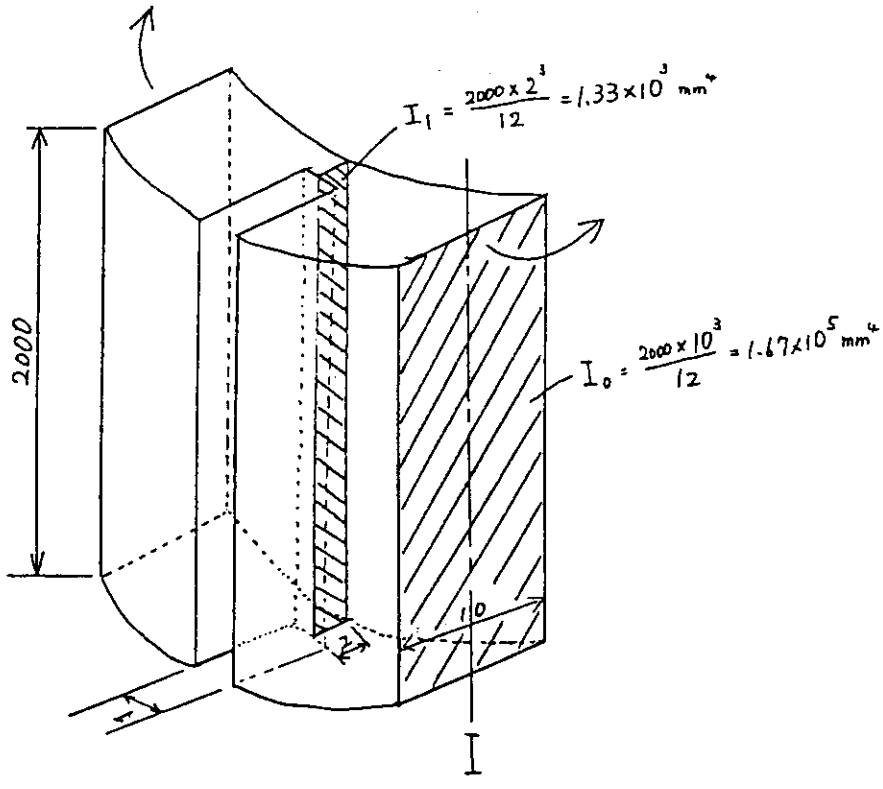

b) Section modulus of Beryllium

Fig. 3.2.2.14 Estimate of Be Young's Modulus

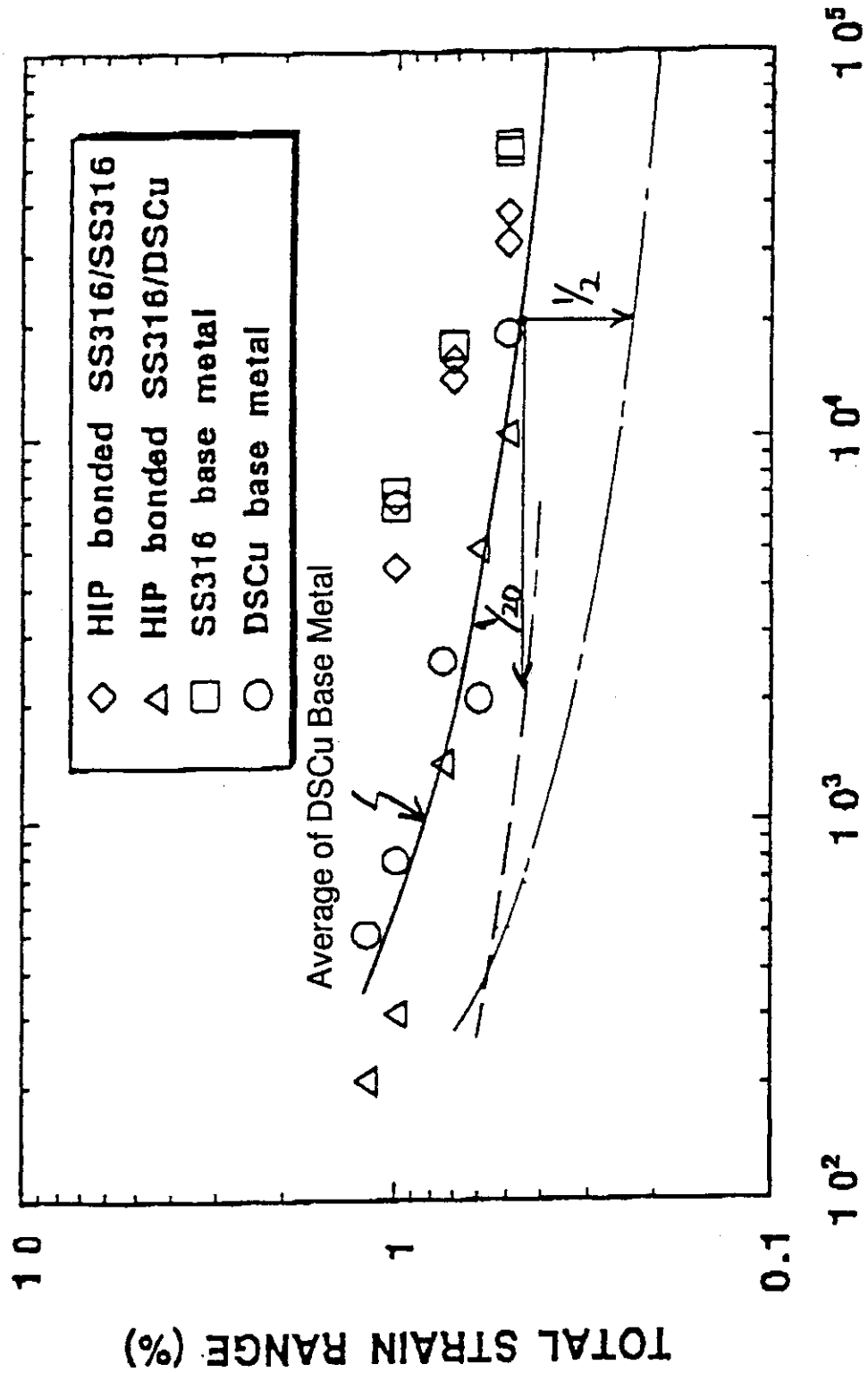

Fig. 3.2.2.15 Fatigue strength of DS-Cu at room temperature

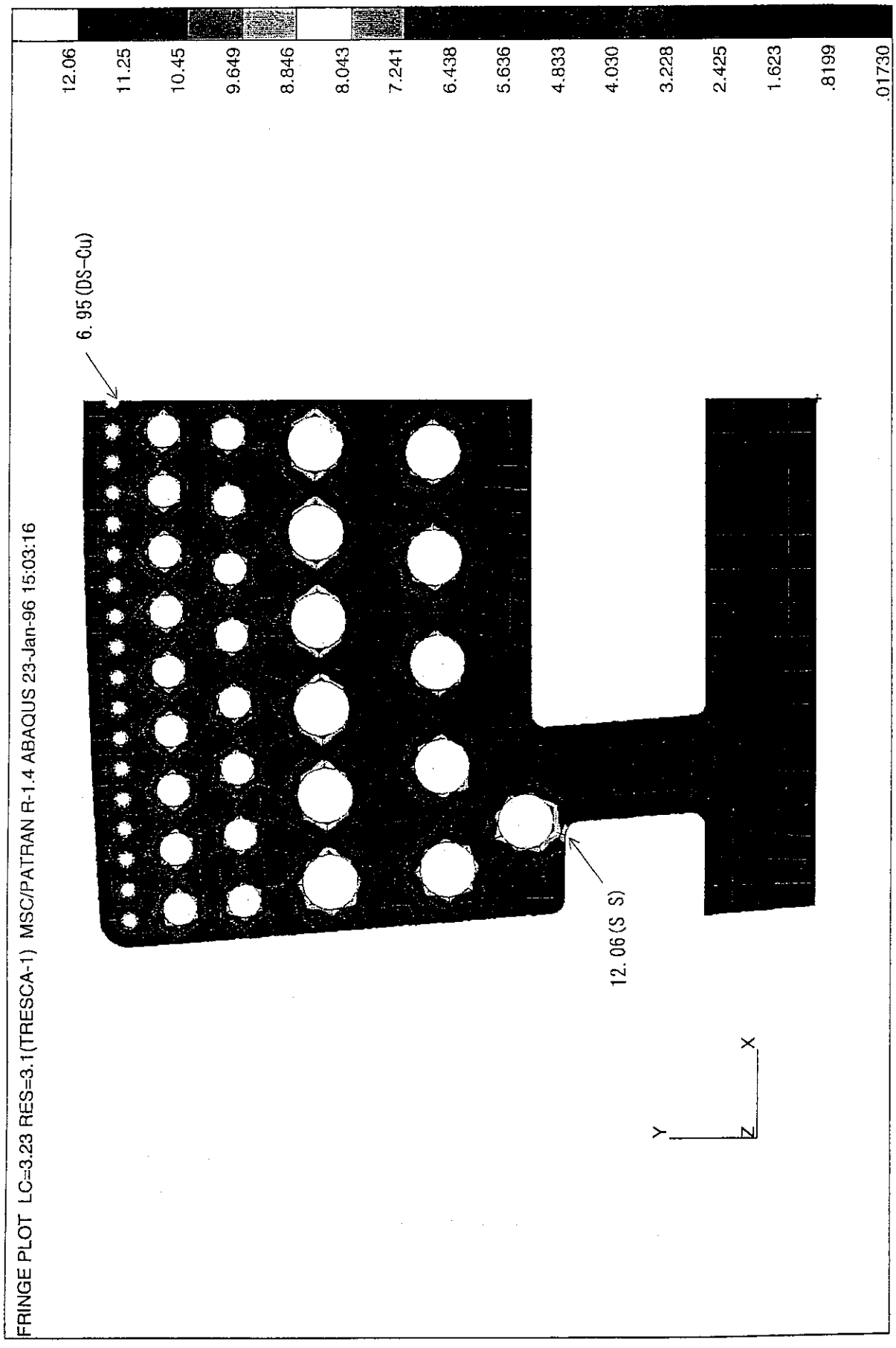

Fig. 3.2.2.16 Stress distribution (Coolant pressure only)

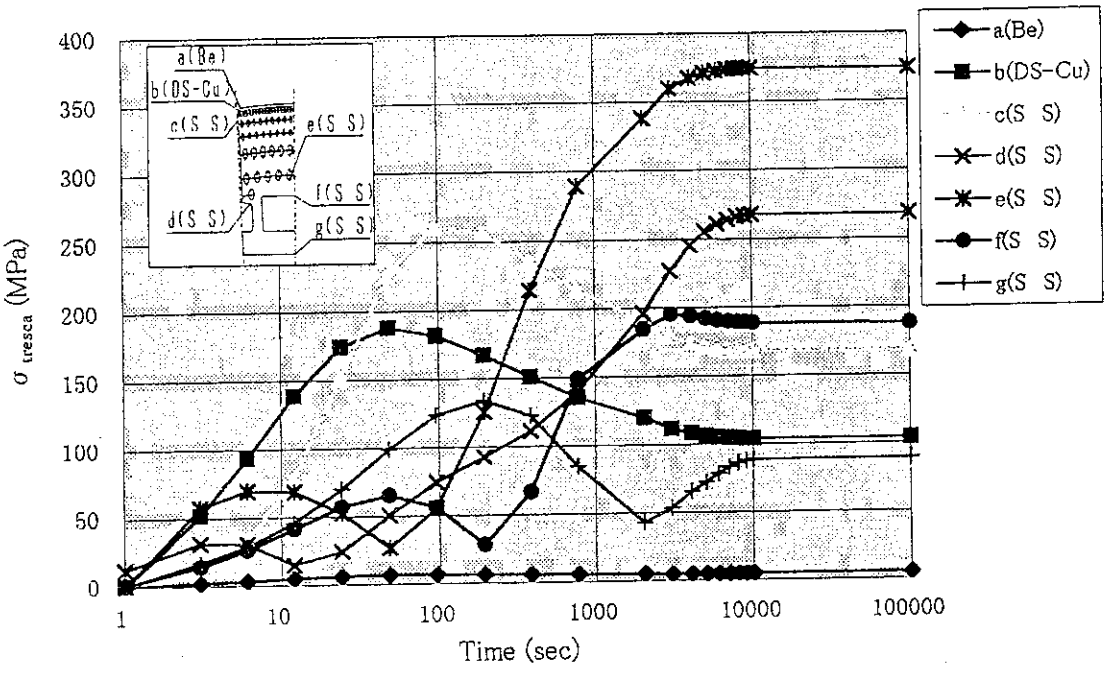

Fig. 3.2.2.17 Relationships between the time and stress

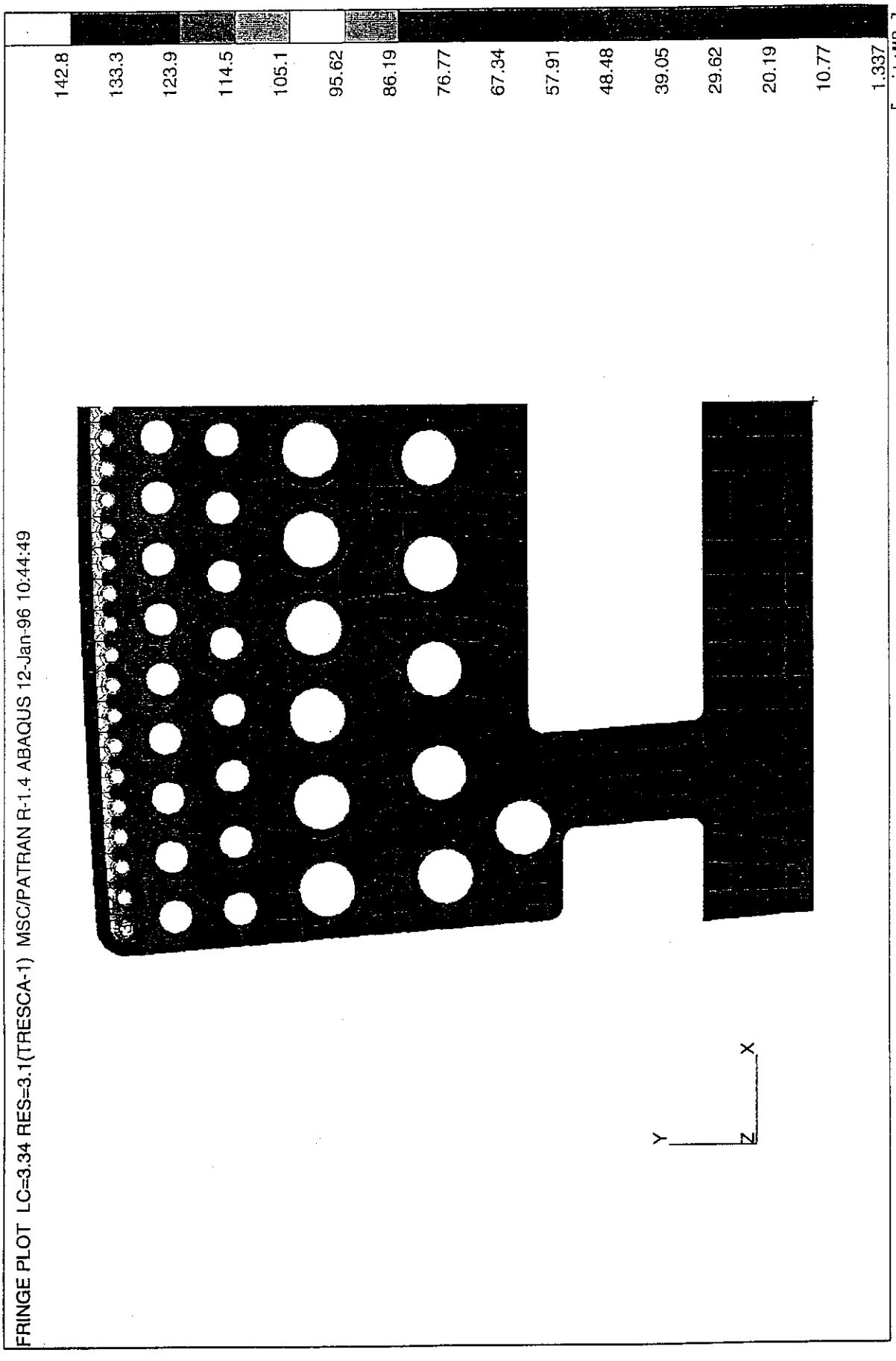

Fig. 3.2.2.18 Stress distribution (after6sec)

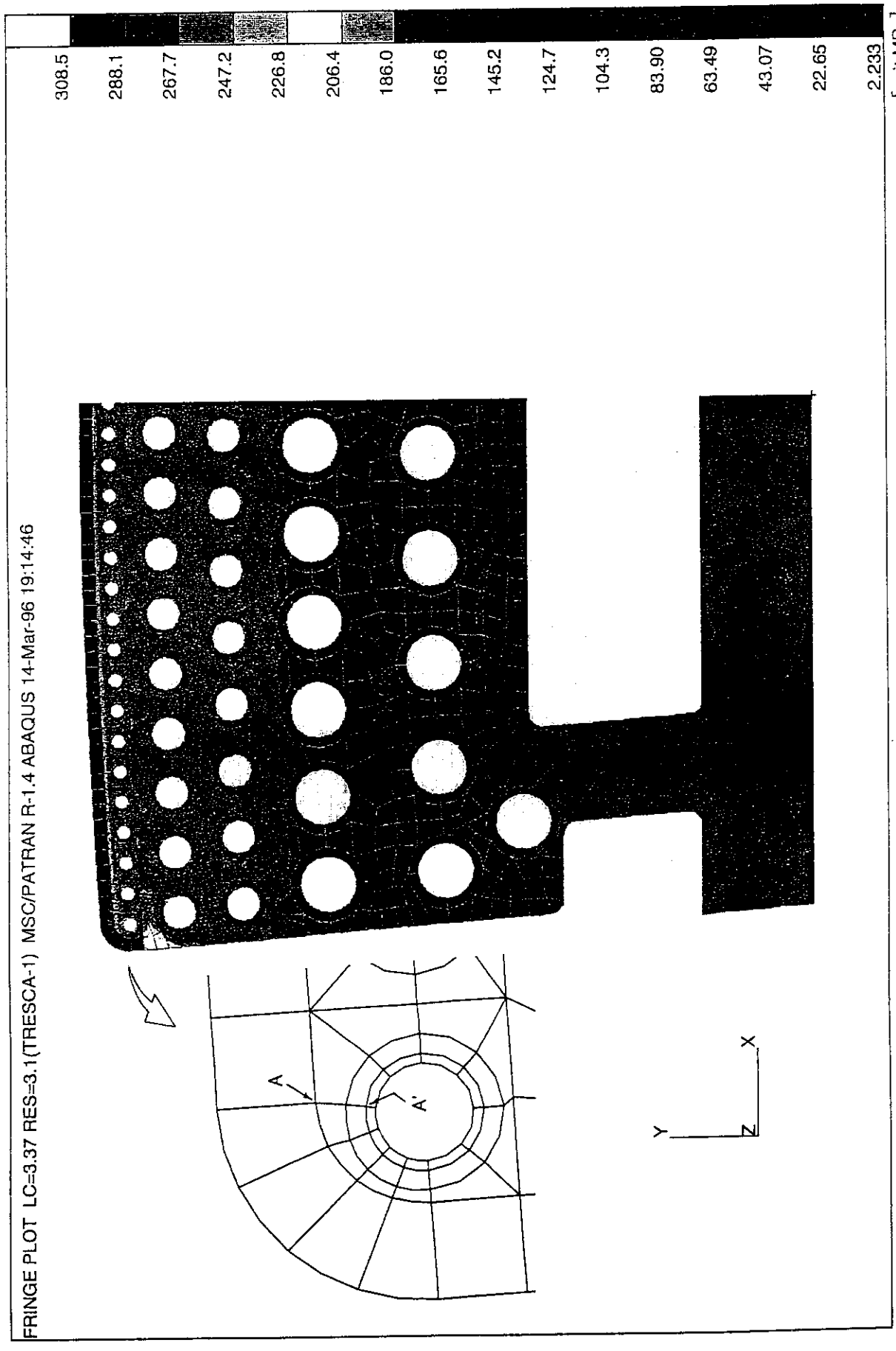

Fig. 3.2.2.19 Stress distribution (after48sec)

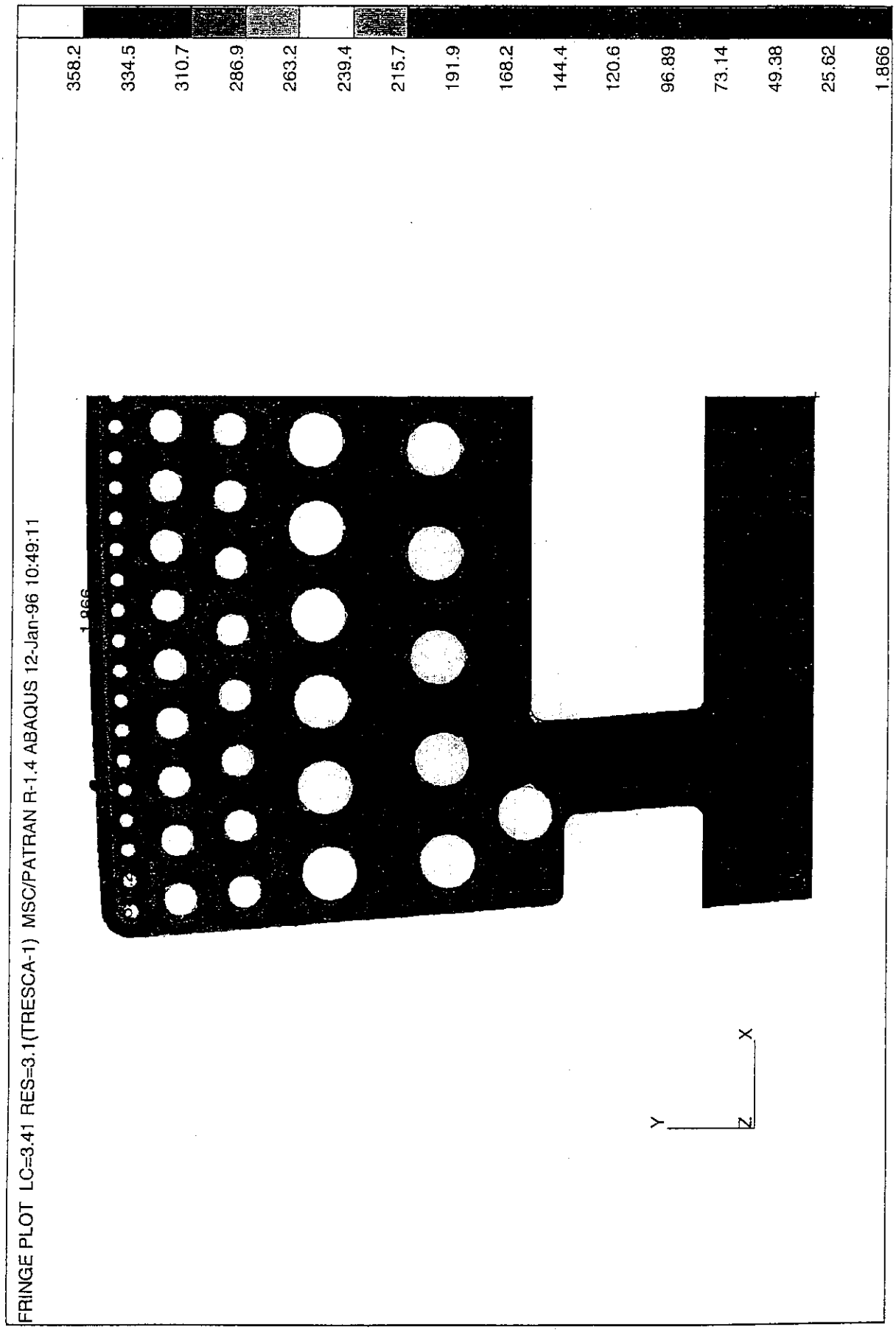

Fig. 3.2.2.20 Stress distribution (after 768sec)

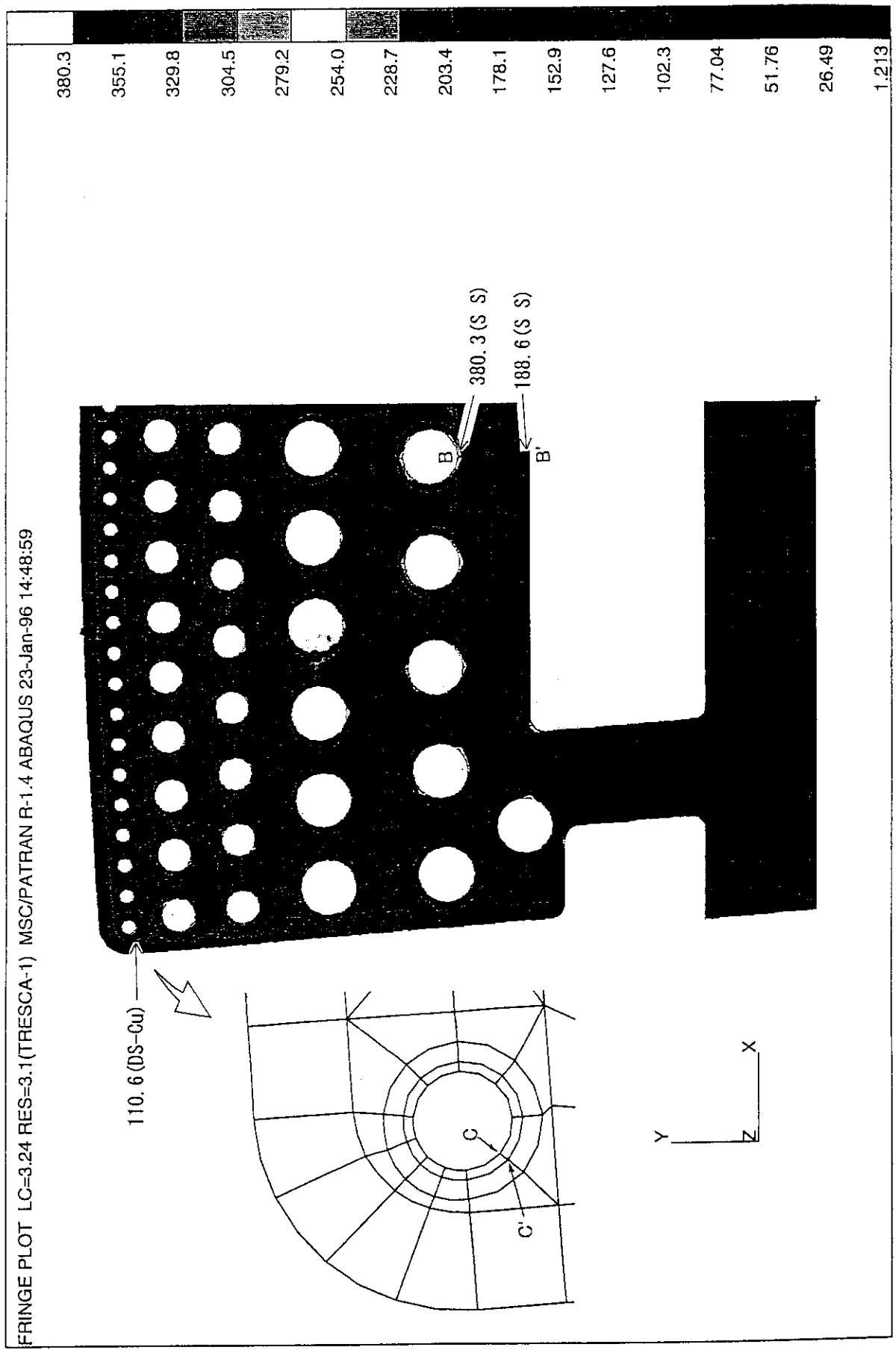

Fig. 3.2.2.21 Stress distribution (Steady State)

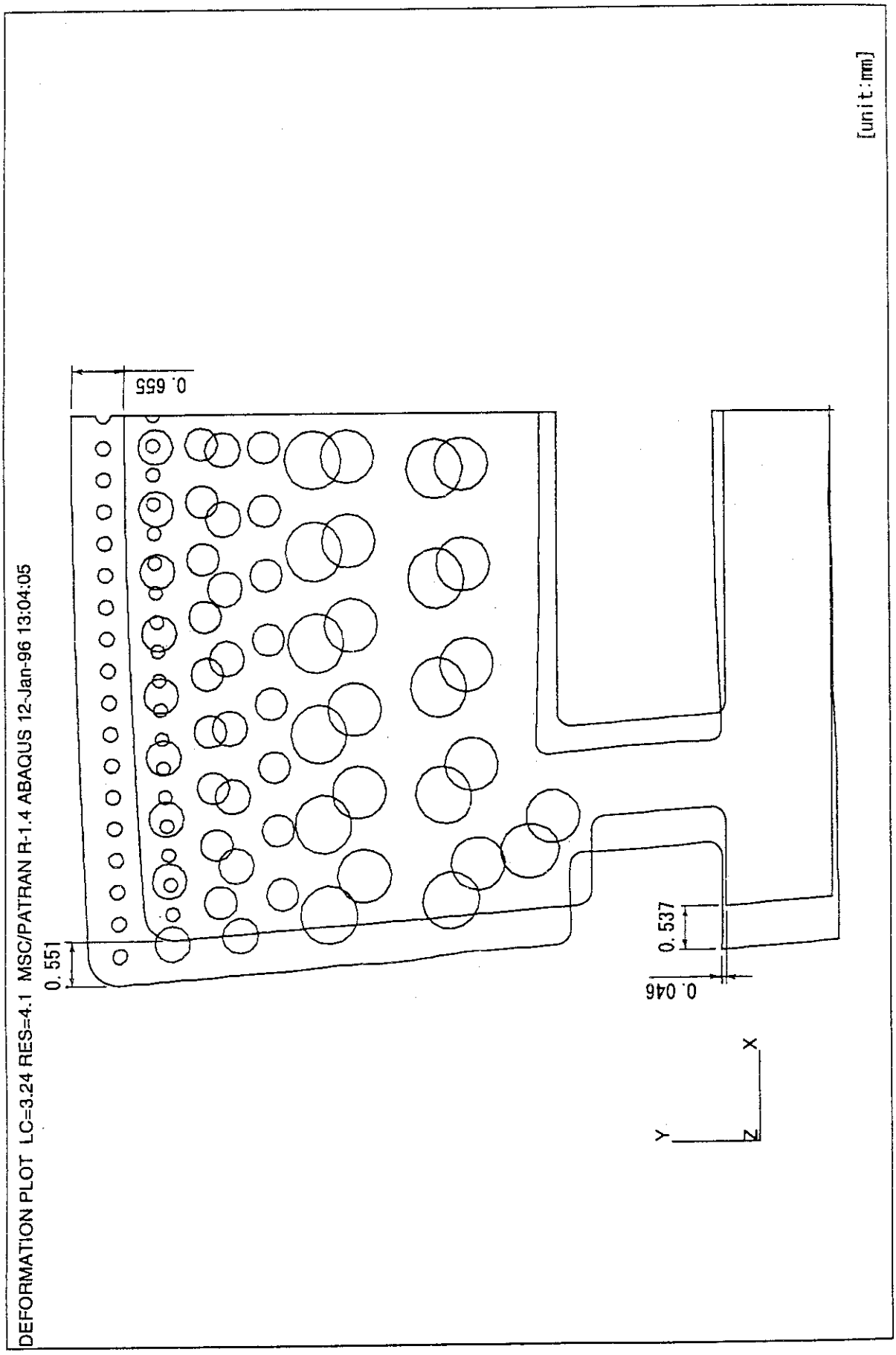

Fig. 3.2.2.22 Distortion (Steady State)

Table 3.2.2.1 Material properties for Berillium

Temp. (℃)	Conductivities (W/mK)	Specific heat (J/KgK)	Density (Kg/m^3)	Young's modules (Gpa)	Poisson's ratio	Thermal expansion (10^{-6}/K)
20	184.51	1807	1822	308	0.071	11.25
50	176.95	1901	1819	306	0.070	11.88
100	165.30	2046	1816	304	0.069	12.88
150	154.77	2176	1812	303	0.068	13.81
200	145.29	2295	1809	302	0.067	14.69
250	136.77	2401	1805	300	0.065	15.51
300	129.14	2497	1801	298	0.064	16.27
350	122.33	2583	1797	294	0.063	16.98
400	116.26	2660	1793	288	0.062	17.65
450	110.86	2729	1789	279	0.060	18.26
500	106.05	2791	1785	267	0.059	18.83
550	101.75	2847	1780	251	0.058	19.36
600	97.89	2898	1776	232	0.057	19.86
650	94.39	2945	1772	207	0.055	20.31
700	91.17	2989	1767	176	0.054	20.73
800	85.30	3071	1758	97	0.052	21.48

Table 3.2.2.2 Material properties for DS－Cu

Temp. (℃)	Conductivities (W/mK)	Specific heat (J/KgK)	Density (Kg/m^3)	Young's modules (Gpa)	Poisson's ratio	Thermal expansion (10^{-6}/K)
20	348.62	384	8860	134	0.343	16.84
50	344.90	389	8860	132	0.343	16.91
100	338.67	396	8860	128	0.343	17.03
150	332.43	402	8860	125	0.343	17.17
200	326.17	408	8860	121	0.343	17.32
250	319.89	413	8860	118	0.343	17.48
300	313.59	418	8860	114	0.343	17.66
350	307.27	422	8860	110	0.343	17.85
400	300.94	426	8860	106	0.343	18.06
450	294.58	429	8860	103	0.343	18.28
500	288.21	432	8860	99	0.343	18.52
550	281.81	434	8860	95	0.343	18.77
600	275.40	435	8860	91	0.343	19.03
650	268.97	436	8860	87	0.343	19.31
700	262.52	437	8860	83	0.343	19.60
800	249.56	436	8860	75	0.343	20.22

Table 3.2.2.3 Material properties for 316LN

Temp. (℃)	Conductivities (W/mK)	Specific heat (J/KgK)	Density (Kg/m^3)	Young's modules (Gpa)	Poisson's ratio	Thermal expansion (10^{-6}/K)
20	13.94	470	7961	192	0.3	15.94
50	14.37	476	7949	190	0.3	16.11
100	15.08	486	7930	186	0.3	16.40
150	15.80	497	7910	182	0.3	16.68
200	16.52	508	7890	178	0.3	16.95
250	17.24	518	7870	174	0.3	17.20
300	17.95	529	7849	170	0.3	17.45
350	18.67	539	7828	166	0.3	17.69
400	19.39	550	7806	161	0.3	17.91
450	20.10	560	7784	157	0.3	18.13
500	20.82	571	7762	153	0.3	18.33
550	21.54	581	7739	149	0.3	18.53
600	22.26	592	7716	145	0.3	18.71
650	22.97	603	7693	141	0.3	18.88
700	23.69	613	7669	137	0.3	19.05
800	25.12	634	7621	129	0.3	19.34

3.3 Fabrication Methods and Procedure

Figure 3.3.1 shows the poloidal segmentation of blanket modules. The curved module, No. 7, that would be one of the most complicated and difficult to be fabricated among the modules is representatively taken here for the investigation of fabrication methods and procedure. Horizontal and vertical cross-sections of the inboard midplane module, No. 4, are shown in Figs. 3.3.2 and 3.3.3, respectively. Though an internal configuration of the module No.7 is not designed in detail yet, it is supposed to be similar to that of the module No. 4, i.e. integrated first wall of SS circular coolant tubes embedded in DSCu heat sink with SS shield block containing drilled coolant channels.

For the fabrication methods, especially the joining of DSCu heat sink, SS coolant tube, SS plates in the first wall and SS shield block, so-called solid HIP, i.e. a HIPping of solid materials such as plate to plate or tube to plate, has been proposed.

Figure 3.3.4 illustrates individual parts of the first wall. Two DSCu plates (1 and 3 in Fig. 3.3.4) are machined to have semicircular grooves to meet SS coolant tubes (2 in Fig. 3.3.4) sandwiched by them. These DSCu plates and SS tubes are bent to meet the required first wall curvature. Short SS plates for top/bottom walls (4 in Fig. 3.3.4) are also machined to have semicircular grooves. A SS back plate of the first wall (5 in Fig. 3.3.4) is machined and bent to meet the DSCu plates and SS top/bottom plates. Then, these parts are assembled as illustrated in Fig. 3.3.5, and edges of SS parts, i.e. tubes, top/bottom plates and back plate, are seam welded.

Fabrication procedure of the shielding block is shown in Figs. 3.3.6 and 3.3.7. A SS block is drilled to have coolant channels of given arrangement, then bent to meet the required curvature. After the bending, support legs protruded from the back of the module and coolant collectors at module top and bottom are machined. Thin SS plates are welded by TIG welding to the collectors in order to provide sealed boundaries for HIPping. This shield block is assembled together with the first wall mentioned above. The assembly is canned by thin SS plates and HIPped. After the HIPping, the SS can is machined away. Cover plates of the first wall coolant manifold are joined by TIG welding. Then, the final machining is carried out.

Beryllium armor would be attached onto the first wall surface, possibly by solid HIP or brazing, after the HIPping of the shield block and first wall. A separate HIP process will be required for the Be armor as the HIP temperature will be different from that for

the HIPping of DSCu and SS. Further investigation needs for the attachment method and procedure for the Be armor.

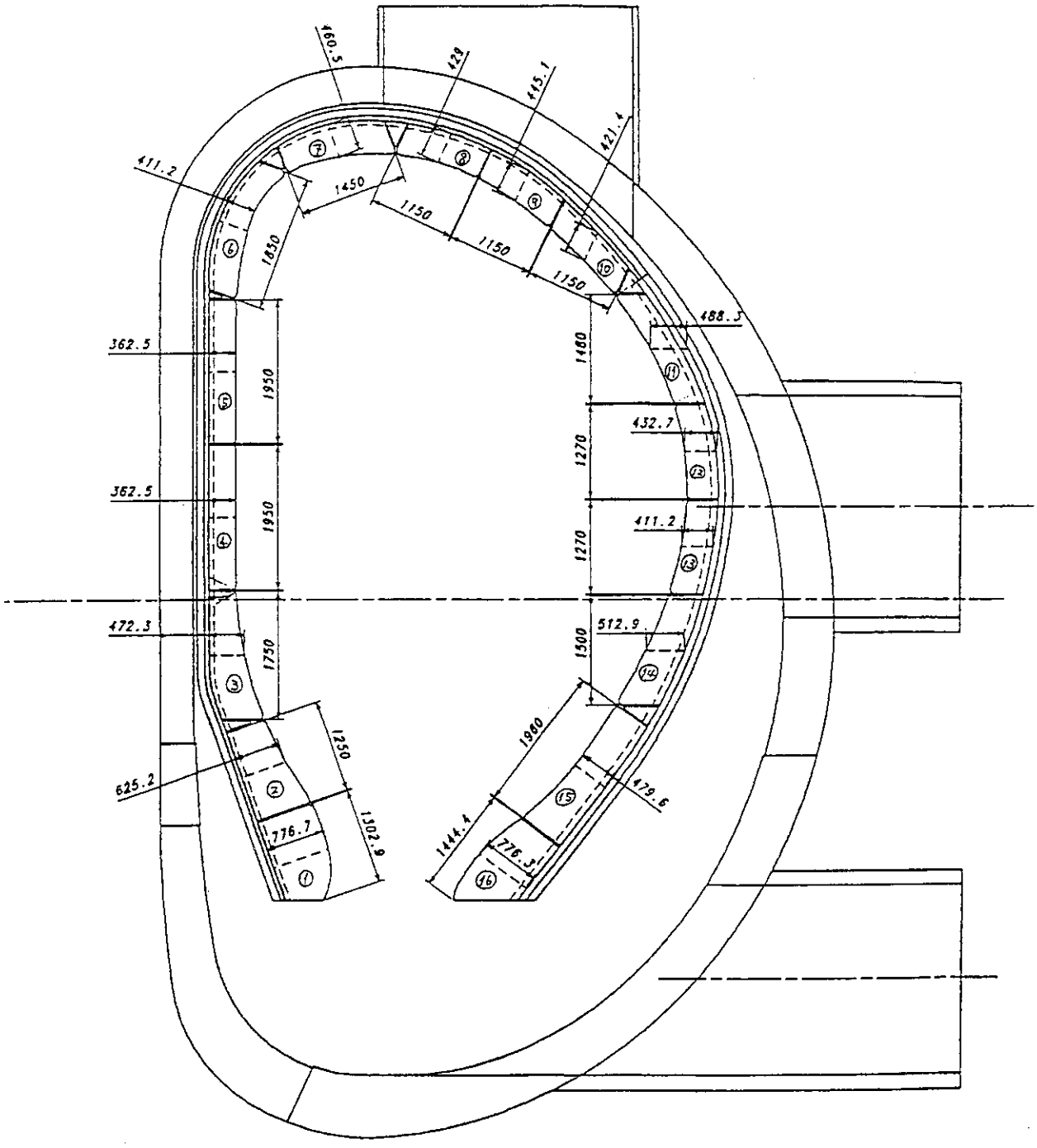

Fig. 3.3.1 Module Segmentation in Vertical Cross Section

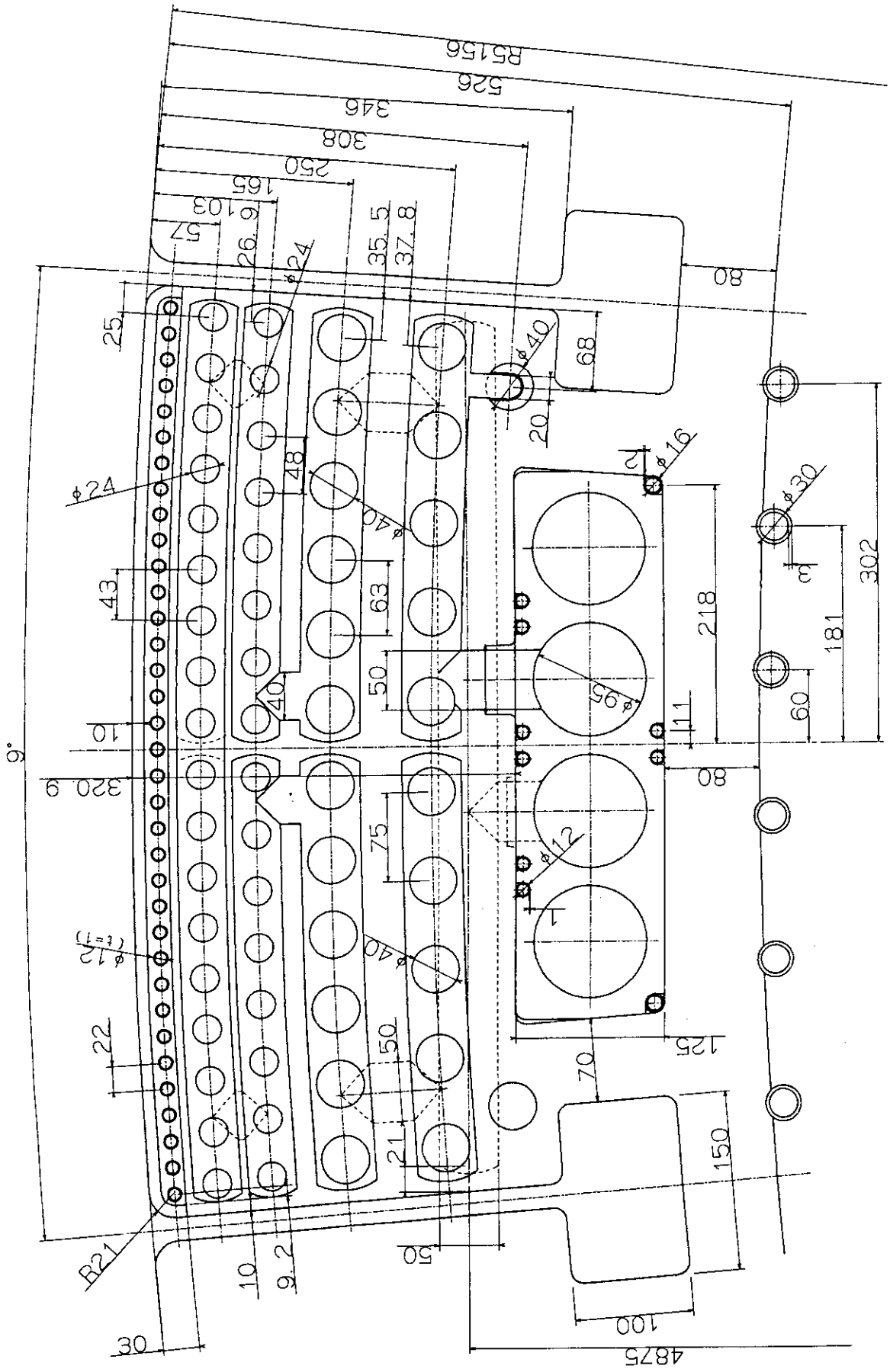

Fig. 3.3.2 A Cross Sectional View of the Inboard Blanket Module

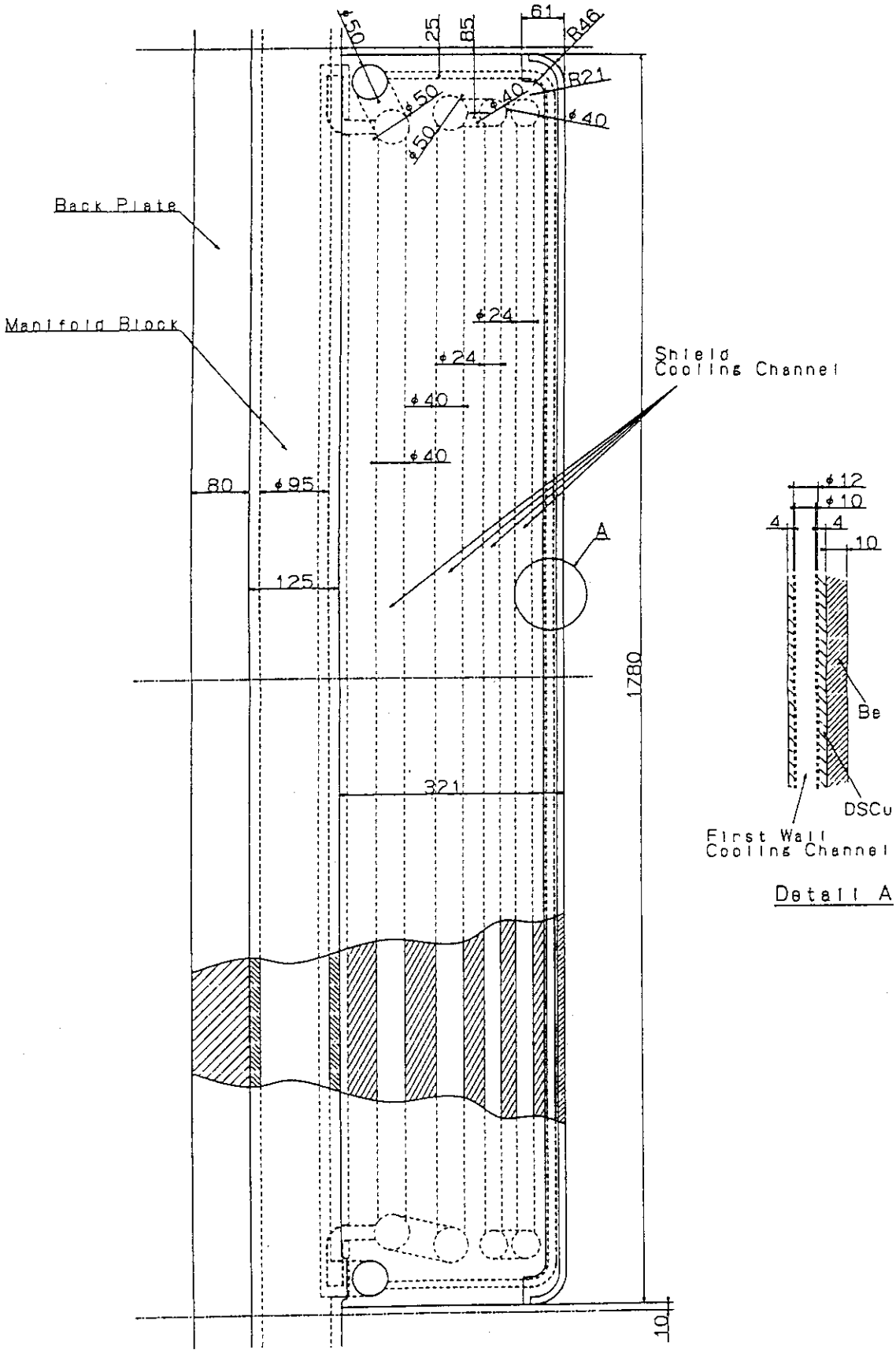

Fig. 3.3.3 A Lateral View of the Inboard Blanket Module

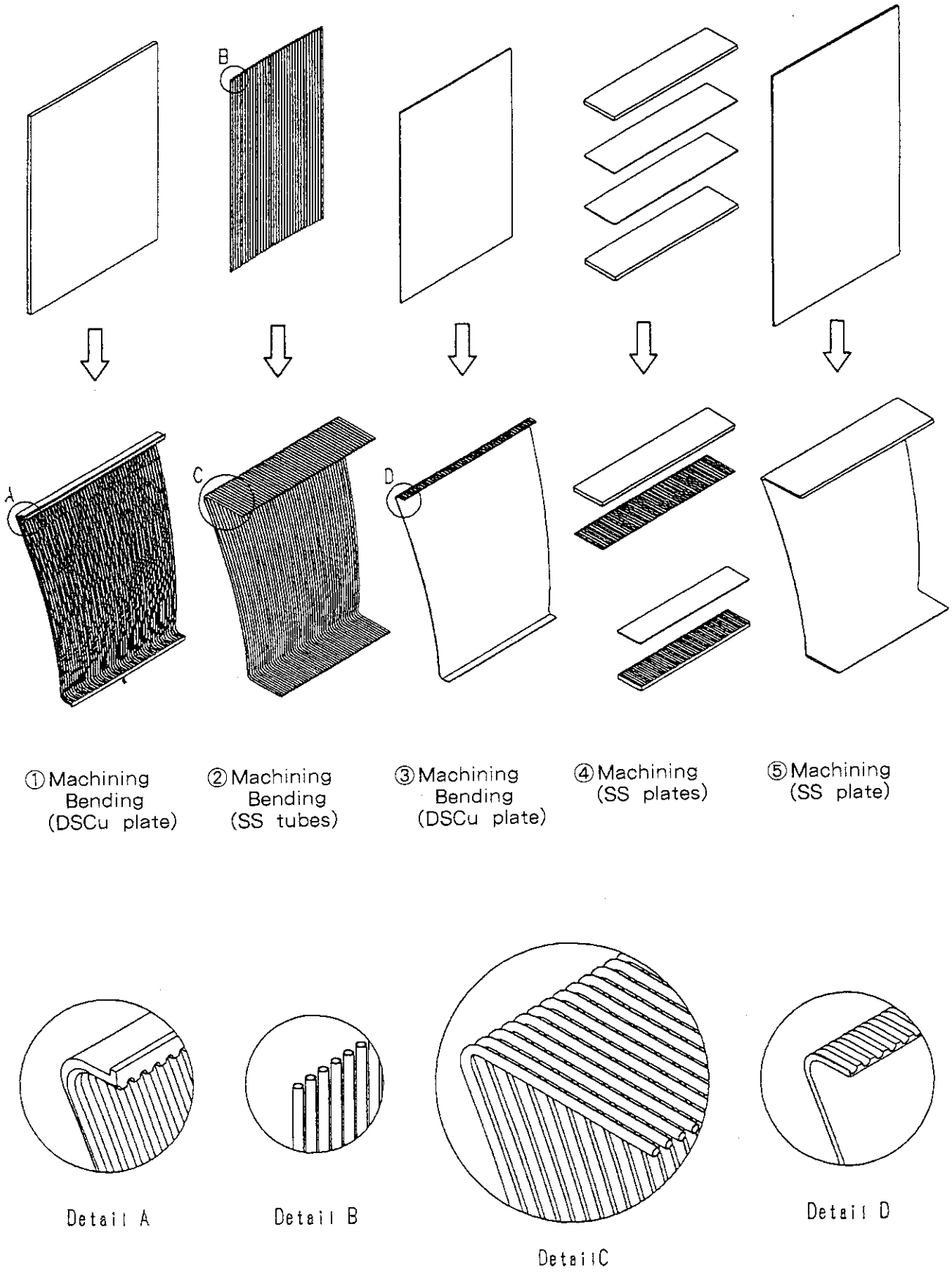

Fig. 3.3.4 Fabrication Procedure of the First Wall Parts for the Module No.7

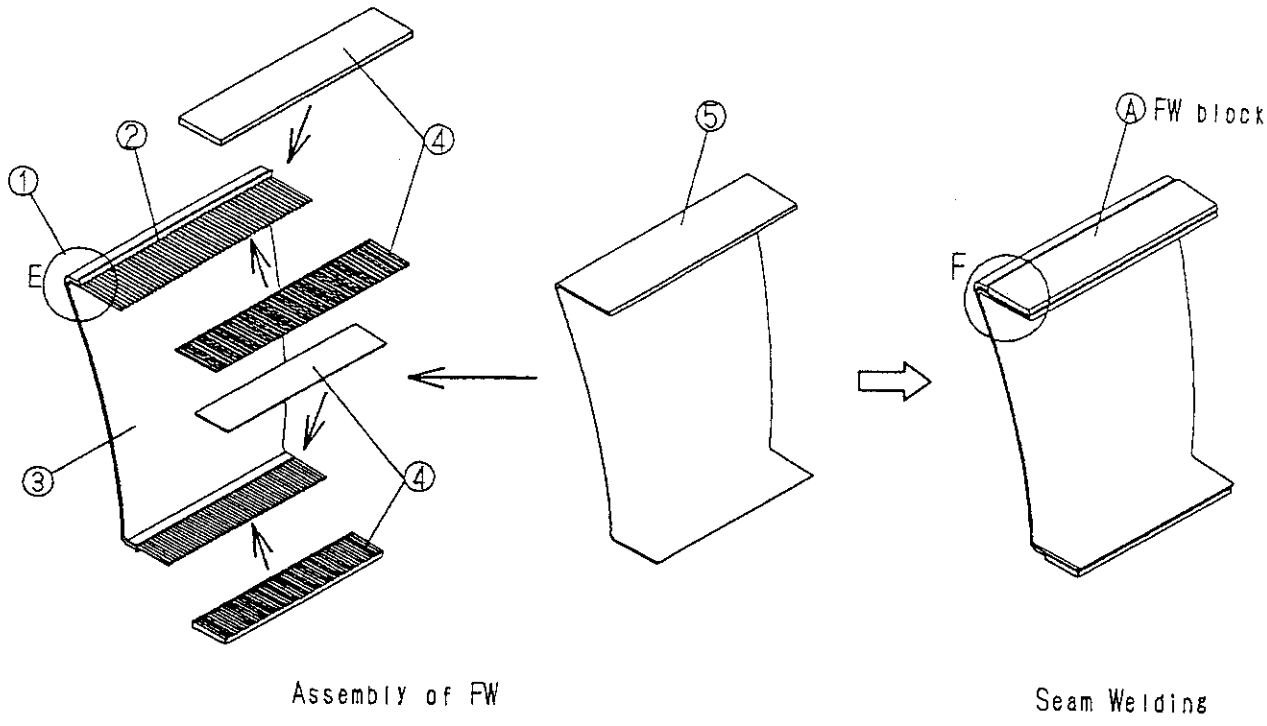

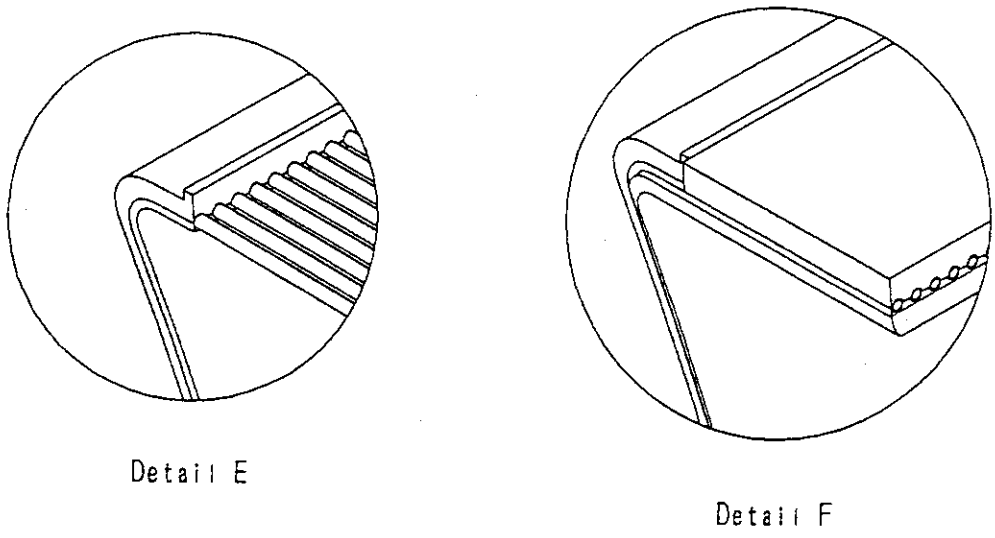

Fig. 3.3.5 First Wall Assembly for the Module No.7

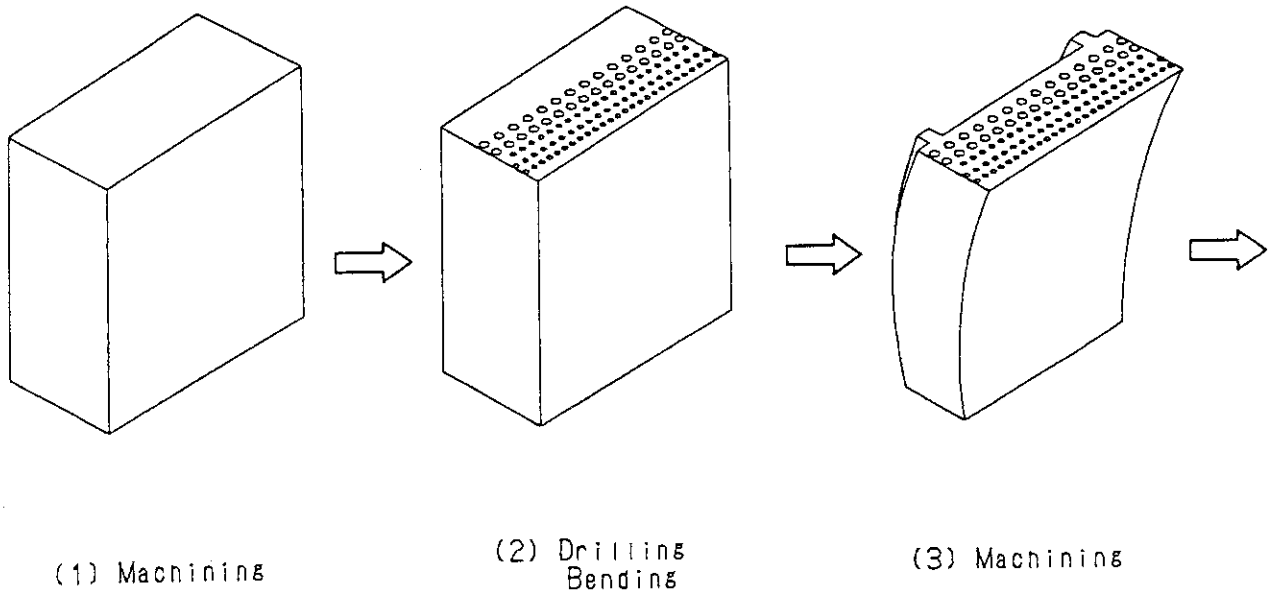

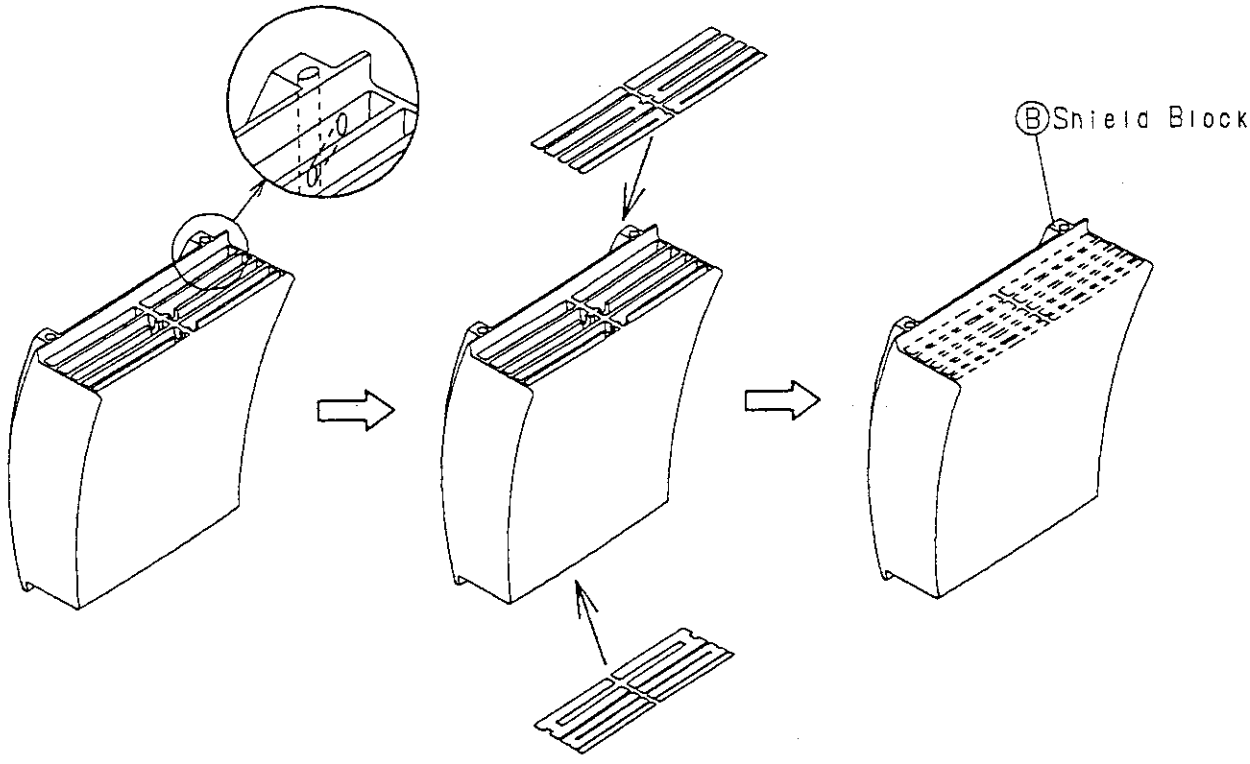

Fig. 3.3.6 Fabrication Procedure of the Shield for the Module No.7

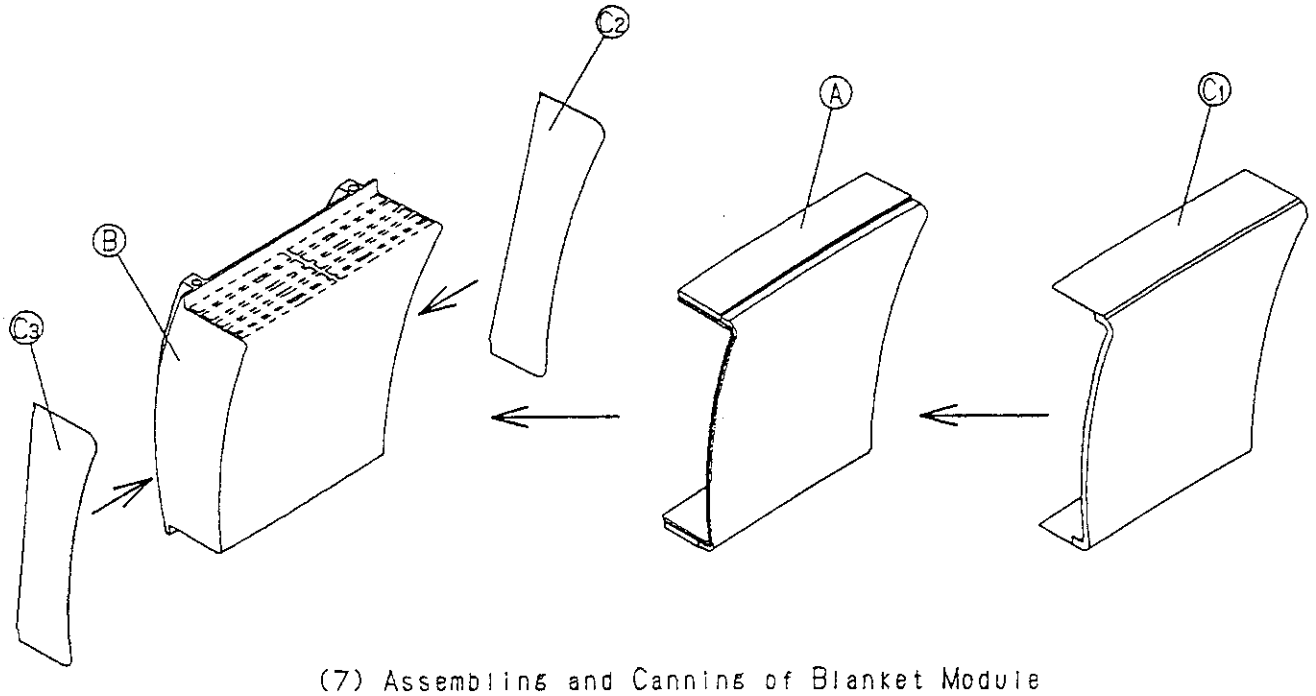

(7) Assembling and Canning of Blanket Module

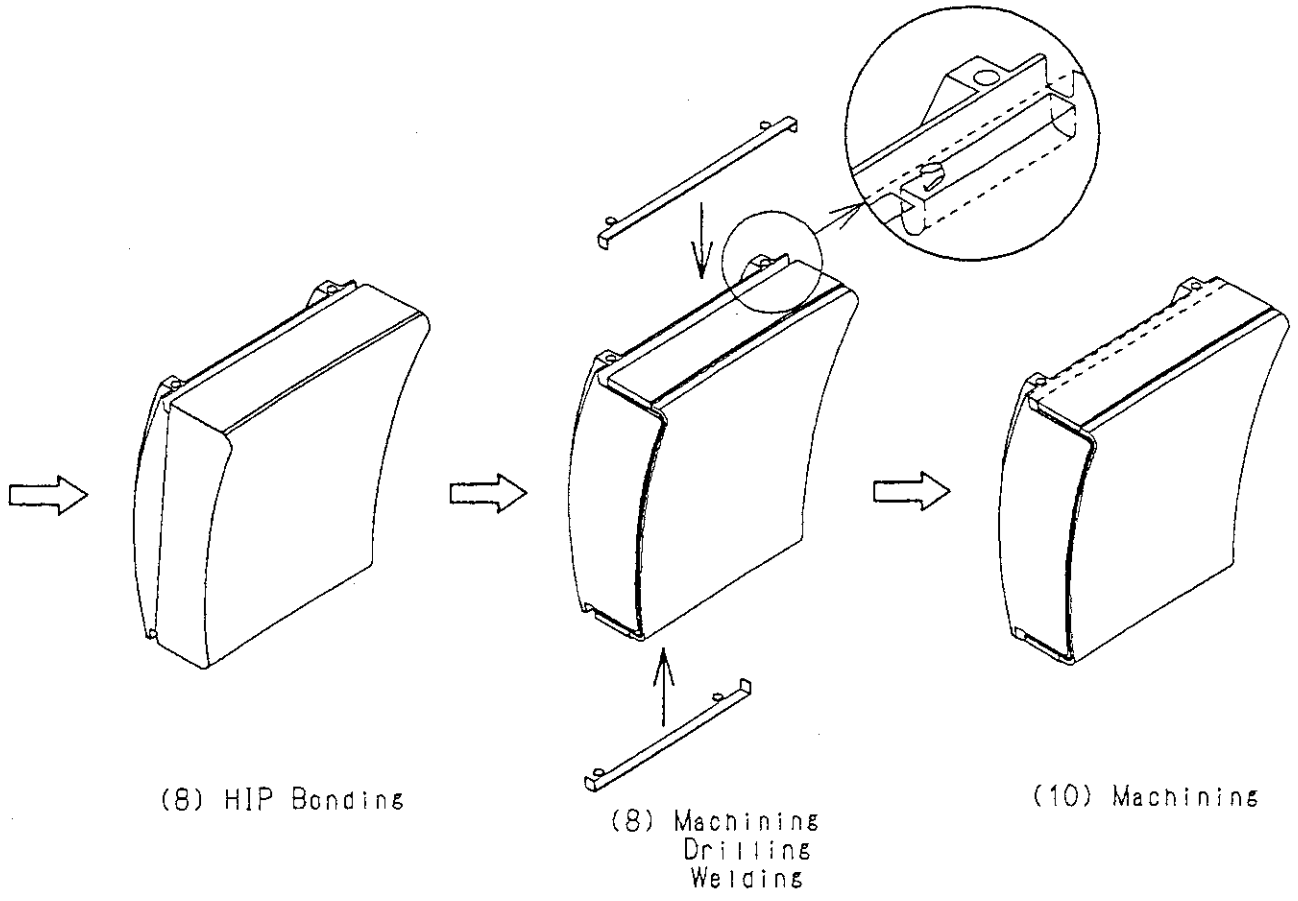

Fig. 3.3.7 Assembling for HIP and Fabrication Procedure After HIP Bonding for the Module No.7

4. Mechanical Design and Thermo-Mechanical Analyses of Separable First Wall

4.1 Concept of the separable first wall

First wall is a component with a potential risk of damage higher than the shielding blanket region because of a stronger interaction with plasma and likely localized heat and particle loads on it. Separable first wall, if it can be realized with a confident design, can reduce the weight of in-vessel components of frequent maintenance, Maintenance Class 1, and drastically relax a big burden onto the remote maintenance equipment and reduce the weight of the radwaste associated with the operation.

JA HT proposed two separable first wall concepts in 1994, and some feasibility studies were developed from the viewpoints of support concept, EM and structural analyses, and thermo-mechanical analysis. We tried to find a structural solution of mechanically-attached separable first wall concept, because it can maximize the advantage of the separable first wall from the maintenance viewpoint. Key points in the design of the separable first wall are 1) reduction of EM loads, 2) attaching concept to accommodate EM and thermal loads, and 3) cooling pipe connection to manifolds. As for the cooling pipe connection, internal-access YAG-laser pipe cutting/welding concept could be applied as the shielding module cooling pipe connection. Electrical insulation from the back plate or electrical breaks within the first wall is an idea to reduce the EM loads, but feasibility of the available electrical insulators under neutron irradiation conditions is questionable. So, basic approach we took was to minimize the weight (and the thickness) of the first wall so as to minimize the weight and EM loads on it during disruptions, and a concept with bolt-connection onto the front surface of the shielding block was considered. Schematic view of one of the proposed separable first wall is shown in Fig. 4.1.1. Two-dimensional thermal and mechanical analyses were conducted to define the number and the dimension of the attaching bolts and to examine the temperature/stress distributions. Detailed information is given in 4.2, and it was found a huge number of M10 bolts were needed to accommodate both of the out-of-plain EM loads and heat loads, which seems quite uncomfortable from the reliability and maintainability viewpoints.

Another concept of mechanically-supported separable first wall was proposed by the JCT during 95-Feb. blanket meeting. It had a feature that the separable

first wall surrounds the shielding block on the top, front surface and the bottom surfaces of it, and is self supporting against the out-of-plain (pulling) EM loads with a thickness of around 10 cm, while shearing EM loads are supported by mechanical locking against the manifold block and the ribs extruding from the back plate. This concept is schematically shown in Fig. 4.1.2. Basic idea of this concept was to reduce the shearing EM loads by eliminating (or minimizing the poloidal length, in reality, of) the side walls of the separable first wall, and to apply mechanical locking as far from the plasma as possible so that thermal and neutron irradiation conditions could be relaxed.

In accordance with the requirement from the JCT, feasibility of this concept was extensively examined. EM and structural analyses were conducted to examine the effect of eliminating the side walls on the magnitude and distribution of the EM loads and on the structural responses. Analyses results, whose detailed information is given in 4.3, showed that a large eddy current was still induced in the first wall through the attaching region and drastic reduction of EM loads onto the first wall was not expected. Furthermore, a peaked distribution of the out-of-plain EM loads on the first wall caused a very large pulling force onto the bolts located at the extremity, which made this design more difficult.

Feasibility of a mechanical locking concept was also examined based on the experiences in JT-60 and the other industrial experiences. Not only for the separable first wall but for the shielding blanket module integrated with the first wall, the JCT has proposed to apply mechanical locking with a number of bolts. But there are a number of fatal concerns on this kind of supporting concept. Mechanical locking has been widely utilized in other industry areas and also in fusion experimental machines. Mechanical locking usually has a geometry as simple as possible, and high dimensional accuracy must be assured by precise machining at factory followed by assembling at factory or on site. Besides it, application of adjustable insertions such as very thin shims, cotters or sleeves is a usual practice to assure a good contact of the mechanical locking.

Tokamak machine is a heavy electrical machine, and large eddy current could be induced in the in-vessel components. So, much attention has been paid on the electrical connection between two components in the process of the design, fabrication and assembly for the past and currently operating tokamak machines. Reliable support without any small clearance gap is essential, and

reliable electrical connection or reliable insulation is a usual practice to assure an electric circuit or to beak reliably the electric circuit, respectively. The mechanical locking concept proposed by the JCT requires a very precise in-situ machining up to an order of 100 μm, after welding the back plate, to get a reliable mechanical locking, but such a machining seems non-realistic due to a limited stiffness of the base or the component itself and also limited space available. Seizing and sticking of the mechanical locking are also concerns under the anticipated load and environment conditions, and it seems very difficult to demonstrate the feasibility by means of a simple set of R&D's.

Bolt connection has also serious concerns. Temperature and stress of the bolts would be excessive even if non-code-relevant special alloy like Inconel 718 is applied. Seizing or sticking due to cyclic heat load, relaxation due to heat load, fatigue and irradiation creep, and periodic maintainability of a huge number of bolts are also serious concerns. Bolts should be designed not to apply shear loads on them, but it could not be guaranteed against lateral movement of the first wall.

In conclusion, we have never reached a reliable concept of the mechanically attached separable first wall, though very ideal if realized. Different approaches were examined; 1) Combination of mechanical locking and welding for the separable first wall, 2) Welding attachment for both of the separable first wall and shielding block, and 3) Welding attachment for the shielding module integrated with the first wall, and through the feasibility study, we have proposed to follow 3) approach from the viewpoints of attachment reliability and higher possibility to demonstrate its feasibility through R&D's.

4.2 Thermal analysis

The concept is shown in Fig. 4.1.1. The separable first wall is attached onto the shielding block by SS316 M10 bolts with toroidal and poloidal pitches of 132 mm and 40 mm, respectively. Accommodation to surface heat flux of 0.5 MW/m2, neutron wall load of 1 MW/m2, and out-of-plain EM loads of 1.5 MPa was considered. This separable first wall panel has a built-in-type cooling channels made by SS316 with a thickness of 2 mm and a cross section of 5 x 10 mm2. A Beryllium plasma facing layer of 5 mm, a Cu-alloy heat sink layer of 5 mm and a SS316 rear wall of 3 mm were assumed. Poloidal cooling flow scheme was applied with top/bottom headers.

A series of two dimensional thermal and stress analyses were conducted to examine the temperature and stress distribution, especially at the location around the attaching bolt. Analysis model and boundary conditions are shown in Figs. 4.2.1 to 4.2.3. Typical results on the temperature and Tresca stress distributions are shown in Figs. 4.2.4 and 4.2.5, respectively. Maximum temperature at the top of the SS316 bolt was found less than 400°C and the peak stresses at the first wall and at the root of the bolt were 329 MPa and 408 MPa, respectively. Though the temperature and stress ranges were within the acceptable values, design activity on this concept was stopped because of the reasons mentioned in 4.1.

4.3 Stress analysis and deflection

Extensive EM and stress analyses were conducted on the separable first wall concept proposed by the JCT. Three-dimensional FEM model for the EM loads analysis (Code: EDDYCAL) is shown in Fig. 4.3.1. It consists of the separable first wall, shield block, back plate and the vacuum vessel (7.5° model in the toroidal direction), and no electrical connection was assumed between the separable first wall and shield block and between two adjacent separable first walls. The separable first wall is assumed 10-mm-thick copper plate. Zoomed-up views showing the induced eddy current distributions in the separable first wall, shield block and the back plate located at the inboard midplane are shown in Figs. 4.3.2 to 4.3.4, respectively. No large reduction of EM loads was observed. And, eddy current components flowing along the side wall of the separable first wall and going up and down on the first wall can be seen in Fig. 4.3.2, which leads to peaked out-of-plain EM loads on the first wall. Resultants EM loads are summarized in Fig. 4.3.5, which are almost the same as those for the case of the integrated first wall, as shown in Fig. 4.3.6.

In the stress analysis, two types of attachment between the separable first wall and the back plate and between the shield block and the back plate were considered, bolt and welding connection. For the welding option 45-mm-thick plate was assumed, while M20 fixing bolts were used for the bolt option. The numbers of the fixing bolts were eight and twenty two for the separable first wall and the shield block, respectively. The analysis models and boundary conditions are shown in Figs. 4.3.7 and 4.3.8 for the bolt and welding options, respectively. Shell elements were used for all of the components (Code: MSC/NASTRAN), while contact stiffness between the shield block and the

separable first wall were modeled with spring elements, manifold blocks were represented with radial and toroidal spring elements and shear elements, and bolts and shear keys were represented with beam elements and shear elements. Zoomed-up analysis was conducted with the results obtained by the previous overall analysis.

Overall deformation of the inboard midplane module is shown in Fig. 4.3.9 with a maximum value of around 3 mm. Typical results showing the Von mises stress distributions are shown in Figs. 4.3.10 to 4.3.13 for the separable first wall, support ribs (legs), back plate and the keys, respectively., and are summarized in Table 4.3.1. Large tensile loads exceeding 500 MPa on the bolts attaching the first wall can be seen in this Table.

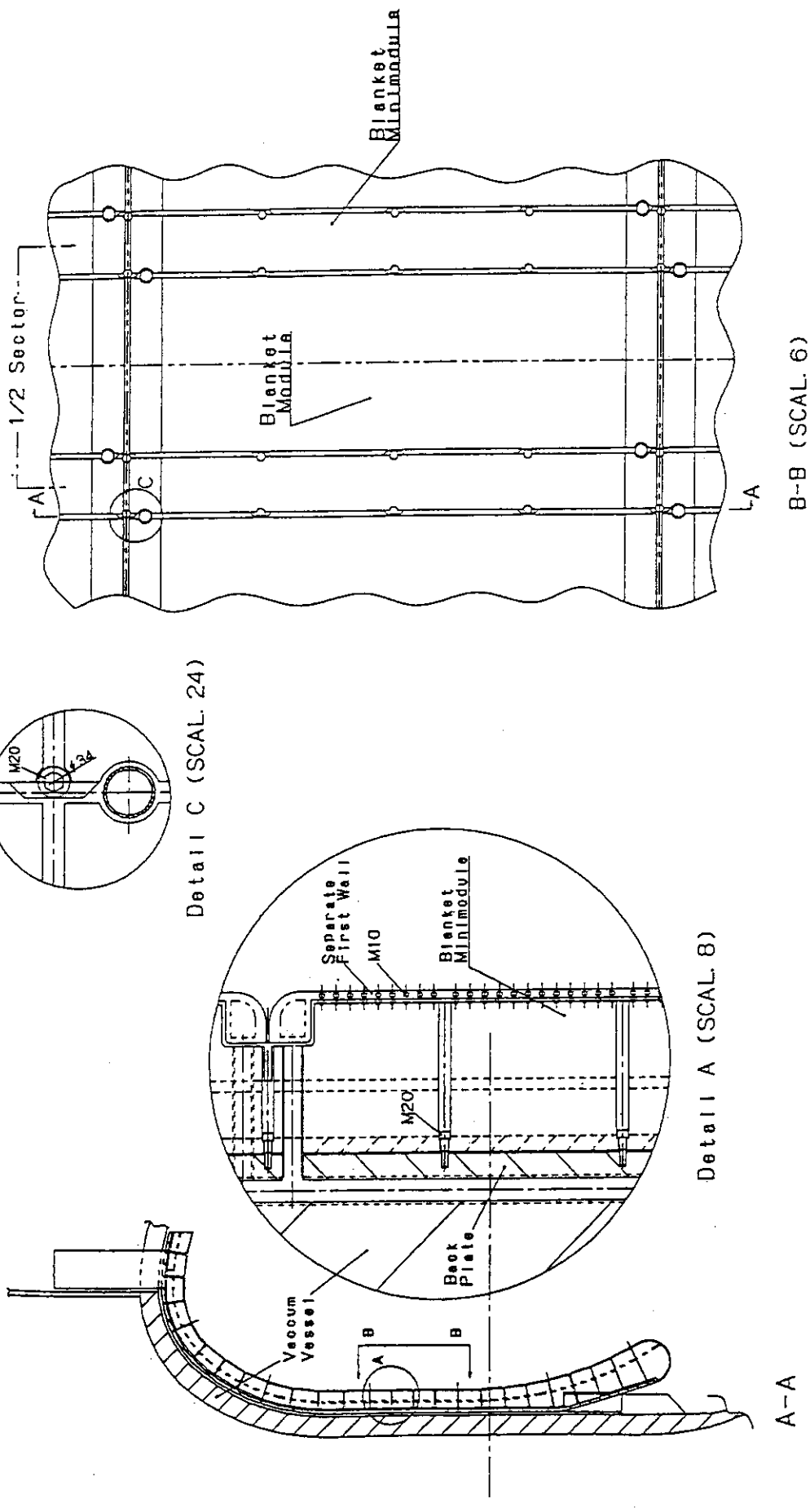

14R50100HA029-01

Fig. 4.1.1 Shield Blanket Integrated Back Plate with Separate First Wall

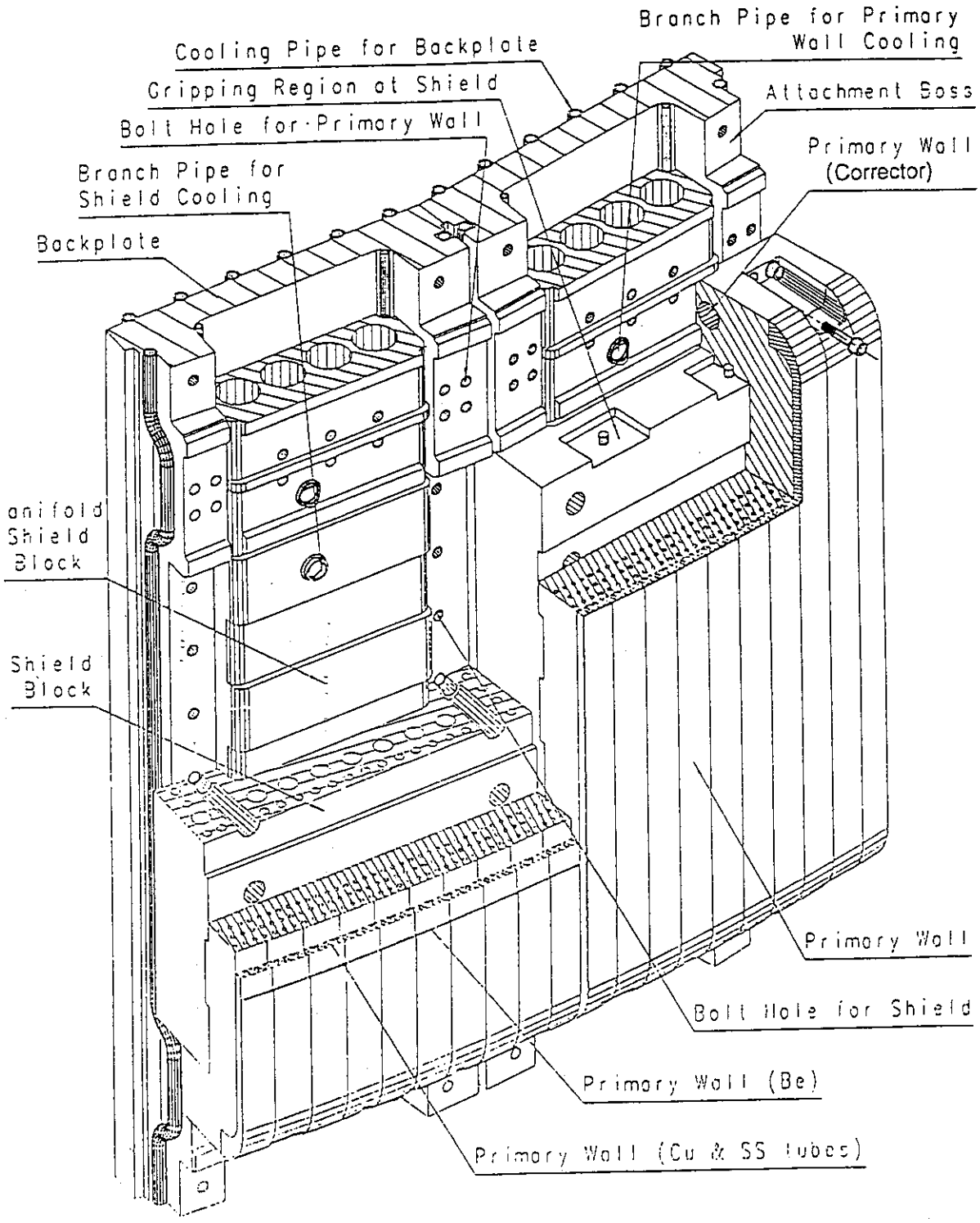

Fig. 4.1.2 Shield Blanket System Concept

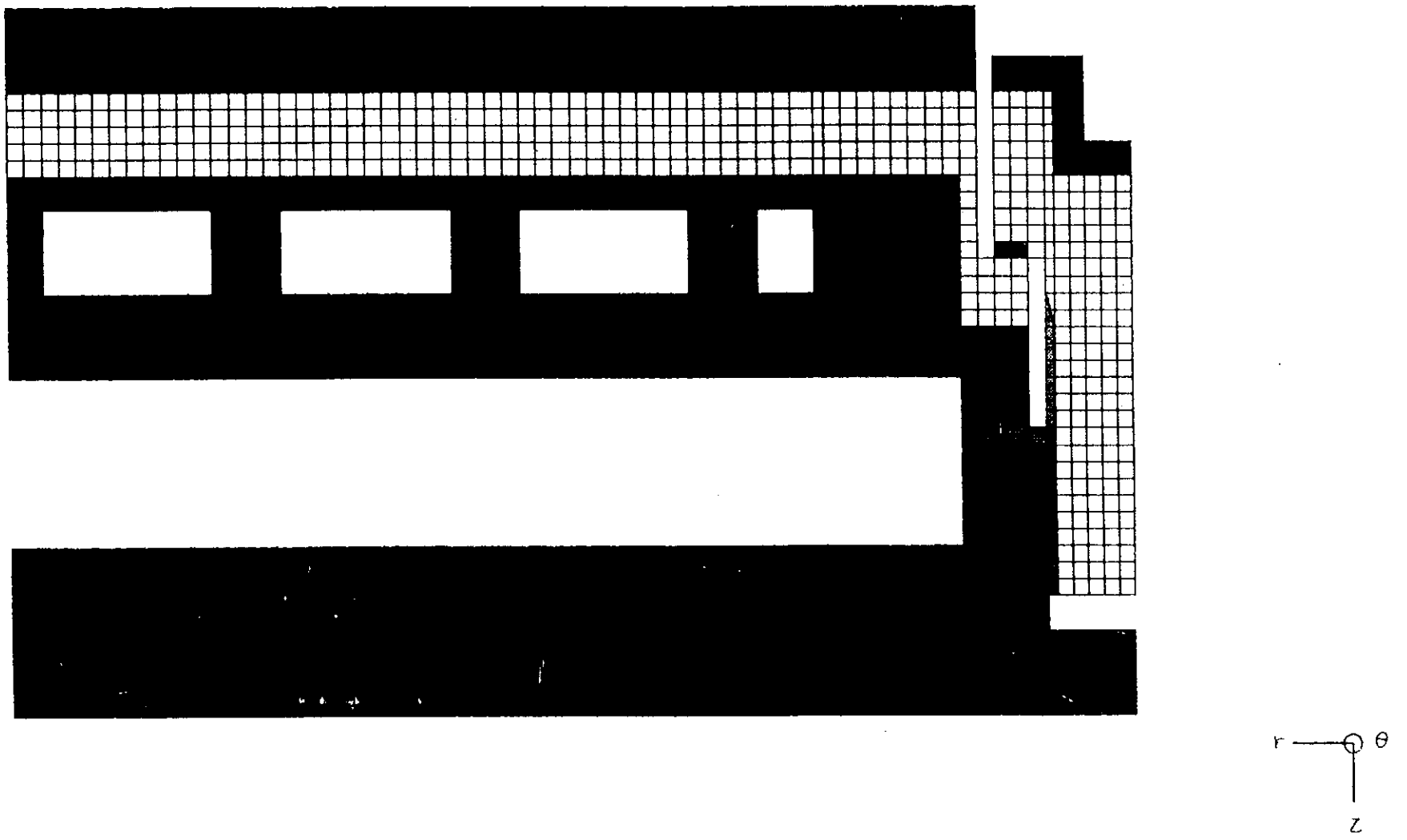

Fig. 4.2.1 Axisymmetric FEM Element Mesh for Temperature Distribution Analysis of Bolt

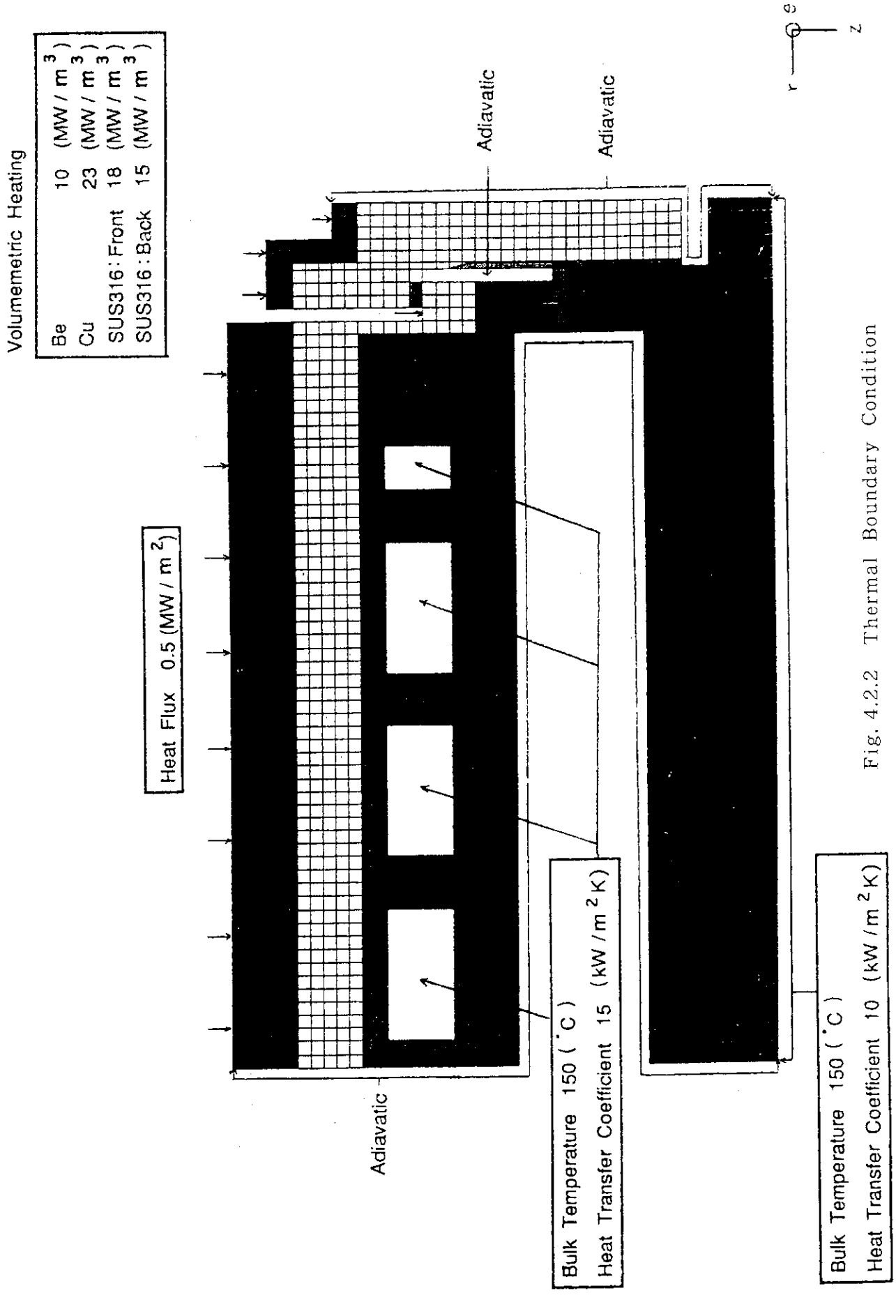

Fig. 4.2.2 Thermal Boundary Condition

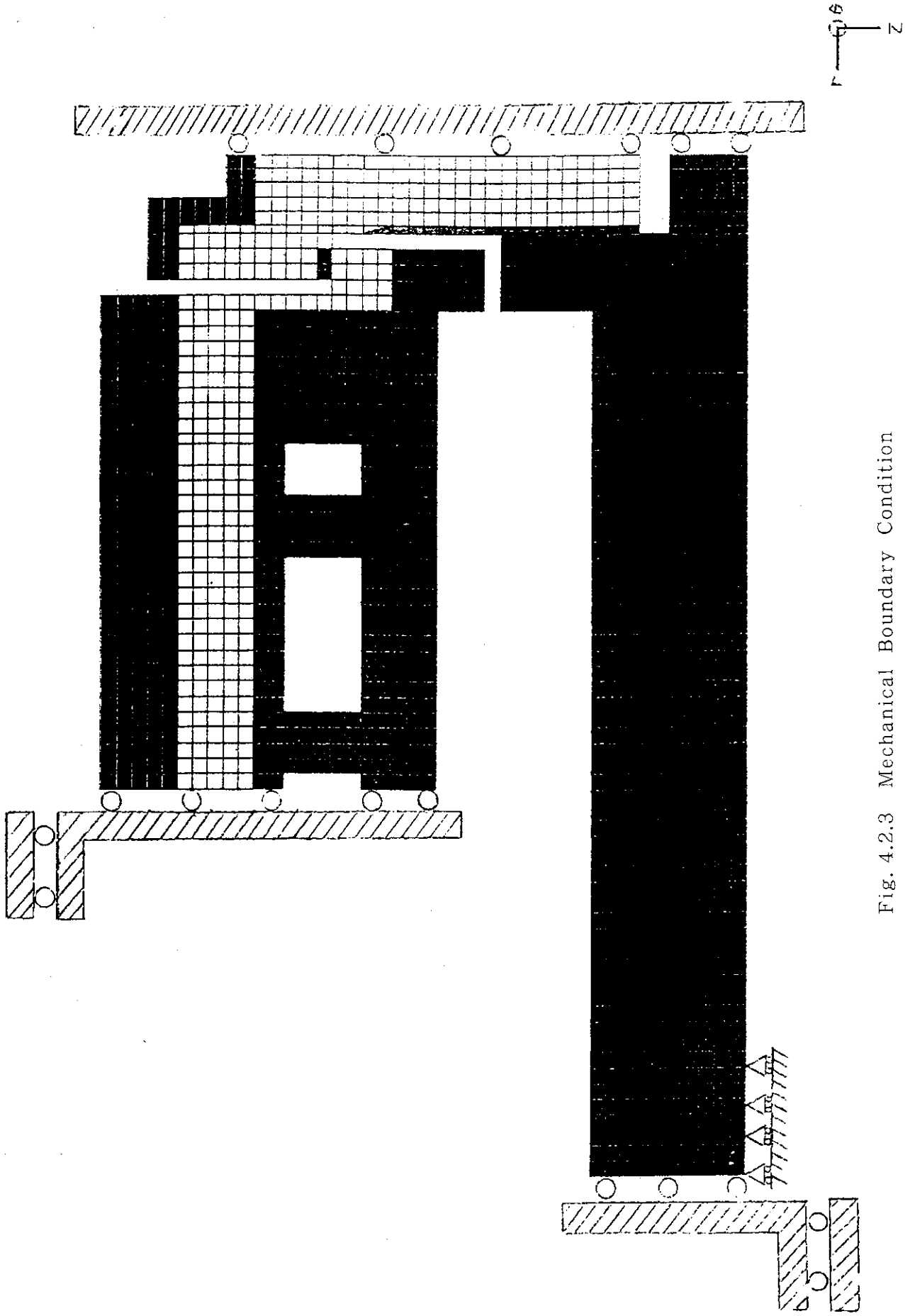

Fig. 4.2.3 Mechanical Boundary Condition

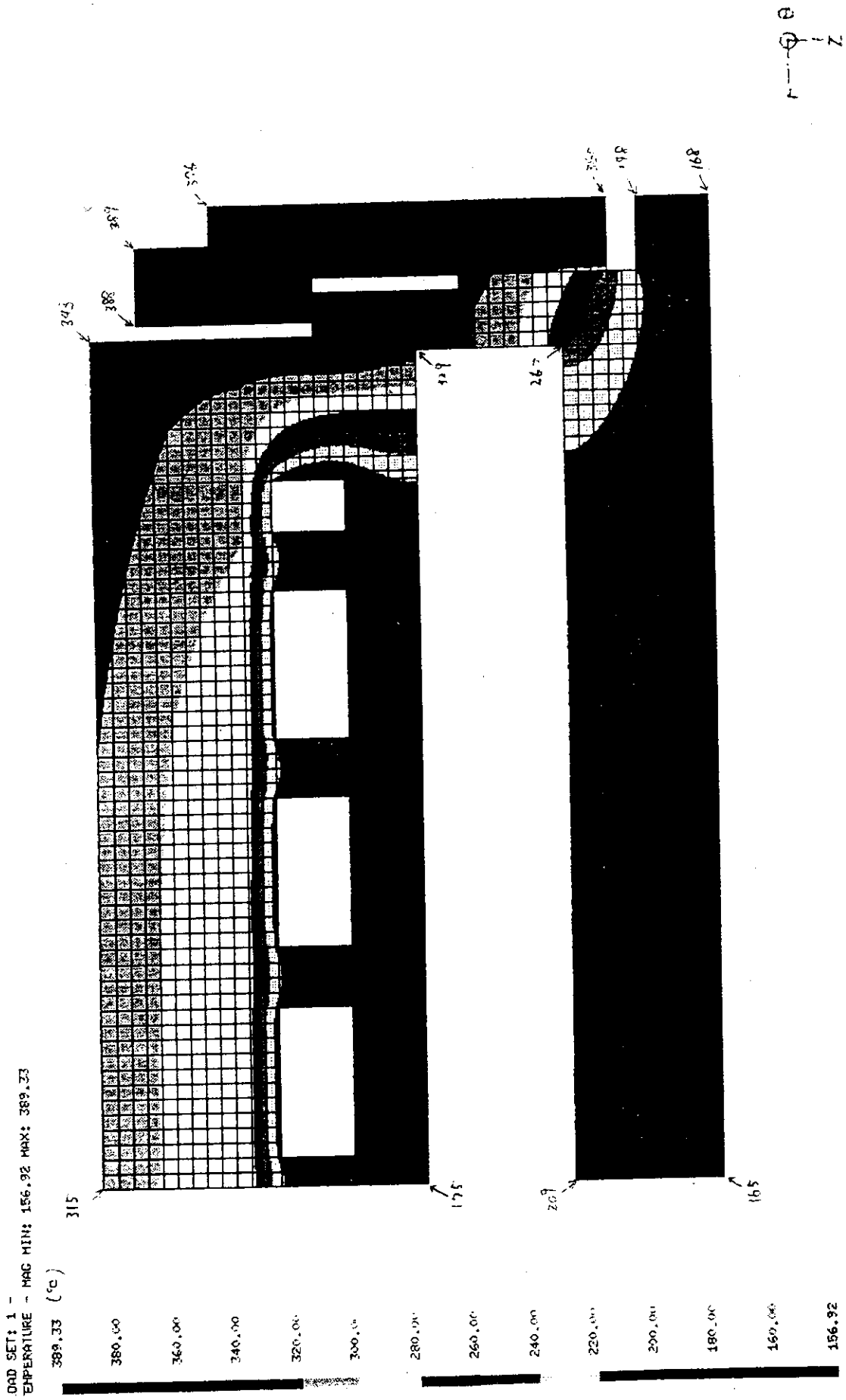

Fig. 4.2.4 Equivalent Temperature Distribution of Bolt

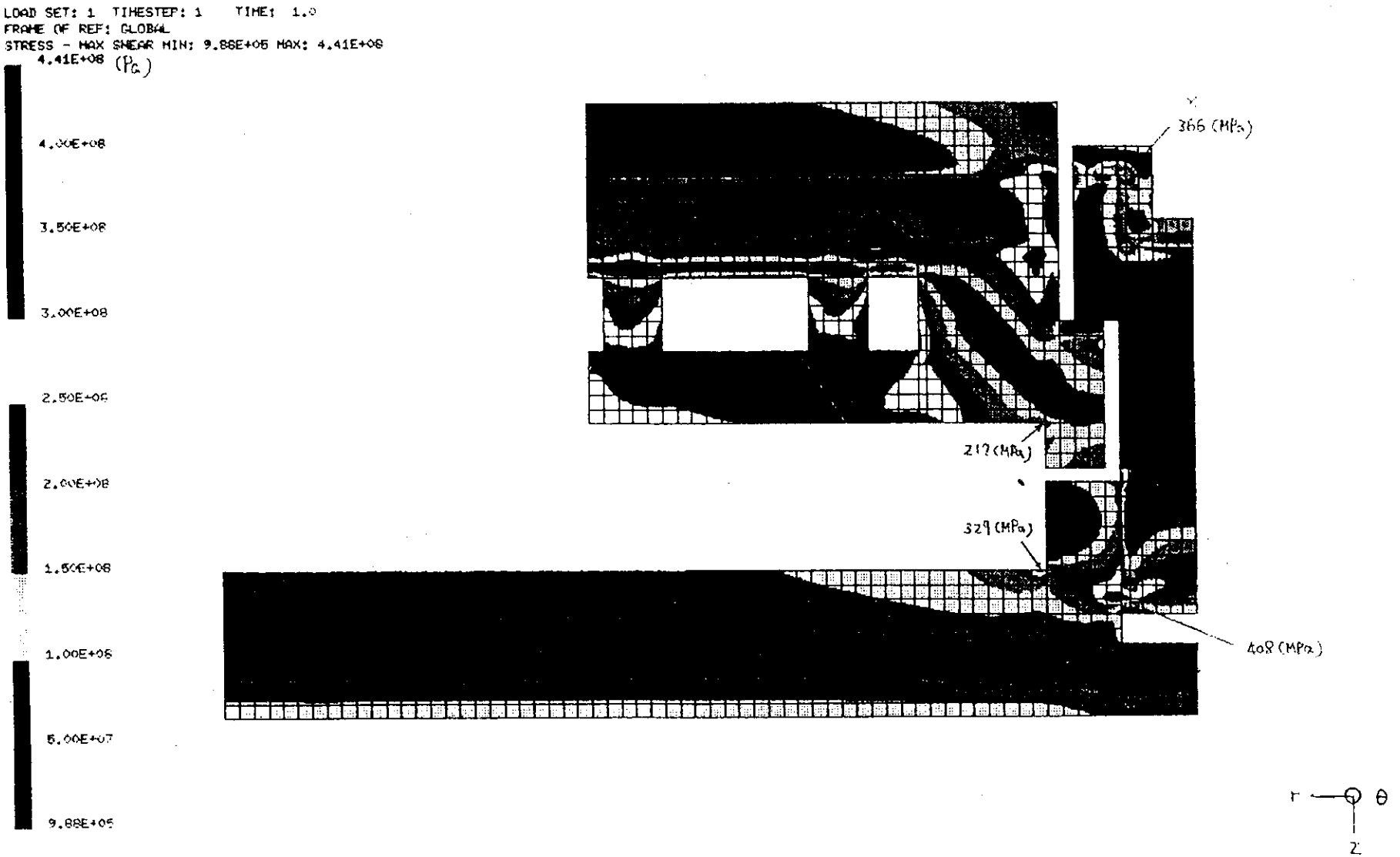

Fig. 4.2.5 Tresca Stress Distribution of Bolt

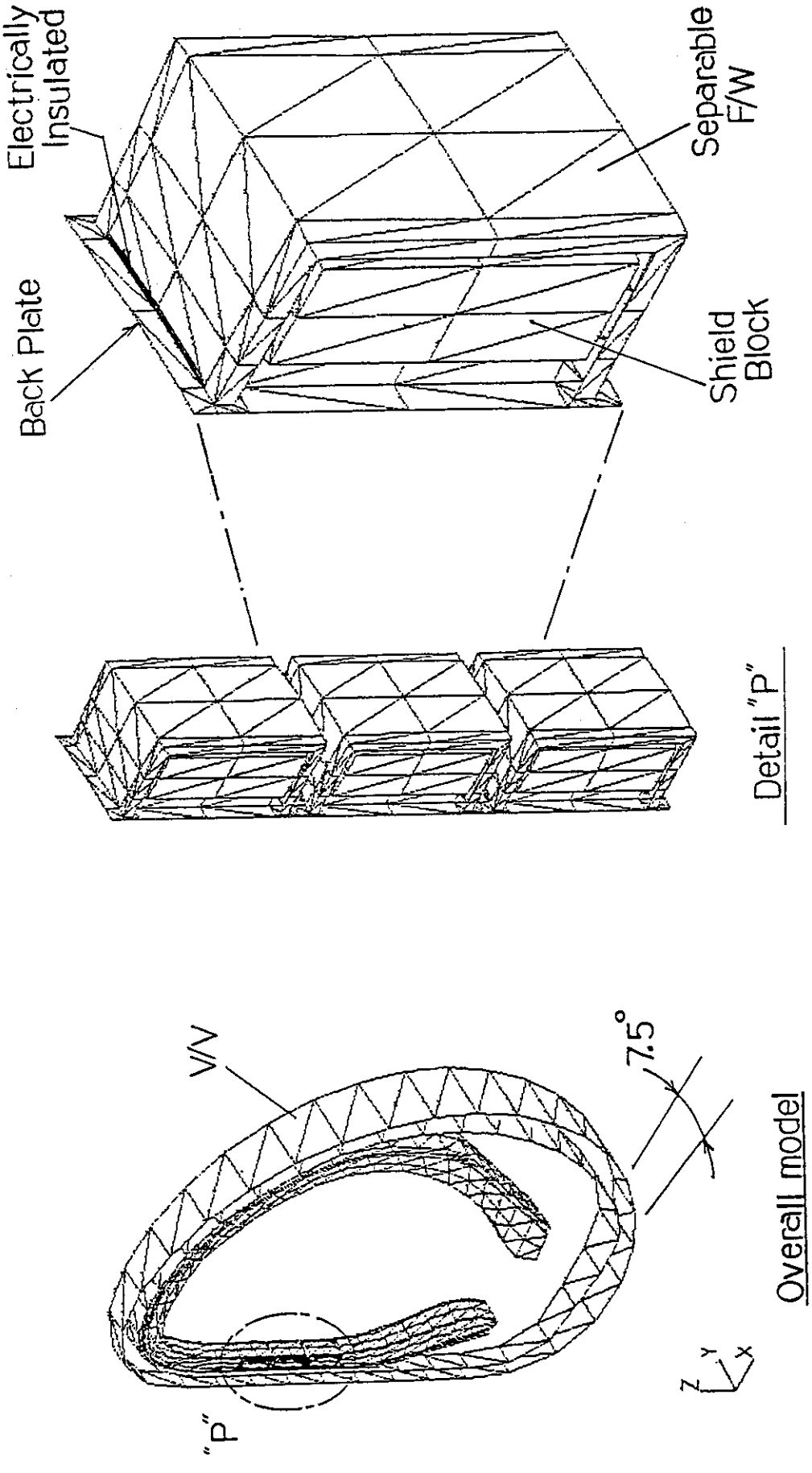

Fig. 4.3.1 Electromagnetic analysis model of blanket structure.

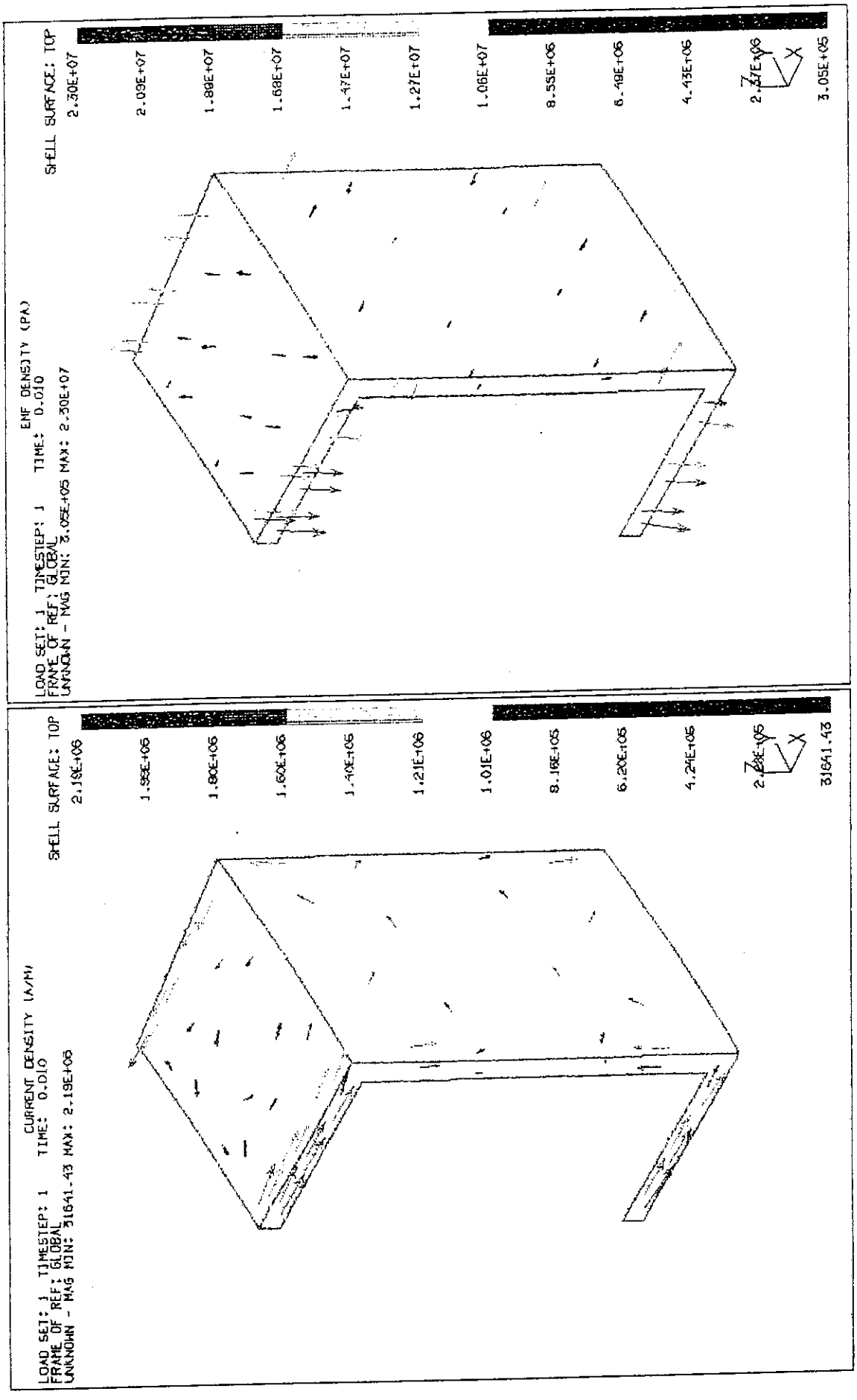

Fig. 4.3.2 Eddy current and EM force distributions on separable first wall in the inboard midplane box module.

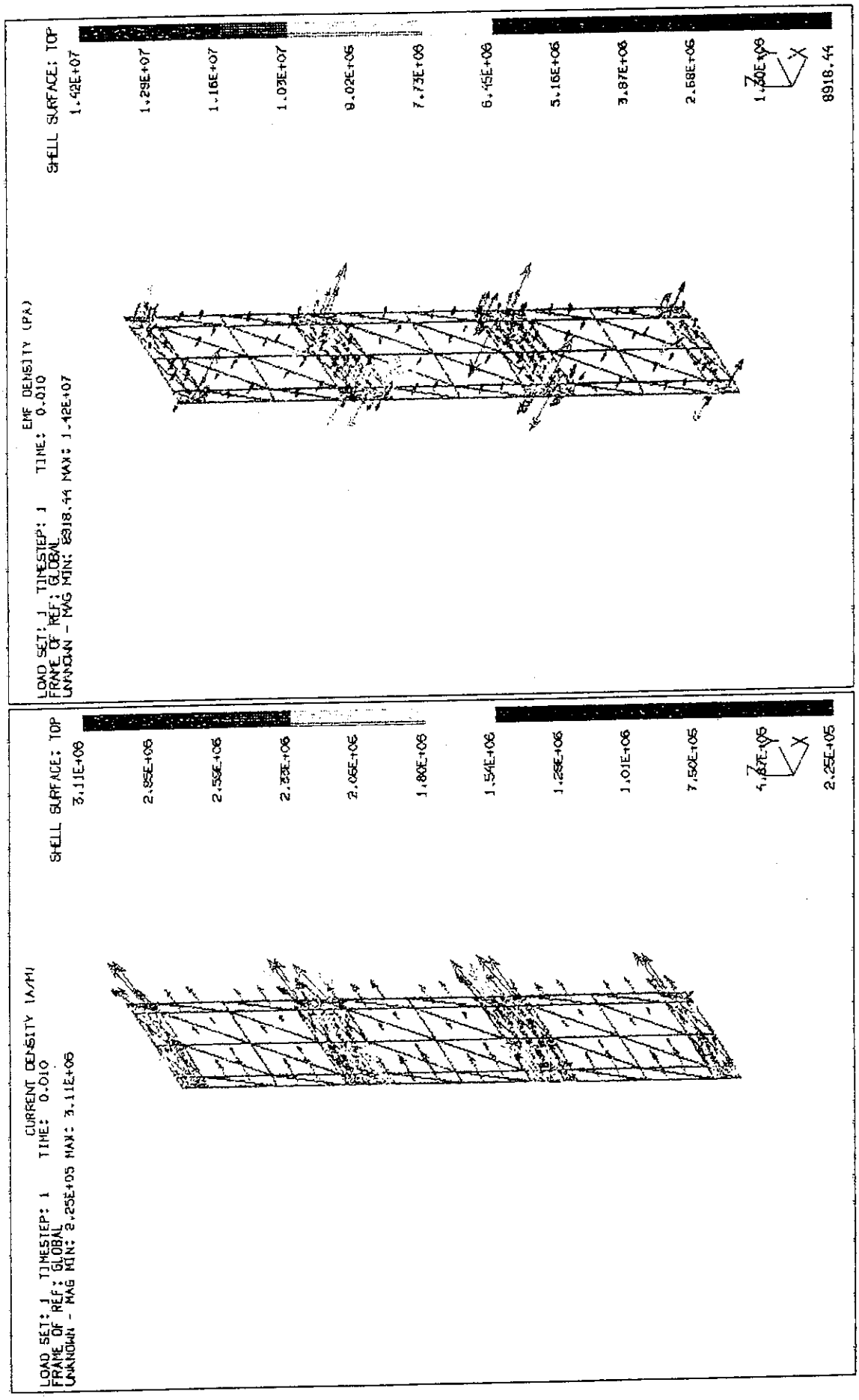

Fig. 4.3.3 Eddy current and EM force distributions on back plate arround 3 inboard box blanket modules.

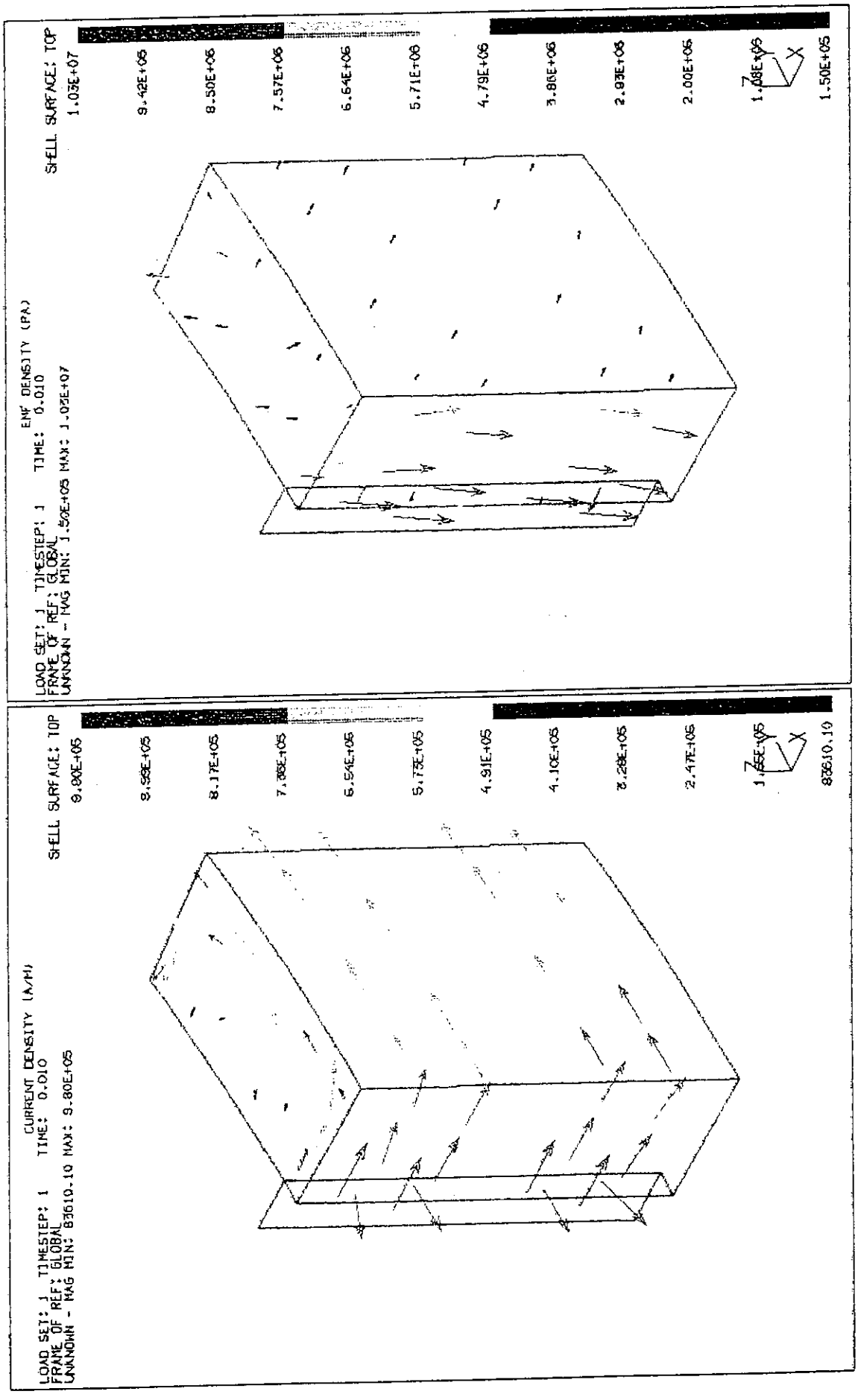

Fig. 4.3.4 Eddy current and EM force distributions on shield block in the inboard midplane box module.

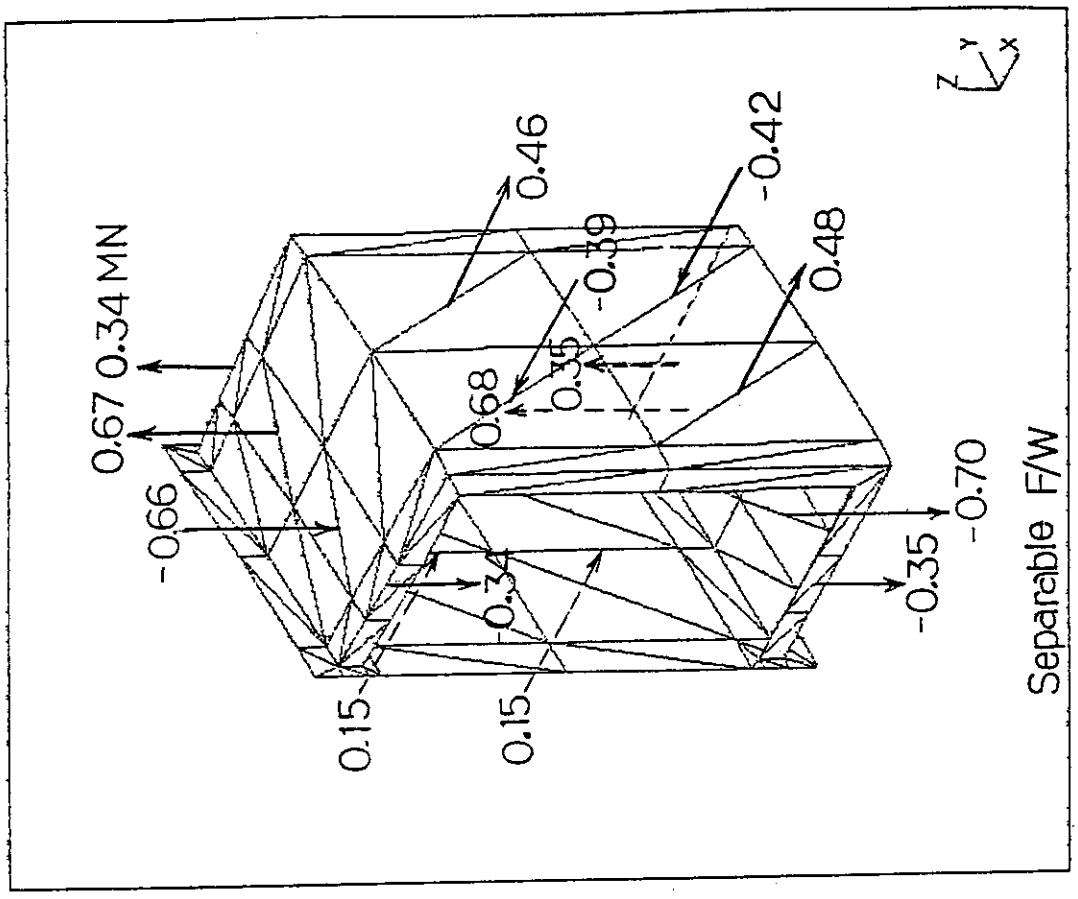

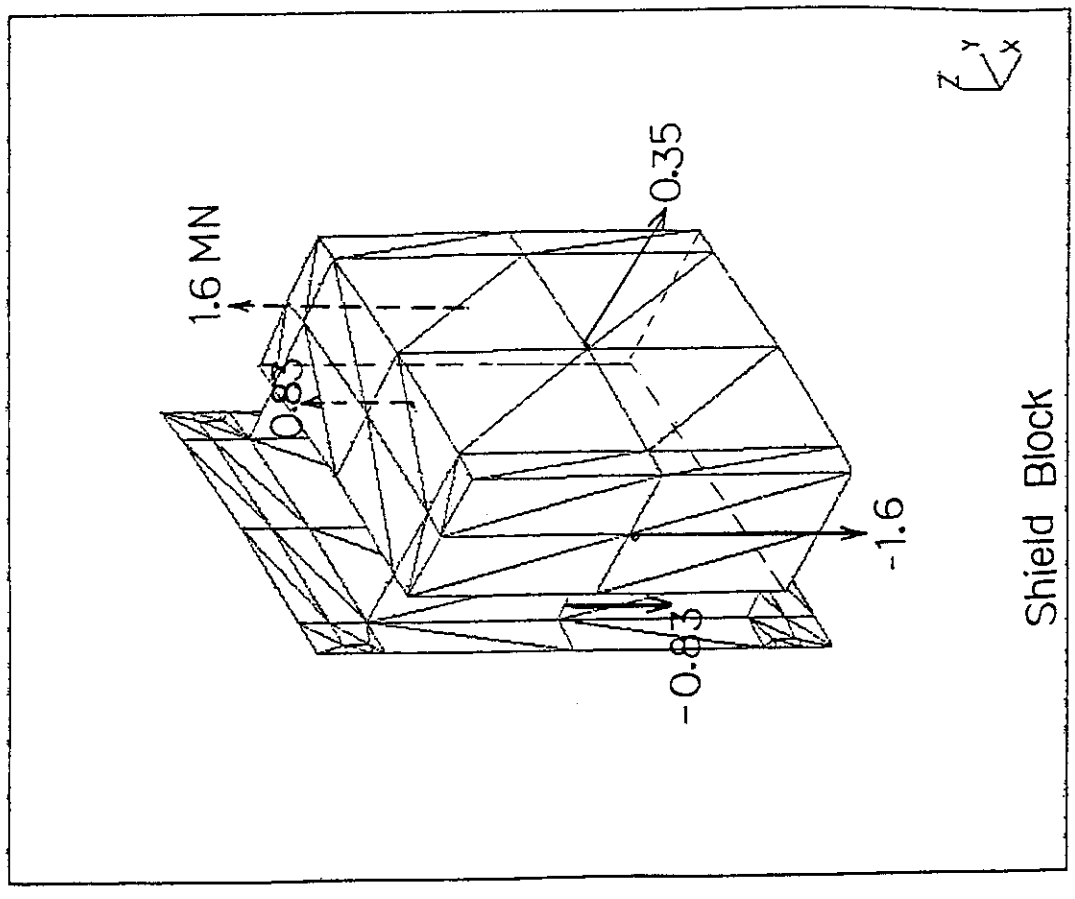

Fig. 4.3.5 Electromagnetic forces on the component parts in the inboard midplane box module.

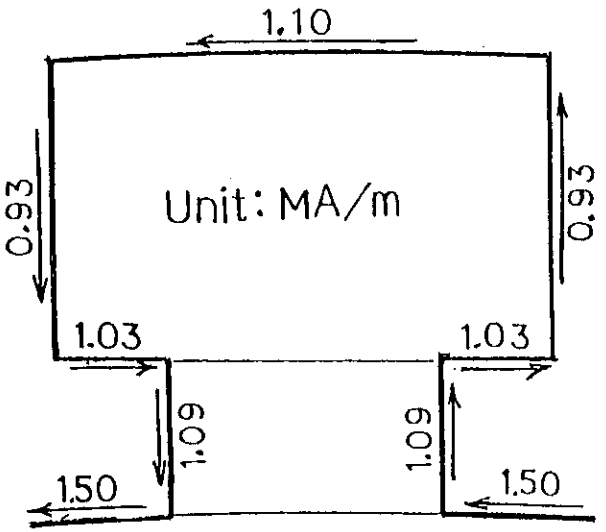

b) θ =7.5°

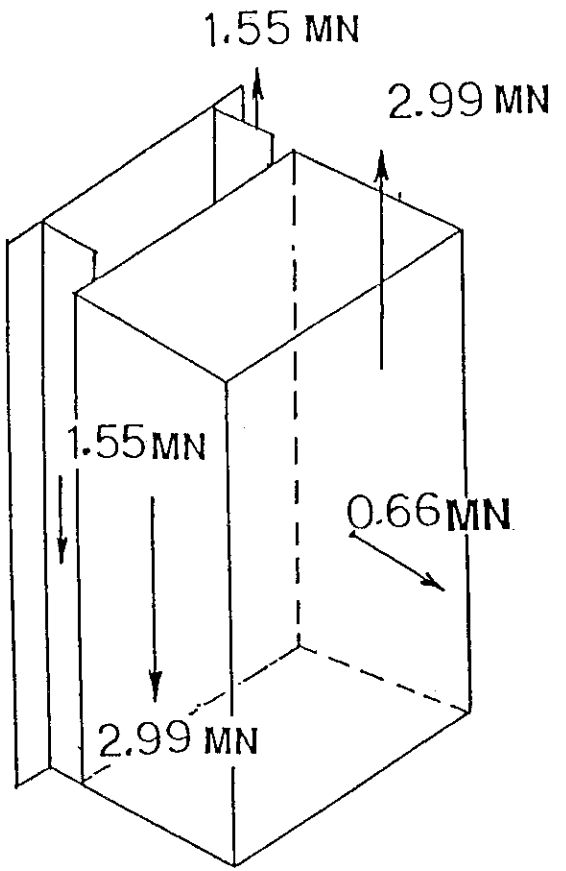

Total vertical load:
±4.54 MN/ 1-m module

b) θ =7.5°

Fig. 4.3.6 Eddy current and EM force on the blanket structure with an integral first wall.

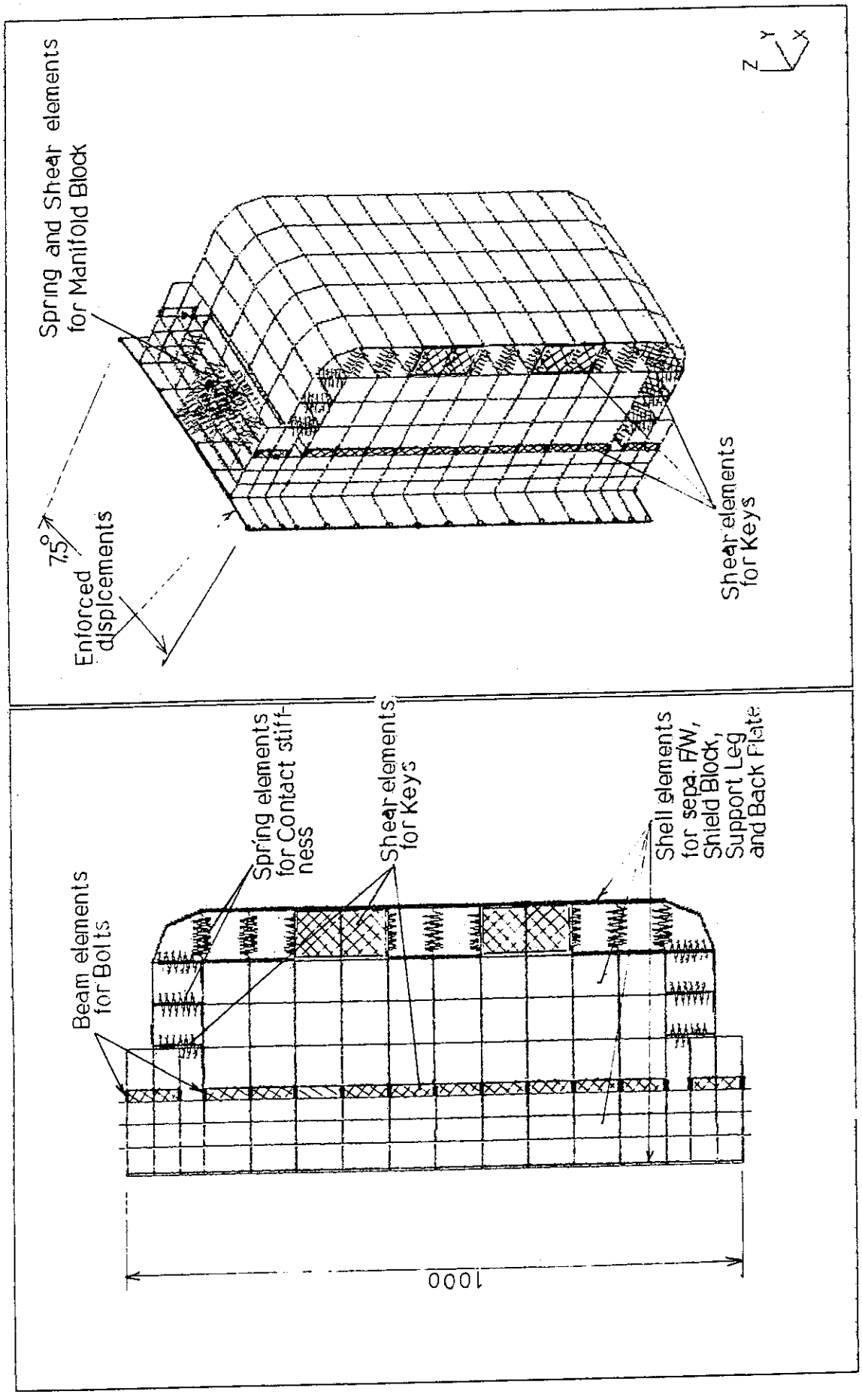

Fig. 4.3.7 FEM model of box blanket module with bolted joint at inboard midplane for stress analysis.

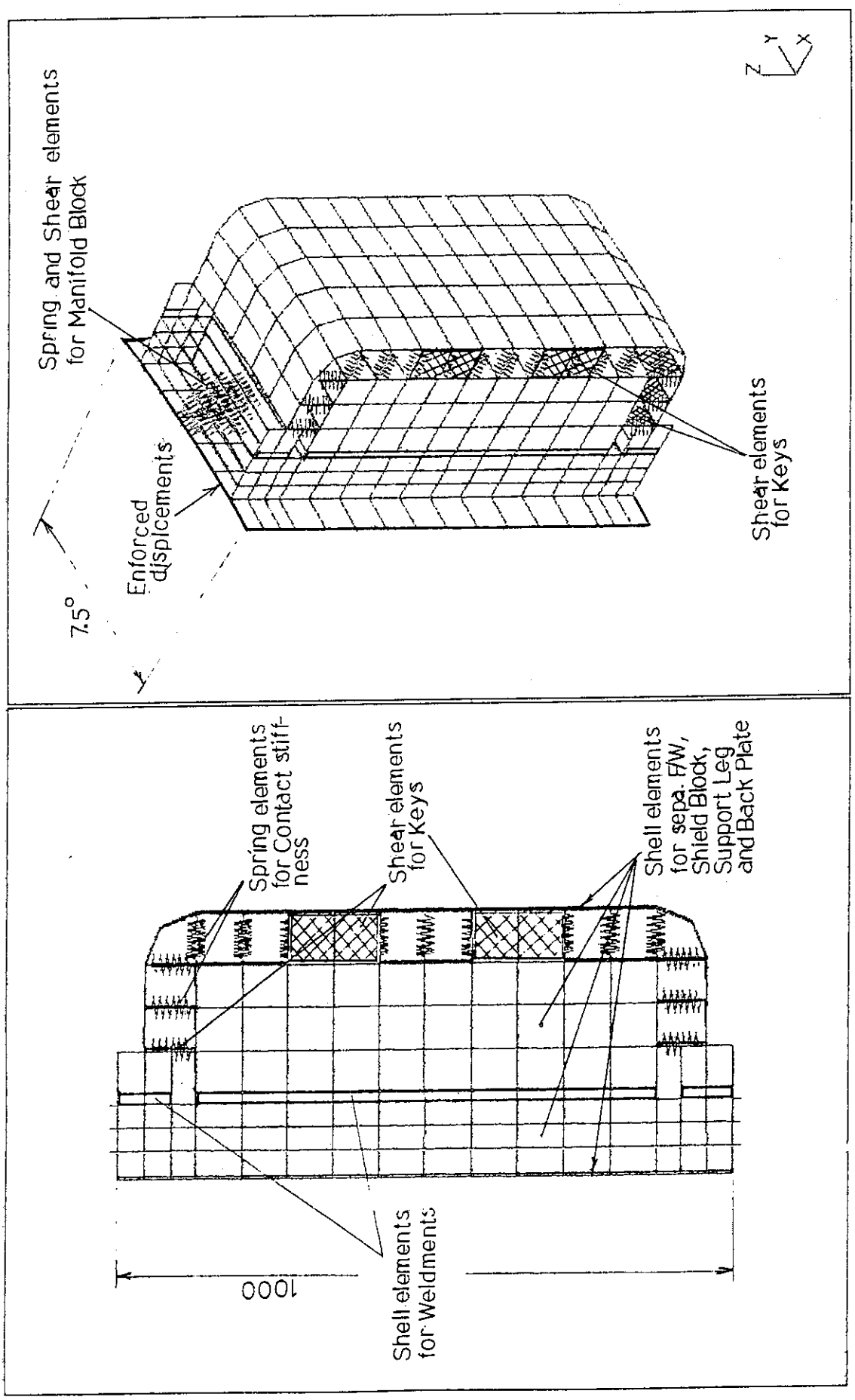

Fig. 4.3.8 FEM model of box blanket module with welded joint at inboard midplane for stress analysis.

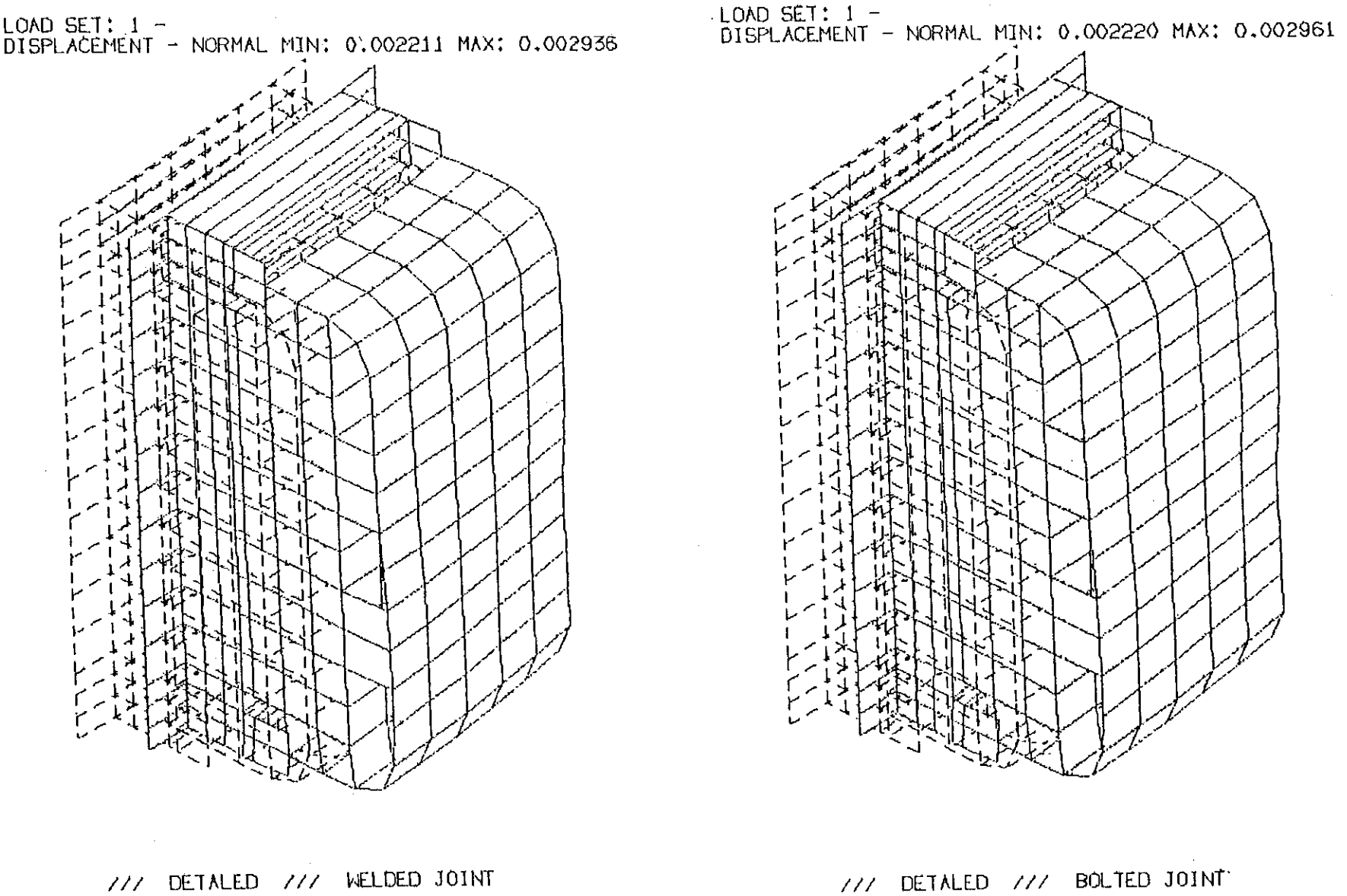

Fig. 4.3.9 Overall deformation of blanket module with separable FW around the inboard mid-plane

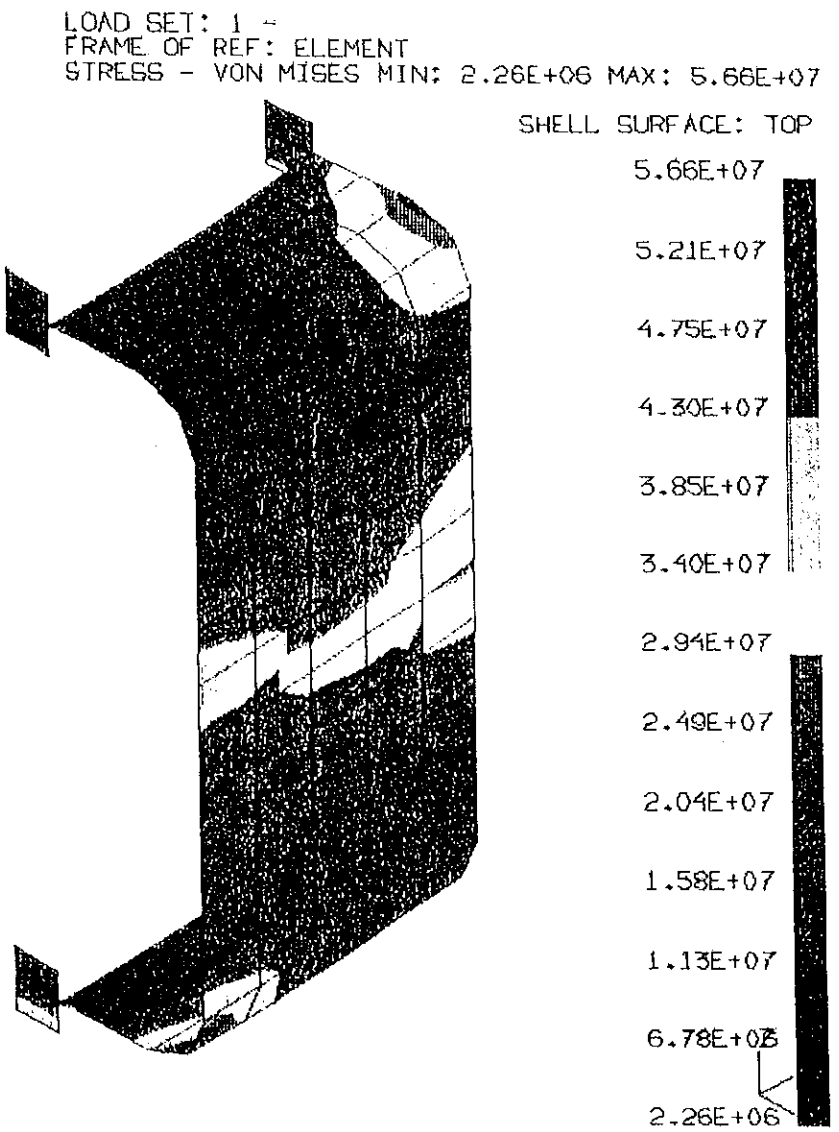

/// DETALED /// WELDED JOINT

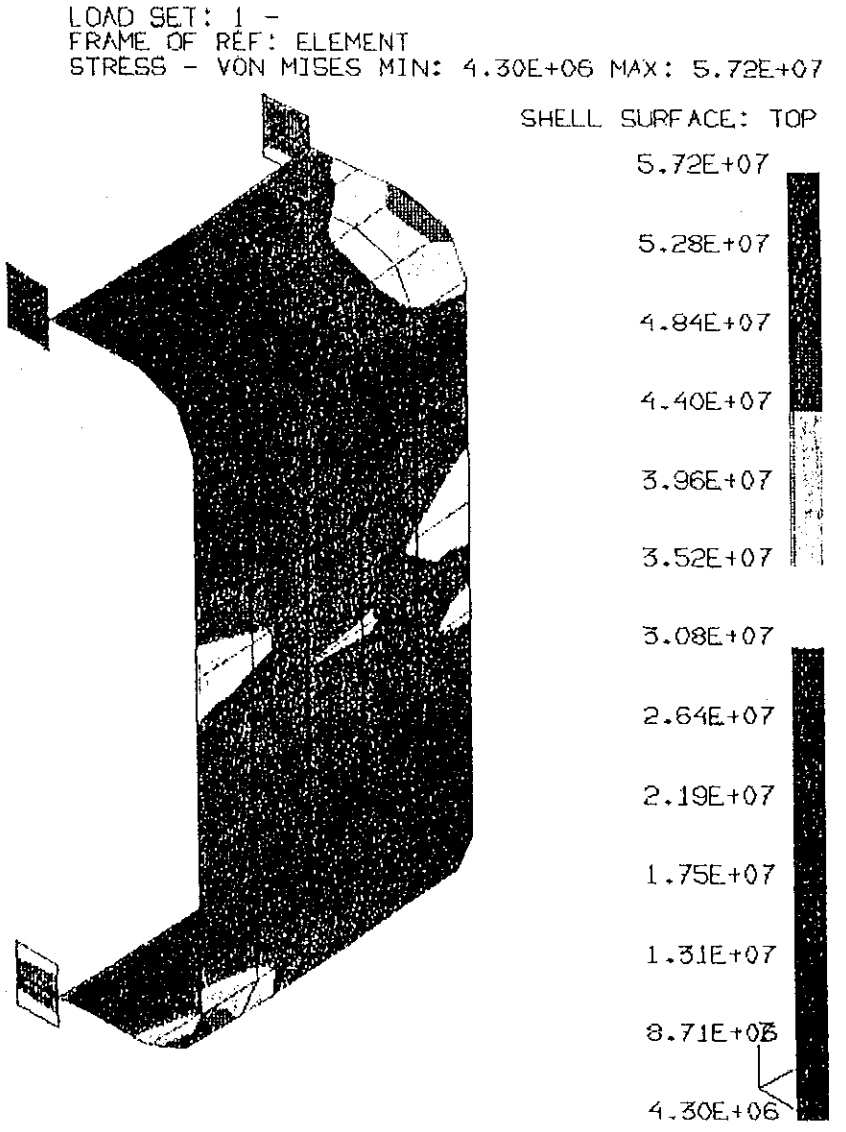

/// DETALED /// BOLTED JOINT

Fig. 4.3.10 Von Mises stress distribution on separable first wall in inboard midplane box module.

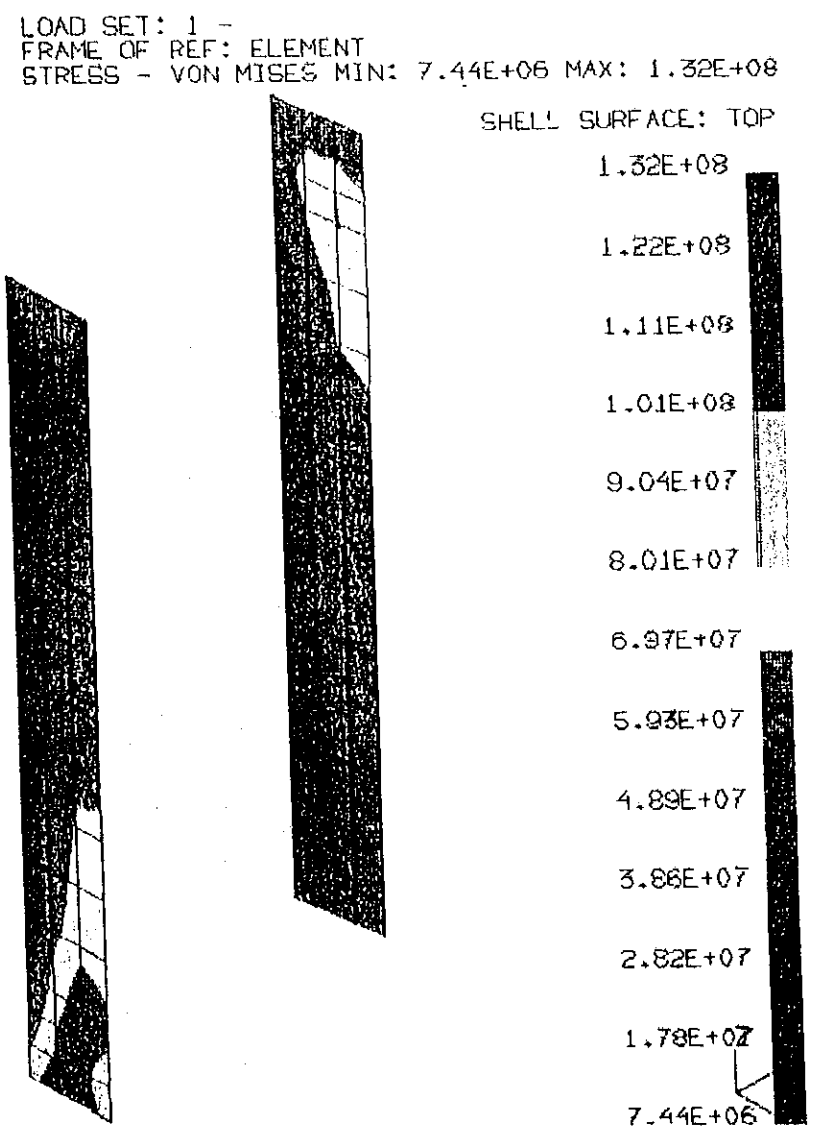

/// DETALED /// WELDED JOINT

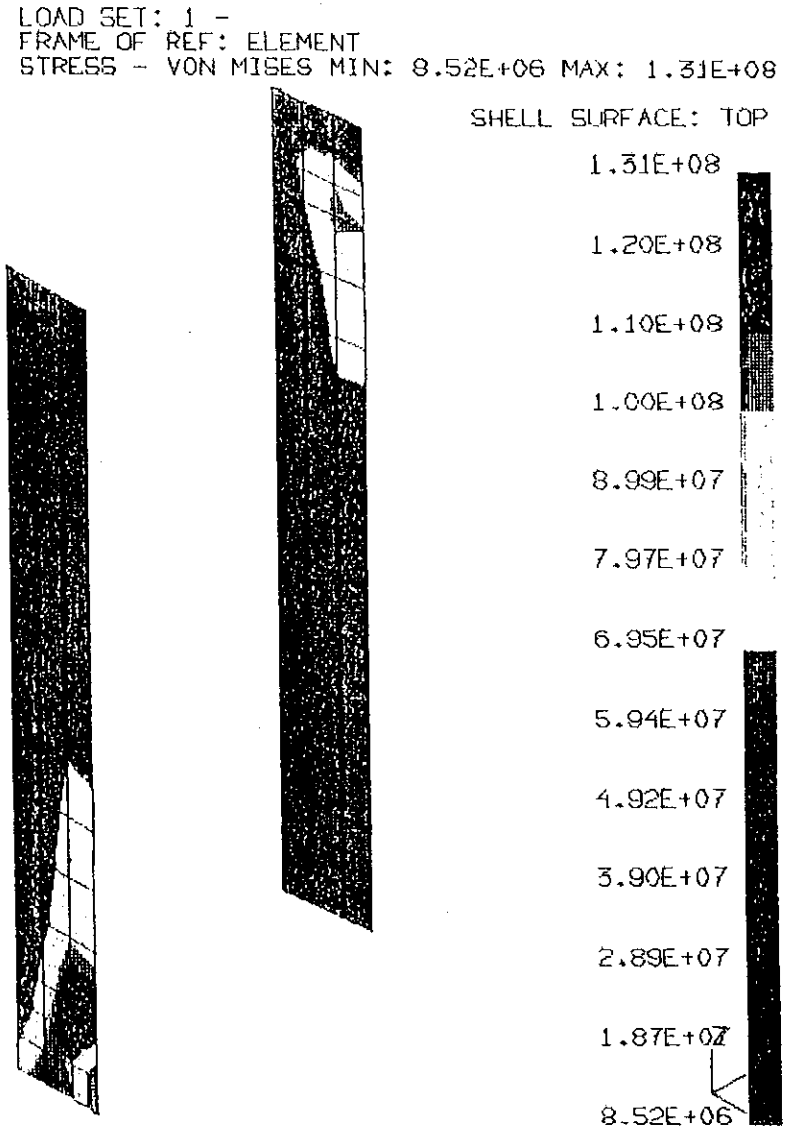

/// DETALED /// BOLTED JOINT

Fig. 4.3.11 Von Mises stress distribution on Support Ribs (Legs) in inboard midplane box module.

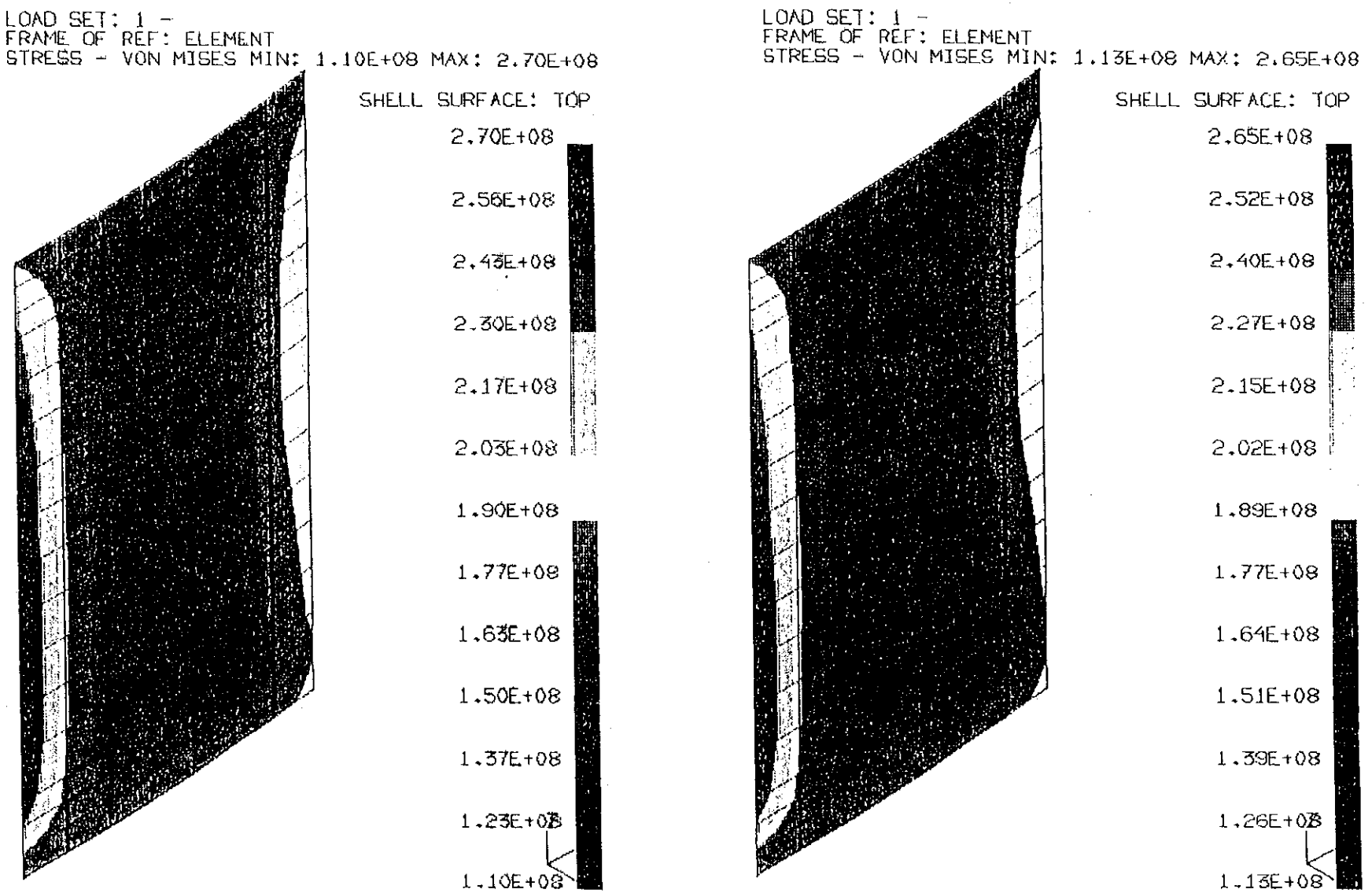

Fig. 4.3.12 Von Mises stress distribution on Back Plate in inboard midplane box module.

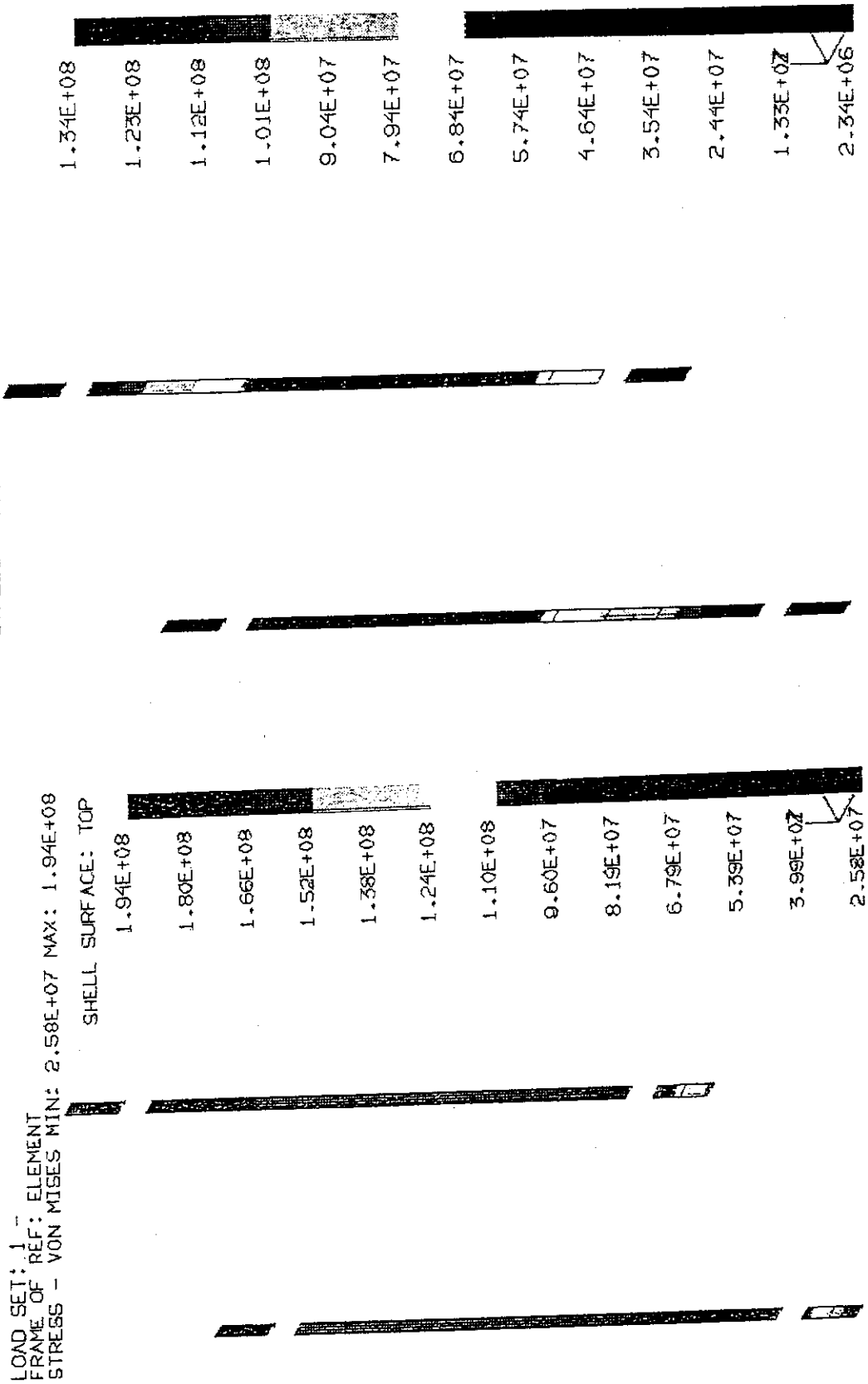

Fig. 4.3.13 Stress distributions on the keys at bolt joint and the weldment at welded joint in support legs.

Table 4.3.1 Max. Stress on the components in inboard midplane module

Components			Thickness (mm)	Bolt & Key Joint (MPa)	Welded Joint (MPa)
Separable F/W			85	64	62
Shield Block	Front		100	32	31
	End		100	35	56
	Side		100	48	52
	Top & Bottom		100	26	26
Support Leg	F/W	Left	75	150	158
		Right	75	120	124
	SHLD	Left	75	158	162
		Right	75	142	148
Keys (F/W & Shield)	Front			23x2	23x2
	Top & Bottom			21x2	26x2
Manifold Block				27x2	22x2
Bolt Joint	F/W	Left	M20	544	-
		Right	M20	562	-
	SHLD	L	M20	299	-
		R	M20	335	-
Key Joint	F/W	L	75/2	78x2	-
		R	75/2	79x2	-
	SHLD	L	75/2	106x2	-
		R	75/2	118x2	-
Welded Joint	F/W	L	45	-	224
		R	45	-	202
	SHLD	L	45	-	244
		R	45	-	262
Back Plate	Edge		80	(228)	(230)
	Center		80	194	192

Note; *1) Key stress is shown by shearing stress(τ)x2.
*2) High stresses at edge sides of back plate are due to enforced displacements on the edge side nodal points.
*3) 'Left' and 'Right' are side directions from plasma center.

Acknowledgment

The authors wish to acknowledge Drs. M. Ohta, T. Nagashima, S. Matsuda, M. Seki and T. Tsunematsu for their support and encouragement. They also would like to express their sincere gratitude to members of Kawasaki Heavy Industries, Ltd., Toshiba Corporation, Hitachi Ltd., and Mitsubishi Heavy Indutries Ltd. for their industrial support.